
Doctoral

Engineering

2009-12-01

Singlemode-Multimode-Singlemode Optical Fibre Structures for Optical Sensing

Agus Muhamad Hatta
Technological University Dublin

Follow this and additional works at: <https://arrow.tudublin.ie/engdoc>



Part of the [Electrical and Computer Engineering Commons](#)

Recommended Citation

Hatta, A. M. (2009) *Singlemode-Multimode-Singlemode Optical Fibre Structures for Optical Sensing*. Doctoral Thesis, Technological University Dublin. doi:10.21427/D7TP5F

This Theses, Ph.D is brought to you for free and open access by the Engineering at ARROW@TU Dublin. It has been accepted for inclusion in Doctoral by an authorized administrator of ARROW@TU Dublin. For more information, please contact yvonne.desmond@tudublin.ie, arrow.admin@tudublin.ie, brian.widdis@tudublin.ie.



This work is licensed under a [Creative Commons Attribution-Noncommercial-Share Alike 3.0 License](#)

Singlemode-Multimode- Singlemode Optical Fibre Structures for Optical Sensing

A thesis submitted for the degree of

Doctor of Philosophy

by

AGUS MUHAMAD HATTA



School of Electronic and Communications Engineering

Faculty of Engineering

Dublin Institute of Technology

Supervisors: Prof. Gerald Farrell and Dr. Yuliya Semenova

Dublin, Ireland

December, 2009

*This thesis is dedicated to:
my late father, my mother,
my wife Dewi, and our son Akram*

Abstract

This thesis describes theoretical and experimental investigations on all-fibre multimode interference (MMI) devices using a singlemode-multimode-singlemode (SMS) fibre structure for use as a new type of edge filter for a ratiometric wavelength measurement system and as novel stand alone sensors. The use of two edge filters, so called X-type edge filters based on SMS fibre structures in a ratiometric wavelength measurement system is proposed and demonstrated. The use of X-type edge filters can improve the resolution and accuracy of wavelength measurement compared to the use of one edge filter in a conventional ratiometric system.

Several aspects of the SMS edge filters have been investigated, including the effect of misalignment the SMS fibre cores due to fabrication tolerances, polarization dependence, and temperature dependence. These aspects can impair the performance of a ratiometric wavelength measurement system. Several approaches have been proposed and demonstrated to achieve high resolution and accuracy of wavelength measurement. Misalignment effects due to the splicing process on the spectral characteristics and PDL of SMS fibre structure-based edge filters are investigated numerically and experimentally. A limit for the tolerable misalignment of the cores of an SMS fibre structure-based edge filter is proposed, beyond which the edge filter's spectral performance degrades unacceptably. It is found that a low PDL for an SMS fibre structure-based edge filter can be achieved with small lateral core offsets. Furthermore, the rotational core offsets position is proposed to minimize the PDL. Analysis of the temperature dependence of SMS

X-type edge filters is presented. The temperature variation in the system can be determined and compensated by using an expanded ratiometric scheme with an additional reference arm.

New sensing applications of multimode interference in an SMS fibre structure are proposed and demonstrated as a temperature sensor, a voltage sensor based on the strain effect, and a strain sensor with very low temperature dependence. All the sensors utilize a simple intensity-based interrogation system using a ratiometric power measurement system. It is found that the temperature and strain characteristics of SMS fibre structures are linear in nature and can be used for temperature and strain sensors. Based on the strain effect in an SMS fibre structure, a voltage sensor is also proposed. The SMS fibre structure is attached to a piezoelectric (PZT) stack transducer. The displacement of the PZT due to the voltage induces a strain on the SMS fibre structure and in turn results in a change in the ratio response. Finally, a strain sensor with very low temperature induced strain measurement error is investigated. For this purpose two SMS fibre structures were proposed and demonstrated in a ratiometric power measurement scheme, one SMS structure acts as the strain sensor and the other SMS structure acts as the temperature monitor. The use of this configuration can effectively minimize the temperature induced strain measurement error.

Declaration

I certify that this thesis which I now submit for examination for the award of Doctor of Philosophy, is entirely my own work and has not been taken from the work of others, save and to the extent that such work has been cited and acknowledged within the text of my work.

This thesis was prepared according to the regulations for postgraduate study by research of the Dublin Institute of Technology and has not been submitted in whole or in part for another award in any Institute.

The work reported on in this thesis conforms to the principles and requirements of the Institute's guidelines for ethics in research.

The Institute has permission to keep, lend or copy this thesis in whole or in part, on condition that any such use of the material of the thesis be duly acknowledged.



Agus Muhamad Hatta

Date: 4th December 2009

Acknowledgment

Hadith

The Messenger of God (may God bless him and grant him peace) said:

“He who does not thank People does not thank God.”

[Abu Dawud]

The work presented in this thesis is a research result within three and half years at DIT Photonics Research Centre (PRC) in School of Electronic and Communications, Dublin Institute of Technology. This thesis would have not been accomplished without support and help from many people. I would like to express my gratitude to people around me for their support, sincere help, guidance, discussions, friendship, and prayers.

First and foremost, I would like to thank my supervisor Prof. Gerald Farrell for giving me an opportunity to work with him, his constant support, advices, encouragements, and guidance on my research. I also would like to thank him for his patience in reviewing and giving many feedbacks on my thesis. I am very thankful to my co-supervisor Dr. Yuliya Semenova for many valuable suggestions and support on my research. Her careful reading, perspectives, and comments to my thesis were really useful.

I also would like to thank Dr. Qian Wang for his guidance and suggestions during my first year at the PRC. I am very grateful to Prof. Jie Zheng for his support and kindness, especially during my visiting research in Jilin University. I would like to thank my thesis examiners, Prof. Elfed Lewis and Dr. Andreas Schwarzbacher, for their careful reading and giving many valuable remarks.

I take many benefits from interaction with people at the PRC. I would like to thank the PRC members: Ginu Rajan, Pengfei Wang, Sunish Mathew, Qiang Wu,

An Sun, Jinesh Mathew, Kalaga Madhav, and Manjusha, for their help, fruitful discussion, and friendship. I am also grateful to the staff of the School of Electronic and Communications Engineering for their kindness and helps.

My gratitude also goes to people in Indonesia. I would like to thanks Mr. Suwarso, Mr. Heru Setijono, Dr. Sekartedjo, Mrs. Apriani, Dr. Aulia Aisyah, Prof. Agus Rubiyanto, and all of my teachers for their inspiration and knowledge. I also would like to thanks Dr. Totok Soehartanto, Dr. Bambang Lelono, and my colleagues at the Engineering Physics Department in Institut Teknologi Sepuluh Nopember (ITS) Surabaya for their encouragements.

Many thanks to my friends in Indo-Irish association; I really enjoyed the programmes and interactions which made life in Ireland more enjoyable. Special thank goes to Mas Syamsul, Mbak Imas, and Mas Dulsono for their kindness. I also thank to all my friends whom are too many to be listed here for being part of my life and for their helps.

I would like to thank Syekh Mustafa Haqqani for his advices and prayers. Many thanks to my brothers and sister: Naufan, Ricky, and Nelly, for their support and prayers. I also would like to thank my entire extended family, my parents in law, uncles, and unties for all their support and prayers.

I am indebted forever to my beloved parents for their love and raising me up. To my late father, I wouldn't be able in this point of my life journey without his sacrifice, support, and prayers to our family during his life. I would like to thanks my mother for her constant prayers, encouragements, and everything. Finally, I would like to thank my beloved wife Dewi and our son Akram for their love, patience, understanding, and prayers.

List of publications arising from the research

Journal papers

- A. M. Hatta, Y. Semenova, G. Rajan, and G. Farrell, "Polarization dependence of an edge filter based on singlemode-multimode-singlemode fibre," *Optics & Laser Technology*, in press, accepted on 19th January 2010.
- A. M. Hatta, Y. Semenova, Q. Wu, and G. Farrell, "Strain sensor based on a pair of singlemode-multimode-singlemode fibre structures in a ratiometric power measurement scheme," *Applied Optics*, vol. 49, no. 3, pp. 536-541, 2010.
- A. M. Hatta, Y. Semenova, G. Rajan, P. Wang, J. Zheng, and G. Farrell, "Analysis of temperature dependence for a ratiometric wavelength measurement system using SMS fibre structure-based edge filters," *Optics Communications*, in press, accepted on 4th November 2009.
- A. M. Hatta, G. Rajan, Y. Semenova, and G. Farrell, "SMS fibre structure for temperature measurement using a simple intensity-based interrogation system," *Electronics Letters*, vol. 45, no. 21, pp. 1069-1071, 2009.
- Q. Wu, A. M. Hatta, Y. Semenova, and G. Farrell, "Use of a single-multiple-single mode fibre filter for interrogating fibre Bragg grating sensors with dynamic temperature compensation," *Applied Optics*, vol. 48, no. 29, pp. 5451-5458, 2009.
- A. M. Hatta, G. Farrell, P. Wang, G. Rajan, and Y. Semenova, "Misalignment limits for a singlemode-multimode-singlemode fibre-based edge filter," *Journal of Lightwave Technology*, vol. 27, no. 13, pp. 2482-2488, 2009.
- A. M. Hatta, G. Farrell, Q. Wang, G. Rajan, P. Wang, and Y. Semenova, "Ratiometric wavelength monitor based on singlemode-multimode-singlemode fibre structure," *Microwave and Optical Technology Letters*, vol. 50, no. 12, pp. 3036-3039, 2008.

Journal paper under review

- A. M. Hatta, G. Rajan, Y. Semenova, and G. Farrell, "A voltage sensor based on a singlemode-multimode-singlemode fibre structure," *Microwave and Optical Technology Letters*, Manuscript ID: MOP-09-1621.

Conference proceeding papers

- A. M. Hatta, G. Farrell, Y. Semenova, and H. Fernando “Ratiometric wavelength monitor using a pair of symmetrical multimode interference structures based on silicon-on-insulator (SOI),” *Photonic Materials, Devices, and Applications III, Proceeding of SPIE*, Vol. 7366,73660S, 2009.
- A. M. Hatta, G. Rajan, G. Farrell, and Y. Semenova, “Ratiometric wavelength monitor based on “X-type spectral response” using two edge filters,” *Optical Sensors 2009, Proceeding of SPIE*, Vol. 7356, 73561N, 2009.
- A. M. Hatta, G. Farrell, and Q. Wang, “A simple integrated ratiometric wavelength monitor based on multimode interference structure,” *Optical Design and Engineering III Proceeding of SPIE*, Vol. 7100, 710023, 2008.
- A. M. Hatta, G. Farrell, Q. Wang, and J. Zheng, “Design on the optical core of an integrated ratiometric wavelength monitor,” *Proceeding of 14th European Conference on Integrated Optics (ECIO)*, 273-276, 2008.
- A. M. Hatta, Q. Wang , G. Farrell, and J. Zheng, “A design method for a ratiometric wavelength monitor using a pair of directional couplers acting as edge filters,” *Silicon Photonics and Photonic Integrated Circuits, Proceeding of SPIE*, Vol. 6996, 69961T, 2008.
- P. Wang, G. Farrell, Y. Semenova, A. M. Hatta, and G. Rajan, “Accurate theoretical prediction on singlemode fibre macrobending loss and bending induced polarization dependent loss,” *Optical Sensors 2008, Proceeding of SPIE*, 7003, 70031Y, 2008.
- A. M. Hatta, G. Farrell, and Y. Semenova, “Design of a multiple MMI structure for (bio-) chemical sensor applications,” *Europtrode IX: Ninth International Conference on Optical Chemical Sensors and Biosensors*, Dublin, Ireland, April, 2008.
- Q. Wang, G. Farrell, and A. M. Hatta, “Global optimization of multimode interference structure for wavelength measurement,” *Third European Workshop on Optical Fibre Sensors, Proceeding of SPIE*, Vol. 6619, 66192M, 2007.

Acronym

ANN	Artificial Neural Network
BPM	Beam Propagation Method
CCD	Charge-Coupled Device
DVD	Digital Versatile Disc or Digital Video Disc
DWDM	Dense Wavelength Division Multiplexing
EM	Electromagnetic
FBG	Fibre Bragg Grating
FDM	Finite Difference Method
LED	Light-Emitting Diode
LP	Linearly Polarised
MMI	Multimode Interference
MPA	Modal Propagation Analysis
OSA	Optical Spectrum Analyser
PDL	Polarisation Dependence Loss
PZT	Piezoelectric
SDL	Strain Dependence Loss
SMF	Singlemode Fibre
SMMS	Singlemode Multimode Multimode Singlemode
SMS	Singlemode Multimode Singlemode
SNR	Signal-to-Noise Ratio
TDL	Temperature Dependence Loss
TE	Transverse Electric
TEC	Thermo Expansion Coefficient
TM	Transverse Magnetic
TOC	Thermo-Optic Coefficient
WDM	Wavelength Division Multiplexing

Contents

Abstract	iii
Declaration	v
Acknowledgment	vi
List of publications arising from the research	viii
Acronym	x
Contents	xi
List of Figures	xiv
Chapter 1 Introduction	1
1.1 Background to the research.....	1
1.1.1 <i>Multimode interference (MMI) effects</i>	3
1.1.2 <i>MMI in optical fibre</i>	6
1.1.3 <i>MPA of SMS structures</i>	7
1.1.4 <i>SMS structures for interrogation of FBG sensors</i>	11
1.1.5 <i>Sensing applications of SMS fibre structures</i>	15
1.2 Motivation and the objectives of the research.....	16
1.3 Research methodology	18
1.4 Layout of the thesis	21
1.5 References	23
Chapter 2 Multimode interference in an SMS fibre structure for an edge filter application	28
2.1 Introduction	29
2.2 Proposed configuration and its design	31
2.3 Design and experimental results	36
2.4 Conclusion	40
2.5 References	41
Chapter 3 Effect of misalignment on an SMS fibre structure-based edge filter	43
3.1 Introduction	45
3.2 SMS-based edge filters	47

3.3 Modal propagation analysis	50
3.4 Design example and spectral response.....	51
3.5 Investigation of misalignment effects for the design example.....	54
3.6 Conclusion	63
3.7 References	64
Chapter 4 Polarization dependence of an SMS fibre structure-based edge filter	65
4.1 Introduction	66
4.2 Calculation of PDL for an SMS fibre structure	68
4.3 Experimental results.....	74
4.4 Conclusion	78
4.5 References	79
Chapter 5 Temperature dependence of an SMS fibre structure-based edge filter	81
5.1 Introduction	83
5.2 Temperature dependence in an SMS edge filter	84
5.3 Temperature dependence in the ratiometric wavelength measurement system.....	90
5.4 Conclusion	97
5.5 References	98
Chapter 6 New standalone sensors based on an SMS fibre structure.....	100
6.1 SMS fibre structure for temperature measurement using a simple intensity-based interrogation system.....	102
6.1.1 Introduction.....	103
6.1.2 SMS fibre structure	104
6.1.3 Temperature dependence	105
6.1.4 Conclusion	109
6.1.5 References	109
6.2 A voltage sensor based on a Singlemode-Multimode-Singlemode fibre structure.....	110
6.2.1 Introduction.....	110
6.2.2 Strain dependence of SMS fibre structure.....	112

6.2.3 <i>Experimental results</i>	116
6.2.4 <i>Conclusion</i>	119
6.2.5 <i>References</i>	120
Chapter 7 Strain sensor based on an SMS fibre structure and its temperature compensation	122
7. 1 Introduction	124
7.2 Strain and temperature dependence of a step index SMS fibre structure .	125
7.3 Experimental results.....	132
7. 4 Conclusions	138
7. 5 References	139
Chapter 8 Conclusions and future research	141
8.1 Conclusions from the research	141
8.2 Overall conclusions from the research.....	149
8.3 Future research	151
Appendix A Statement of Contribution	154
Appendix B Ratiometric wavelength monitor based on “X-type spectral response” using two edge filters	155
Appendix C Design of the optical core of an integrated ratiometric wavelength monitor	169
Appendix D A simple integrated ratiometric wavelength monitor based on multimode interference structure	177
Appendix E Flowchart of the Modal Propagation Analysis	190
Appendix F Equipment and accessories	193

List of Figures

Figure 1 Schematic of a multimode waveguide placed between input and output singlemode waveguides	5
Figure 2 Field profile within the multimode waveguide showing self-imaging of the input field	5
Figure 3 SMS fibre structure.....	6
Figure 4 (a) light propagation in the MMF section (b) calculated transmission loss to the output SMF versus the length of MMF section [23] (c) calculated spectral response	10
Figure 5 FBG sensing system	11
Figure 6 Schematic configuration of ratiometric wavelength monitor (a) using one edge filter (b) using two edge filters, (c) the desired spectral response of the edge filter-1 and edge filter-2 arms, and (d) the output ratio of two arms using one edge filter and two edge filters.....	14
Figure 7 Block diagram of the experimental set-up.....	20
Figure 8 Schematic structure of (a) a ratiometric wavelength measurement system (b) an SMS fibre-based edge filter (c) the desired spectral response of the two edge filter arms and (d) the output ratio between the two arms	32
Figure 9 Spectral responses at re-imaging distance for different core radii and MMF section lengths	35
Figure 10 Calculated and measured spectral responses of the SMS edge filters .	39
Figure 11 Measured ratio	39
Figure 12 Measured ratio as the wavelength is tuned	40
Figure 13 (a) Schematic configuration of a ratiometric wavelength measurement (b) desired spectral responses of the SMS-based edge filter, negative (solid line) and positive (dash line) slope versions, and (c) the output ratio between two output SMS-based edge filters.....	48
Figure 14 (a) Schematic configuration of the SMS fibre structure (b) concentric alignment (c) misalignment condition	49

Figure 15	Transmission loss responses of the two SMS-based edge filters	54
Figure 16	Calculated transmission loss response due to misalignment effect of the SMS-based edge filter (a) negative slope (b) positive slope.....	56
Figure 17	The MMF field amplitude profile at $\lambda = 1537$ nm for the negative slope (a) $a = 0$ μm , (b) $a = 10$ μm ; for the positive slope (c) $a = 0$ μm , (d) $a = 10$ μm	58
Figure 18	Correlation coefficient of the spectral response for different offsets ..	60
Figure 19	Measured and calculated transmission loss with misalignment of the SMS-based edge filters	61
Figure 20	Measured ratio	62
Figure 21	Schematic structure of an SMS fibre structure (inset). Calculated spectral response of SMS fibre structure	69
Figure 22	Interfaces of input/output SMF core to the MMF core (a) position of input SMF core, and (b) position of output SMF core.....	70
Figure 23	Calculated PDL for several lateral core offsets at the rotational core offset from 0 to 180°	71
Figure 24	Field amplitude profile at the output end of the MMF section (a) TE mode, (b) TM mode; close up images: (c) TE mode, (d) TM mode, and (e) the difference in the amplitude profiles between TE and TM modes	73
Figure 25	Measured results of SMS edge filters using the automatic splicing mode (a) spectral responses, (b) PDL	75
Figure 26	Screenshot of the splicing process using attenuation splicing mode...	77
Figure 27	Measured results of SMS edge filters with the rotational core offsets of 180° and 90° (a) spectral responses, (b) PDL.....	78
Figure 28	Calculated and measured two edge filters X-type spectral response...	85
Figure 29	Schematic set-up for measuring the temperature dependence on the SMS edge filter transmission loss	87
Figure 30	Transmission loss response at the temperature of 10 and 40 °C: (a) calculation results (b) measurement results	88
Figure 31	Transmission loss change as a function of temperature at a wavelength of 1545 nm for a reference temperature of 20 °C.....	89

Figure 32	Calculated transmission loss change due to temperature change for TEC, TOC separately and also for TEC and TOC together.....	90
Figure 33	Measured ratio at different temperatures within the wavelength range. Schematic configuration of ratiometric wavelength measurement (inset figure). Temperature response at 1545 nm (inset graph)	92
Figure 34	Updated schematic ratiometric system to allow self-monitoring of temperature.....	94
Figure 35	(a) wavelength coefficients at the temperature of 10 °C, and (b) temperature coefficients at the wavelength of 1540 nm	95
Figure 36	Calculated and measured of SMS fibre structure spectral response (Inset: a schematic structure of an SMS fibre structure).....	105
Figure 37	Temperature dependence of SMS fibre structure (Inset: schematic of the measurement set-up)	108
Figure 38	Transmission of the SMS structure against temperature at the wavelengths of 1509.5 nm and 1554 nm	108
Figure 39	Schematic configuration of SMS fibre structure voltage sensor system	112
Figure 40	Transmission loss response of the SMS fibre structure. SDL of the SMS fibre structure (inset figure)	114
Figure 41	Transmission loss vs applied strain to the SMS fibre structure at a wavelength of 1556.8 nm.....	116
Figure 42	Measured ratio spectral response at 0 V and 100 V (inset: ratio difference)	117
Figure 43	Ratio response of system against voltage at the operational wavelength 1556.8 nm (inset: variation in ratio for a step change of 0.5 V)	118
Figure 44	(a) Single SMS fibre structure (b) Schematic structure of strain measurement with a self-temperature monitoring in a ratiometric power measurement scheme using a pair of SMS fibre structures ...	127
Figure 45	SDL and TDL of the SMS fibre structure (Inset, spectral response).	129
Figure 46	Transmission loss responses at the operating wavelength of 1539 nm (a) strain responses at different ambient temperatures, (b) temperature response for an applied strain of 500 $\mu\epsilon$	131

Figure 47 Measured spectral response of two SMS fibre structures.....	132
Figure 48 Ratio of SMS-1 as a function of strain with temperature variation at an operating wavelength of 1539 nm: (a) measured (b) calculated.....	134
Figure 49 Ratio response of SMS-2 due to temperature variation at an operating wavelength of 1539 nm: (a) measured (b) calculated	136
Figure 50 Calculated ratio response of SMS-2 with MMF length errors due to temperature variation at an operating wavelength of 1539 nm.....	137
Figure 51 Schematic configuration of the proposed MMI ratiometric wavelength monitor (a) using two edge filters (b) using one edge filter, (c) Desired spectral response of two edge filter arms and (d) The output ratio between two arms (e) SMS fibre edge filter	158
Figure 52 Calculated and measured two SMS fibre edge filters X-type spectral response.....	159
Figure 53 Measured ratio response for the use of two edge filters and one edge filter	160
Figure 54 Calculated ratio with tuning increment from 2 to 10 pm (a) two edge filters, (b) one edge filter.....	163
Figure 55 Measured ratio with tuning increment from 10 to 30 pm (a) two edge filters, (b) one edge filter.....	164
Figure 56 Measured variation in ratio (a) and wavelength (b) due to the PDL of the system for the use of two edge filters and one edge filter.....	166
Figure 57 (a) Schematic configuration of ratiometric structure with two edge filter arms with MMI structures (b) Desired spectral response of two edge filter arms and (c) The output ratio between two arms.....	171
Figure 58 (a) Spectral response of optimised edge filters with opposite slopes (b) Spectral response of the ratiometric	174
Figure 59 Output ratio as the wavelength is tuned.....	175
Figure 60 Schematic configuration of the proposed MMI ratiometric wavelength monitor (b) Desired spectral response of two edge filter arms and (c) The output ratio between two arms	181
Figure 61 Figure of merit of the appropriate structures with a set of parameter $[L_m, x_1, x_2]$	186

Figure 62 Spectral responses of the output ports of the optimal structure	187
Figure 63 The output ratio calculated using BPM	187
Figure 64 Output ratio as the wavelength is tuned.....	188

Chapter 1

Introduction

This chapter introduces the background, motivation and objectives of the research, along with the research methodology employed, and layout of the thesis.

1.1 Background to the research

The range of applications for optoelectronics and fibre optic communications has grown significantly in the last few decades. Today, one can find a broad range of consumer and industrial optoelectronic products on the market such as DVD players, CCD cameras, laser printers, laser pointers, LED lights, scanners, etc [1]. The internet and a variety of telecommunication technologies are growing rapidly supported by the very large data transmission capacities of optical fibre, in some cases enhanced by dense wavelength division multiplexing (DWDM) optical fibre communication systems.

Current optoelectronic and fibre optic technologies have reached levels of technical maturity, quality, and cost effectiveness that are far beyond those available a few decades ago [1]. Correspondingly, fibre optics sensor systems based on optoelectronic and fibre optic technologies have also grown in technical sophistication and in the range of applications possible in a variety of industries. Fibre optic sensors are replacing traditional sensors for strain, temperature,

humidity, position, vibration, acoustics, electric and magnetic field measurement, and bio-chemical measurement [2]-[6]. Fibre optic sensors have the advantages of light weight, very small size, low power consumption, isolation from EM interference, and ease of remote operation [2]-[6]. Many sensor types also demonstrate additional advantages, such as high sensitivity and the ability to multiplex a number of sensors on one fibre.

A number of approaches have been adopted in fibre optic sensors for the measurement of a change in an external measurand, for example evanescent field effects, taper effects, Bragg resonance, and multimode interference (MMI) [7]-[10]. Bragg resonance effects in fibre-Bragg grating (FBG)-based sensors have been widely used for strain and temperature measurement [9], [11], [12]. FBG-based sensors have a number of advantages: 1) they are simple, intrinsic sensing elements, 2) they can be directly written into the fibre without changing the fibre diameter, making them compatible with a wide range of situations where small diameter probes are essential, and 3) the signal obtained from an FBG sensor is encoded directly in the wavelength domain and this facilitates wavelength division multiplexing (WDM) of multiple sensors [12]. Implementation of an FBG-based optical sensing system requires an interrogator, in effect a wavelength measurement system, for determining the wavelength shift in the reflected light from an FBG element induced by strain or temperature changes.

Recently, MMI effects occurring in singlemode-multimode-singlemode (SMS) fibre structures were investigated and utilized for both sensing and signal processing applications [10], [13]-[15]. These optical devices offer an all-fibre solution with the advantages of ease of fabrication, packaging, and

interconnection to other optical fibres and in addition the possibility of interrogation by a simple system based on intensity measurements.

In this thesis, SMS fibre structures are investigated for interrogation of FBG sensors and as standalone novel sensors for a variety of measurands. A simple all-fibre ratiometric wavelength measurement utilizing an SMS fibre structure-based edge filter is proposed and demonstrated for interrogation of FBG sensors. The SMS fibre structures are also proposed and demonstrated as novel standalone sensors for strain, temperature, and voltage using a simple interrogation system based on intensity measurement.

1.1.1 Multimode interference (MMI) effects

MMI is a useful basis for the implementation of a number of optical waveguide devices. MMI was investigated and proposed at first for planar waveguides. MMI-based devices implemented in planar waveguides have been developed for optical signal processing applications [16], [17], and for optical sensing applications [18], [19].

A useful basis for visualizing and gaining a better understanding of MMI in a multimode waveguide is the phenomenon of self-imaging. Self-imaging can be defined as a property of multimode waveguides by which an input field profile is reproduced due to constructive interference to form single or multiple images of the singlemode input field at periodic intervals along the propagation direction of the guide. The self-imaging phenomenon in a waveguide due to MMI was studied and described in [20]. Self-imaging in a planar waveguide can be analyzed using a modal propagation analysis (MPA) [20], a hybrid method [21], and a beam propagation method (BPM) [22]. An MPA is a comprehensive theoretical tool to

describe self-imaging phenomena in multimode waveguides [20]. It also provides an insight into the mechanism of multimode interference as well as the basis for numerical modelling and design.

To illustrate self-imaging due to MMI in a multimode waveguide, a structure consisting of a multimode waveguide placed between input and output singlemode waveguides is presented in Fig. 1. The waveguide parameters are also presented in Fig. 1, the width of the multimode waveguide is W_M and the width of the singlemode waveguide of W_s . The length of the multimode waveguide is L . Using an MPA as in [20], an input field profile existing at $Z = 0$ will be decomposed into the modal distribution of all possible modes in the multimode waveguide. The field profile at a distance $Z = L$ can be expressed as a superposition of the modal distribution of all possible modes. Under certain circumstances, the field at $Z = L$ will be a reproduction or self-image of the input field at $Z = 0$. Fig. 2 shows the simulated field profile within the multimode section and it is clear that self-imaging of the input field takes place so that at periodic intervals, a single image of the input field is reproduced. This occurs in Fig. 2 at 2708, 5415, and 8122 μm . Multi-fold images of the input field can also be found, for example, two-fold images can be found at 1354, 4062, 6770, and 9478 μm . Self-imaging occurs at specific lengths only for certain wavelengths. The spectral response of an MMI-based device is therefore not flat and in fact has a bandpass type response, where the bandpass peak wavelength corresponds to the wavelength value where the self-imaging distance is exactly equal to the multimode section length [20].

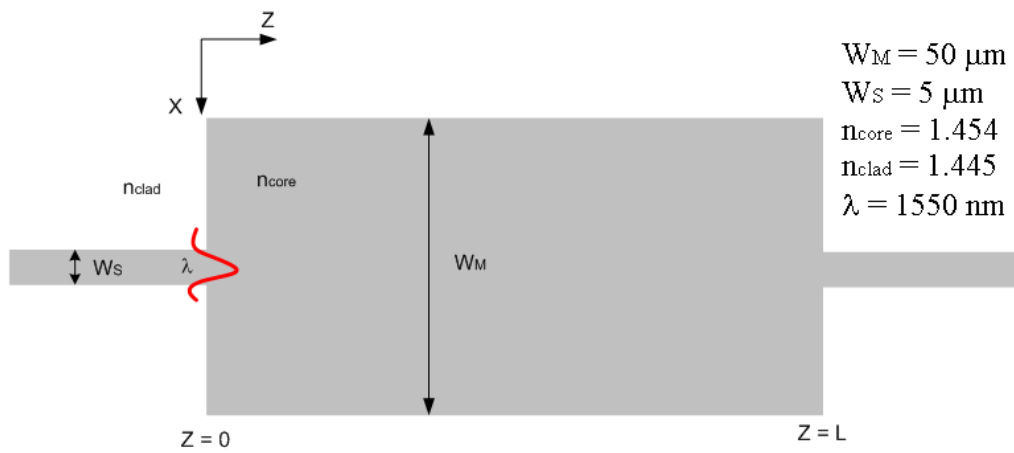


Figure 1 Schematic of a multimode waveguide placed between input and output singlemode waveguides

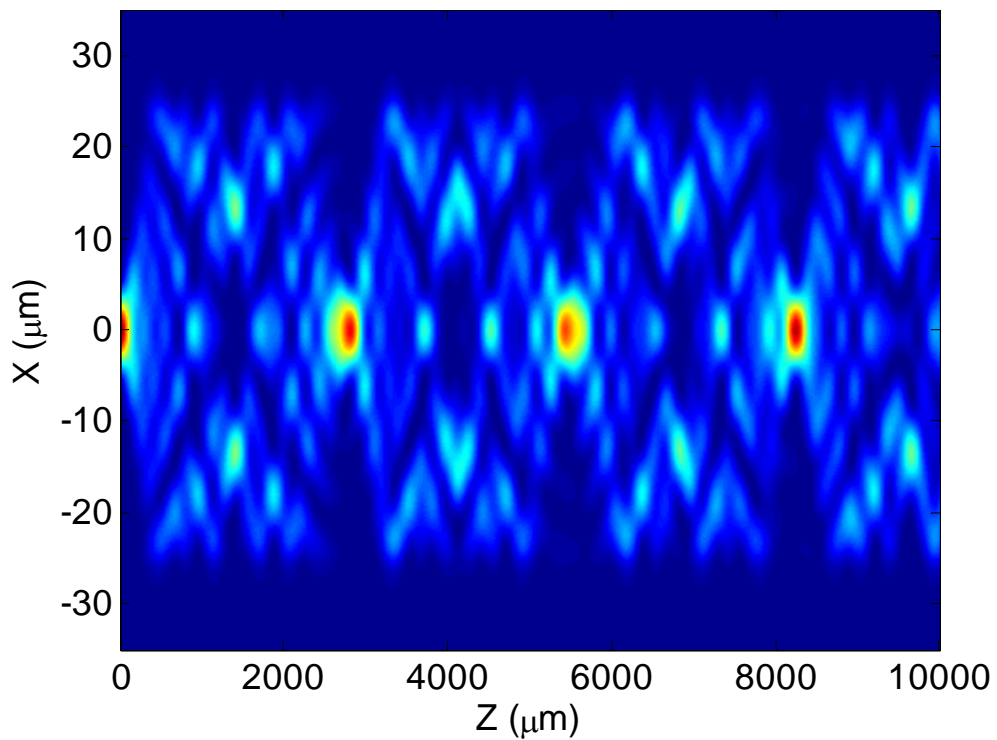


Figure 2 Field profile within the multimode waveguide showing self-imaging of the input field

1.1.2 MMI in optical fibre

In an optical fibre, MMI can be implemented using a fibre hetero-structure consisting of a singlemode-multimode-singlemode (SMS) fibre structure with a step index profile [14], [23]. An SMS fibre structure can be fabricated by splicing a precisely dimensioned multimode fibre (MMF) section between two singlemode fibres (SMFs). Fig. 3 shows a schematic diagram of an SMS fibre structure. SMS fibre structures can utilize either a step index or a graded index profile MMF. SMS structures using a graded index profile MMF section have been demonstrated by several authors where the effects of modal interference were investigated and microbend, strain, and temperature sensors were demonstrated [15], [24]-[26]. In this thesis, SMS fibre structures utilizing a step index MMF section are considered and investigated. The primary reason for this choice is that the spectral response resulting from a step index MMF section is more suitable for the development of edge filters [15], a key issue in this thesis.

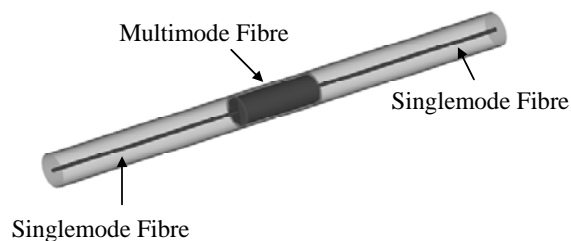


Figure 3 SMS fibre structure

As in a planar waveguide, the MMF section can support many guided modes and the input field to the MMF section is reproduced as single or multiple

images at periodic intervals along the propagation direction due to the interference between these guided modes. MMI in fibre optics can be analyzed using the MPA in cylindrical coordinates as in [23].

1.1.3 MPA of SMS structures

As a starting point for an MPA using cylindrical coordinates for an SMS fibre structure, the input light to the MMF section is assumed to have a field distribution $\psi(r,0)$ which is equal to the fundamental mode of the SMF. The input field can be decomposed into the eigenmodes of LP_{nm} of the MMF when the light enters the MMF section. The eigenmodes and eigenvalues of the MMF can be obtained by solving the eigenmodes and eigenvalues equations as in [24]. Because of the circular symmetry of the input field and assuming perfect alignment of the central axes of the fibres cores of the SMF and MMF, only LP_{0m} can be excited. The reduction in the number of modes is an advantage as it reduces the computational complexity and computational time.

The field profile of LP_{0m} is defined as $F_\nu(r)$ and the eigenmodes of the MMF are normalized as $\int_0^\infty |\psi(r,0)|^2 r dr = \int_0^\infty |F_\nu(r)|^2 r dr$, $\nu = 0, 1, 2, \dots, m-1$, where m is the number of modes in the MMF. The number excited modes of LP_{0m} can be calculated using $m \approx \frac{V}{\pi}$, where $V = \frac{2\pi}{\lambda} a \sqrt{n_{core}^2 - n_{clad}^2}$ is the normalized frequency, λ is a wavelength in free space, a is core diameter, n_{core} and n_{clad} is core and cladding refractive index, of the MMF respectively. The input field at the MMF can be written as:

$$\psi(r,0) = \sum_{\nu=0}^{m-1} c_\nu F_\nu(r) \quad (1.1)$$

where c_ν is the excitation coefficient of each mode. The coefficient c_ν can be calculated by an overlap integral between $\psi(r,0)$ and $F_\nu(r)$ thus:

$$c_\nu = \frac{\int_0^\infty \psi(r,0)F_\nu(r)rdr}{\int_0^\infty F_\nu(r,0)F_\nu(r)rdr}. \quad (1.2)$$

As the light propagates in the MMF section, the field at a propagation distance z can be calculated by

$$\psi(r,z) = \sum_{\nu=0}^{m-1} c_\nu F_\nu(r) \exp(j\beta_\nu z) \quad (1.3)$$

where β_ν is the propagation constant of each eigenmode of the MMF. The propagation constant can be calculated from the eigenvalues of the MMF [27].

The transmission loss in dB can be calculated by using overlap integral method between $\psi(r,z)$ and the eigenmode of the output SMF $E_0(r)$ as in [10]

$$L_s(z) = 10 \cdot \log_{10} \left(\frac{\left| \int_0^\infty \psi(r,z)E_0(r)rdr \right|^2}{\int_0^\infty |\psi(r,z)|^2 rdr \int_0^\infty |E_0(r)|^2 rdr} \right). \quad (1.4)$$

Self-imaging occurs at the so called self-imaging distance (L_z).

$L_z = 10L_\pi = 10 \frac{\pi}{(\beta_0 - \beta_1)}$, where L_π is a beat length between the first two eigenmodes

and β_0 and β_1 are the first two of propagation constants of the MMF [23]. As an

example, assume the SMF type is SMF28 with core diameter of 8.3 μm and MMF

type is AFS105/125Y with core diameter of 105 μm . Fig. 4(a) and 4(b) show the

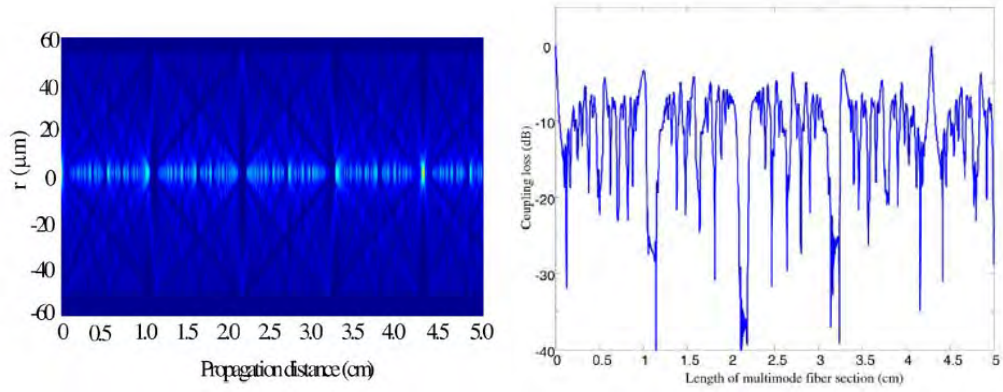
light propagation in the MMF section and corresponding transmission

loss/coupling loss to the output SMF as functions of MMF length, respectively.

The self-imaging distance is 4.28 cm for a wavelength of 1550 nm as in Fig. 4(a)

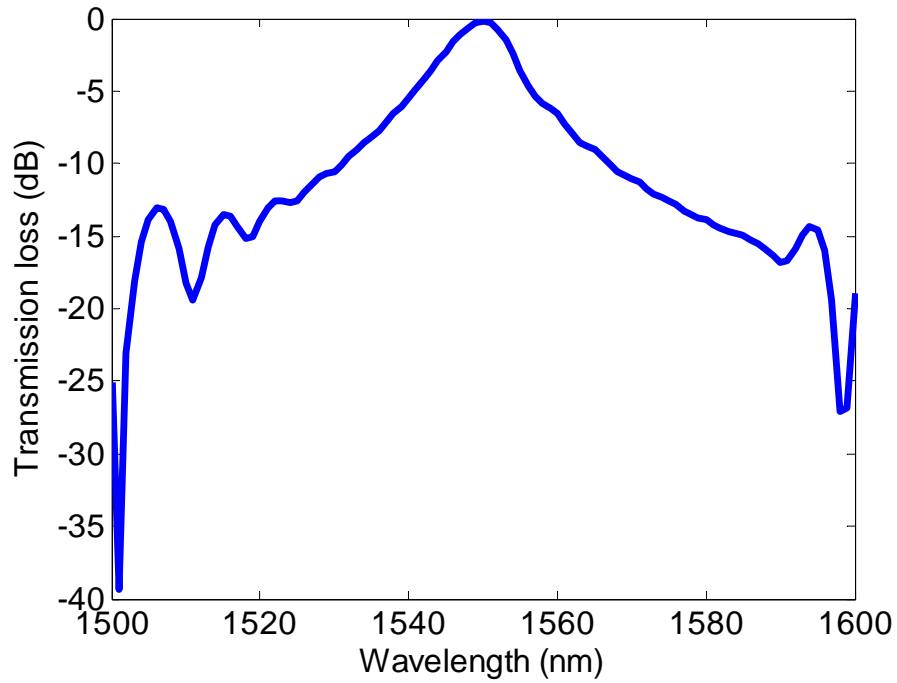
[23]. At the self-imaging distance, the input field (at a propagation distance of 0 cm) is reproduced and thus, the transmission loss/coupling loss value is close to zero. For a fixed MMF length, an SMS fibre structure provides a wavelength dependent spectral response. In Fig. 4(c), the spectral response of the SMS fibre structure is shown for a wavelength range of 1500 to 1600 nm. It is clear that the SMS fibre structure provides a bandpass spectral response and could be used as a bandpass filter [14], [23].

As previously mentioned, an SMS fibre structure can be fabricated by using a fusion splicer. A commercial fibre fusion splicer is normally used to splice SMF to SMF or MMF to MMF with very low loss and also low lateral core offsets [28]. However, fusion splicers are not pre-programmed to deal with splicing SMF to MMF so that during the splicing process for SMF to MMF or vice-versa, significant lateral core offset errors may arise. When lateral core offsets exist, the MPA based on LP_{0m} cannot be used as it is not possible to assume a perfect alignment between the axes of the fibres. Thus, to investigate the effect of misalignment of SMS fibre cores using an MPA, it is necessary to calculate all possible modes in the MMF section and not only the LP_{0m} modes.



(a)

(b)



(c)

Figure 4 (a) light propagation in the MMF section (b) calculated transmission loss to the output SMF versus the length of MMF section [23] (c) calculated spectral response

1.1.4 SMS structures for interrogation of FBG sensors

An FBG sensor requires a wavelength measurement system to extract temperature or strain information. Fig. 5 shows a typical configuration of an FBG-based sensor system. Light from the broadband source is launched via a circulator into the fibre containing the FBG. Only one wavelength is reflected back from the FBG and the shift in the reflected wavelength caused by the changes in temperature or strain is monitored by a wavelength discriminator. A wavelength discriminator provides a known stable relationship between attenuation and wavelength. Assuming this relationship is known, then with a suitable calibration, the wavelength can be measured by means of an intensity measurement.

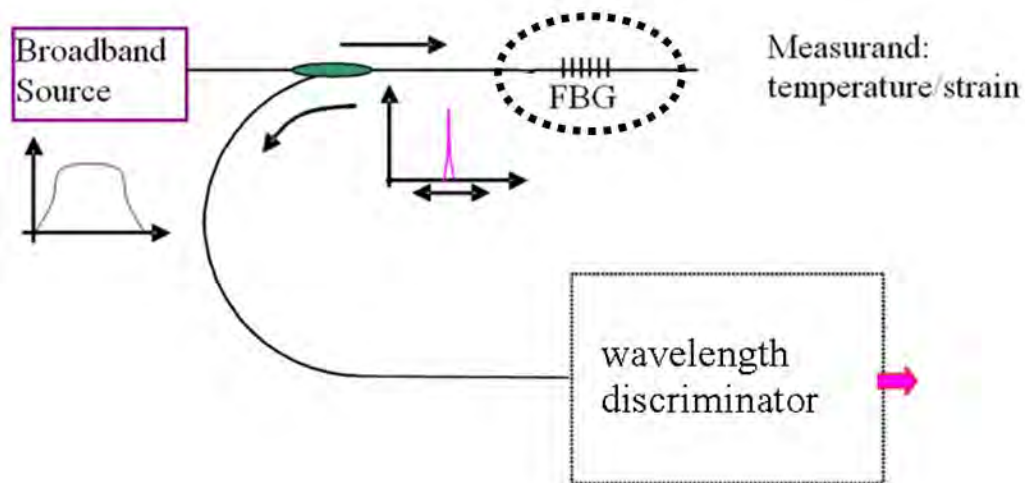


Figure 5 FBG sensing system

The general requirements for an ideal discriminator in a wavelength measurement system are as follows: 1) high resolution (better than 10 pm) and high accuracy, 2) high measurement speed to allow measurement of dynamic

strain, and 3) cost effectiveness. In addition a wide wavelength range (> 10 nm) is needed where wavelength division multiplexed FBGs are used.

One approach to wavelength discrimination that satisfies the above requirements is a ratiometric power measurement technique [29]. When compared to a wavelength-scanning-based active measurement scheme, it has the advantages of a simple configuration, the potential for high-speed measurement, the absence of mechanical movement, and a low cost [29]. A ratiometric wavelength monitor conventionally consists of a splitter with two outputs to which an edge filter arm with a well-defined spectral response and a reference arm are attached [29]. Two photodetectors are placed at the end of both arms. The wavelength of an unknown input signal can be determined by measuring the ratio of the electrical outputs of the two photodetectors, assuming a suitable calibration has been carried out.

Fig. 6(a) shows schematic structure of a typical ratiometric wavelength measurement system. A modified ratiometric wavelength measurement system containing two edge filter arms with opposite slope spectral responses is also shown in Fig. 6(b). The use of two edge filters can increase sensitivity and resolution of wavelength measurements [30]. Fig. 6(c) shows the target spectral responses of the edge filters and the reference arm in a wavelength range from λ_L to λ_H . The corresponding ratios of the two outputs over the wavelength range are presented in Fig. 6(d) for the systems with one and two edge filters.

An edge filter can be implemented either by a bulk thin filter [30], tilted chirped grating structure [31], biconical fibre coupler [32], a wavelength division multiplexer [33], or a bending fibre [34]. All-fibre edge filters have several

advantages in comparison to bulk filters, for example, ease of interconnection, mechanical stability, and low polarization sensitivity [29]. In this thesis, an SMS fibre structure is investigated as a new type of an edge filter. Previous studies showed that an SMS fibre structure can be operated as a bandpass filter [14], [23]. On either side of the centre wavelength in the bandpass response shown in Fig. 4(c), there are monotonically increasing or decreasing spectral responses over a limited wavelength range which can be utilized as the basis of either a positive or negative slope edge filter. Two SMS fibre structures with opposite slope spectral responses are investigated in this thesis for their use in a ratiometric wavelength measurement scheme.

Several factors, such as noise, polarization dependent loss (PDL), and temperature dependent loss (TDL) can influence the resolution and accuracy of wavelength measurement in an all-fibre ratiometric system [35]-[38]. It is shown in [34], that an acceptable slope for the edge filter is determined by the signal-to-noise ratio (SNR) of the input signal. The noise of the photodetectors also affects the resolution of the ratiometric wavelength measurement system [36]. In [36], it is demonstrated theoretically and experimentally that the SNR of the signal source, the noise of the photodetectors, and the other noise sources, such as receiver shot and thermal noise in the ratiometric system, have a significant impact on the resolution of the wavelength measurement.

Polarization dependence in an all-fibre ratiometric wavelength measurement system can also degrade measurement accuracy [37]. It is well known that in standard optical fibres, the state of polarization varies. For a macrobending fibre-based edge filter, it has been shown that the fibre structure

needs to be optimized to minimize the effects of input polarization [39]. For an SMS fibre structure used as an edge filter, the polarization dependence has not been previously investigated. In this thesis, the polarization dependence of an SMS fibre structure is investigated theoretically and experimentally.

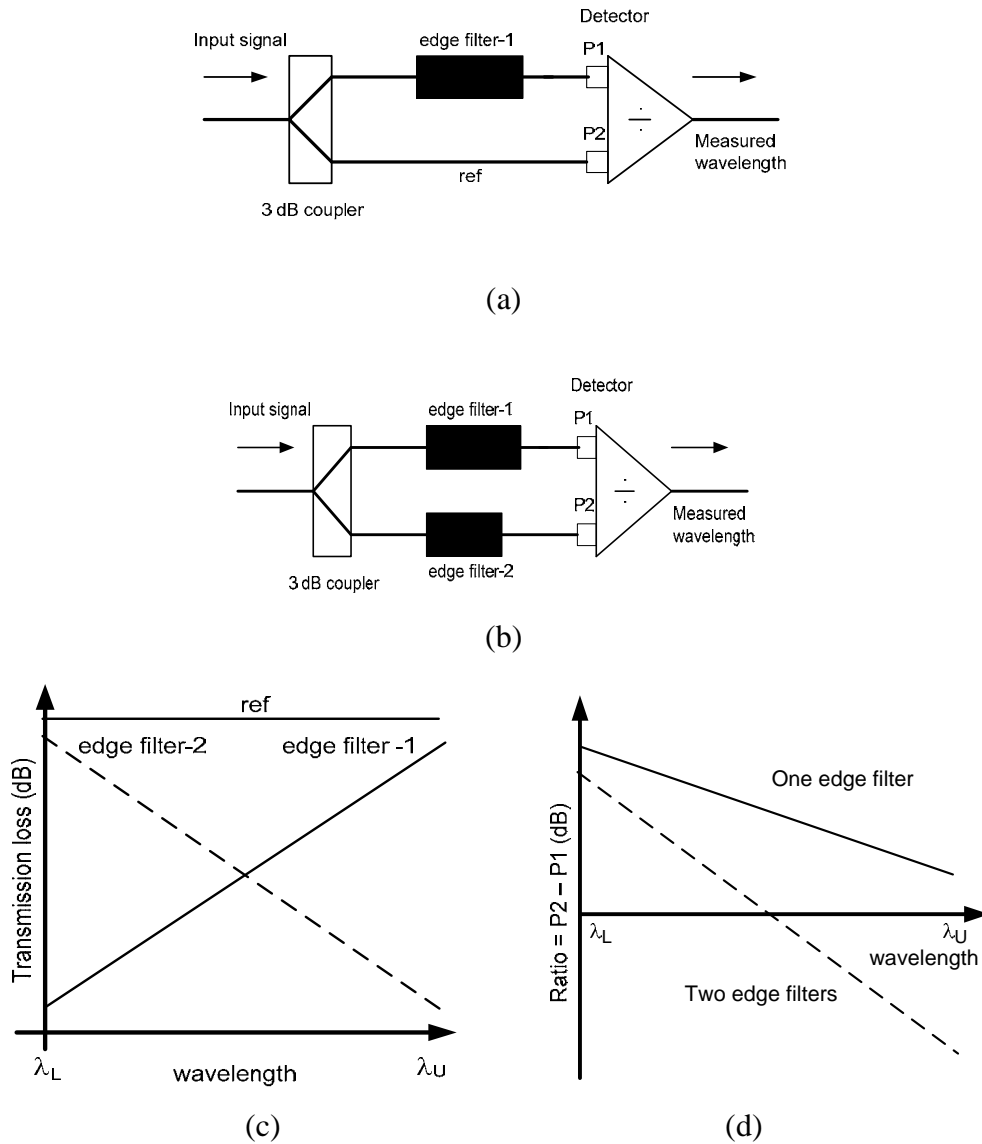


Figure 6 Schematic configuration of ratiometric wavelength monitor (a) using one edge filter (b) using two edge filters, (c) the desired spectral response of the edge filter-1 and edge filter-2 arms, and (d) the output ratio of two arms using one edge filter and two edge filters

The effect of temperature on the optical and mechanical properties of silica means that temperature changes could affect the performance of fibre-based edge filters. Thus, it can have a significant influence on the accuracy of wavelength measurement. An investigation has been carried out previously [40] on the peak wavelength shift of the transmission spectral response of an SMS fibre structure due to temperature change and the reduction of this peak shift to a low value by a temperature compensation scheme. However, in an edge filter-based ratiometric wavelength measurement scheme, even low values of peak wavelength shift can still induce sufficient ratio variation to degrade wavelength measurement accuracy [38]. Therefore, an investigation of the temperature dependence of an SMS-based edge filter needs to be carried out to implement a suitable temperature compensation scheme.

1.1.5 Sensing applications of SMS fibre structures

As an alternative to FBG sensors, SMS fibre structures can be used as temperature and strain sensors with the advantages of low cost and simple fabrication by comparison to FBGs. SMS fibre structure sensors can be interrogated in a number of ways, either by tracking the wavelength of a peak or dip in the spectral response using an optical spectrum analyzer (OSA) or by tracking the position of an edge in the SMS spectral response using a ratiometric intensity measurement system. The characteristics of the wavelength shift of the SMS spectral response due to strain and temperature applied to a step index SMS fibre structure have been investigated previously in [38]. In [15], an SMS fibre structure employing a graded index MMF was studied in regard to the sensing applications of wavelength shift due to strain and temperature. In [41], an SMS fibre structure

combined with an FBG is utilized to enhance the sensitivity of strain measurement. An FBG combined with an SMS fibre structure has also been reported for simultaneous strain and temperature measurement [42]. However, all of these demonstrated temperature or strain measurement techniques required the use of an OSA which is costly and low speed.

In this thesis, SMS fibre structure-based sensors in an intensity measurement scheme using ratiometric power measurement are investigated, offering low cost, simple configuration, and the potential for high speed measurement compared to sensors which employ an OSA.

1.2 Motivation and the objectives of the research

The core aim of this research is to investigate all-fibre multimode interference (MMI) devices based on a step index singlemode-multimode-singlemode (SMS) fibre structure for use as (A) a new type of edge filter for a ratiometric wavelength measurement system and as (B) novel stand alone sensors.

The research investigates edge filter based on SMS fibre structures and introduces this novel fibre filter type into a ratiometric wavelength measurement system for the first time. The use of two edge filters with opposite slope spectral responses, so-called X-type edge filters, based on SMS fibre structures is proposed and demonstrated for a ratiometric wavelength measurement system to improve the performance of the measurement system compared to a conventional single filter ratiometric wavelength measurement system. The proposed wavelength measurement system provides high resolution, high accuracy, high speed measurement and low cost.

Several aspects of SMS fibre structure-based edge filters are investigated including the effect of misalignment of the SMS fibre cores along with polarization and temperature dependence effects. Specifically, the fabrication process for an SMS fibre structure-based edge filter can introduce SMS core offsets. A limit of tolerable misalignment of SMS fibre cores is investigated and proposed to maintain the spectral performance of the edge filter based on an SMS fibre structure. The polarization dependence of the SMS fibre structure has not been previously investigated. It is known that the polarization dependence on the edge filter can affect the performance of wavelength measurement. Therefore, in this thesis the polarization dependence of an SMS fibre structure-based edge filter is investigated numerically and experimentally, specifically polarization dependence due to the SMS fibre core offsets. It is well known that devices based on optical fibre are sensitive to temperature variations. Calibration of a ratiometric wavelength measurement system takes place at a fixed temperature, any temperature induced variations in the spectral response of an edge filter can impair the performance of wavelength measurement. This temperature dependence is investigated and a suitable scheme to compensate for temperature dependence in a ratiometric wavelength measurement system is proposed.

The research also investigates novel SMS-based fibre sensors for temperature and strain measurements in an intensity-based measurement system. Three novel applications of SMS fibre structures are proposed and demonstrated as a temperature sensor, a voltage sensor utilizing the strain effect, and a strain sensor with self-temperature monitoring. The proposed sensors provide high

resolution with the advantages of low fabrication cost for an SMS fibre structure and the use of a simple intensity-based interrogation system.

The objectives of the research are as follows:

A. Edge filter based on SMS fibre structure

- Investigate MMI in SMS fibre structures for the use as X type edge filters.
- Investigate the effect of SMS fibre core offsets arising during the fabrication process on the parameters of SMS-based edge filters.
- Investigate polarization dependence for an SMS-based edge filter.
- Investigate temperature dependence for an SMS fibre structure-based edge filter and its temperature compensation.

B. Novel standalone sensors based on SMS fibre structure

- Investigate the use of an SMS fibre structure for a temperature sensor.
- Investigate an SMS fibre structure for voltage measurement based on strain effect.
- Investigate for the use of an SMS fibre structure as a strain sensor and its temperature compensation.

1.3 Research methodology

For the various research strands pursued in this thesis, the typical research methodology employed consists of a sequence of steps as follows:

1. Carry out a theoretical study.

Theoretical studies and analysis of multimode interference in SMS fibre structures were carried out to understand light propagation behaviour and to underpin the development of numerical simulations.

2. Develop a numerical model for simulations.

Based on the theoretical studies of the light propagation in SMS fibre structures in Step 1, appropriate models were developed to simulate the SMS fibre structure under a variety of conditions. The computer programmes were developed based on custom source code in Matlab performed on a personal computer with Intel® Core™ 2 Duo CPU E7200 @ 2.53 GHz, 2 GB RAM and 500 GB hard disk storage.

3. Fabricate the SMS fibre structure.

In this research, all the SMS fibre structures were fabricated using common technique based on a Fujikura CT-07 cleaver and a Sumitomo type-36 fusion splicer. First, the input SMF and the input end of the MMF were cleaved and spliced together. The cleaver was then used again to cleave the other end of the MMF fibre to the required length. The length of the MMF fibre needs to be accurately controlled during cleaving to provide the desired design device. The length of the cleaved MMF section was checked using a precision calliper. Finally, the output end of MMF section was spliced to the cleaved end of the output SMF.

4. Develop an experimental set-up and verify simulation results.

A block diagram of the experimental set-up used in this research is presented in Fig. 7. The SMS fibre structure within the ratiometric system

as in Fig. 6(a) or 6(b) was connected to a tunable laser and a ratiometric power measurement system or an optical spectrum analyzer (OSA), depending on the experiment to be performed. A personal computer with a LabView program was used to control the tunable laser TUNIC PLUS and either the ratiometric power measurement system or an Agilent 86140B OSA, as appropriate. To conduct polarization or temperature studies, a Thorlabs FPC560 manual polarization controller or a thermoelectric Peltier cooler with temperature controller (ITC 510, Thorlabs) was used within the experimental set-up, respectively. Where the SMS structure is utilised as a sensor, strain could be applied by using Max303 NanoMax Thorlabs micro-positioning stage attached to the SMS fibre structure to study the effect of strain. A piezoelectric transducer (PZT) of PZT stack AE0505D18 (from Thorlabs) was used for voltage measurements using the SMS fibre structure.

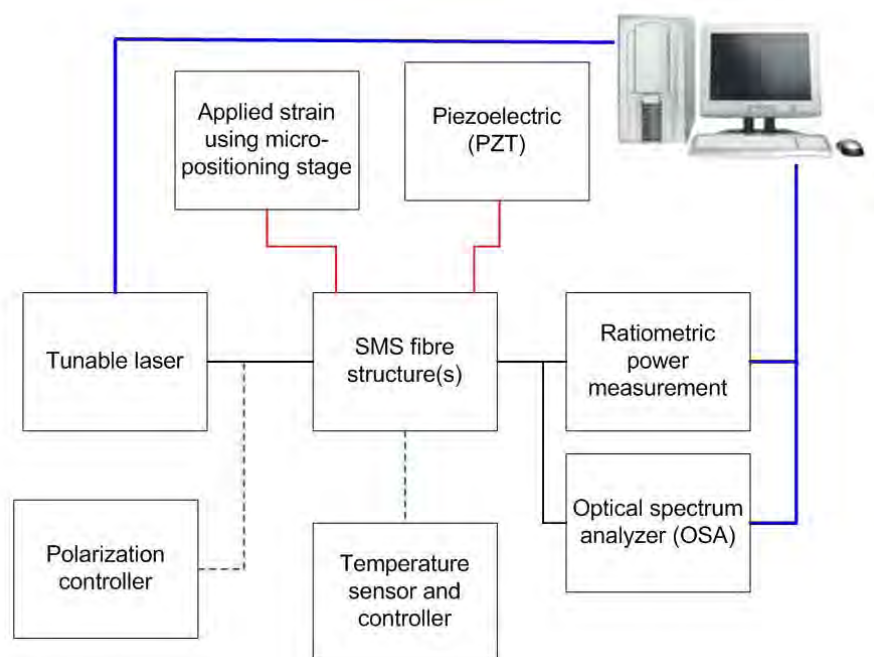


Figure 7 Block diagram of the experimental set-up

1.4 Layout of the thesis

This thesis is based on a series of linked journal publications prepared during the period of the PhD research. The publications are all first author publications by the author of this thesis. There are several authors for each publication. A signed statement from all the co-authors is included in Appendix A, confirming that the first author undertook all aspects of the research described in each paper, including preparation and submission of the paper, with the support and advice of the co-authors.

Chapter 1 is an introduction chapter which introduces the background, motivation and objectives of the research, research methodology and an outline of the thesis.

Chapter 2 presents a new type of the edge filter based on an SMS fibre structure. Firstly, the numerical design for edge filter is presented. Two SMS fibre structures were optimized to provide an X-type spectral response as an alternative to a conventional single filter ratiometric wavelength measurement. The experimental results are presented and ratiometric wavelength measurement is demonstrated.

Chapter 3 analyzes the effect of misalignment of the SMS fibre cores on the edge filter spectral response. A numerical model was developed to investigate the effect of misalignment of SMS fibre cores. A limit of tolerable misalignment of SMS fibre cores beyond which the spectral performance of the edge filter-based SMS fibre structure degrades unacceptably is proposed. An experimental verification is also presented.

Chapter 4 presents the studies of polarization dependent loss (PDL) of the SMS-based edge filter. The PDL due to lateral and rotational SMS fibre cores offsets is investigated numerically and experimentally. It is shown that small core offsets are necessary to achieve low PDL for an SMS fibre structure-based edge filter. It is also proposed and demonstrated that when lateral core offsets are unavoidable, the PDL of an SMS fibre structure-based edge filter can still be minimized by introducing a rotational core offset of 90^0 .

Chapter 5 analyzes temperature dependence of an edge filter based on SMS fibre structure numerically and experimentally. In a ratiometric wavelength measurement scheme using two SMS edge filters, a small temperature variation can induce a ratio variation and in turn a wavelength measurement error. It is proposed and demonstrated that self monitoring of temperature can be carried out using an expanded ratiometric scheme, regardless of the ambient temperature variation.

Chapter 6 is dedicated to new applications of an SMS fibre structure as standalone sensors of temperature and voltage. The temperature dependence of the SMS fibre structure is investigated for the use as a temperature sensor. Temperature measurement using an SMS fibre structure in a simple intensity-based interrogation system is demonstrated. A voltage sensor based on an SMS fibre structure attached to a piezoelectric transducer utilized in a ratiometric power measurement scheme is also proposed and demonstrated numerically and experimentally.

Chapter 7 presents a strain sensor with very low temperature induced strain measurement error using a pair of SMS fibre structures. For intensity-based

strain measurement using a single SMS fibre structure, it is found that there is a high strain dependence, but also a temperature dependence that will induce strain measurement error. It is proposed and demonstrated that the use of two SMS fibre structures can minimize the temperature induced strain measurement error, where one SMS structure acts as the strain sensor and the other SMS structure acts as the temperature monitor.

Finally the conclusions arising from the research and future research plans are presented in Chapter 8.

Several Appendices detail other publications at international conferences related to the research. In Appendix B, a comparison of performance for the use of one edge filter and X-type edge filters based on SMS fibre structure(s) is presented. Appendix C presents an integrated optic version of X-type edge filters based on MMI. A Y-branch and two MMIs based on a planar lightwave circuit (PLC) of silica on silicon buried channel waveguides were designed and optimized to provide the X-type spectral response. A simple configuration for an integrated ratiometric wavelength monitor with the X-type spectral response based on a single MMI structure is also proposed and presented in Appendix D.

1.5 References

- [1] S. Sudho and K. Okamoto, *New Photonics Technologies for The Information Age: The Dream of Ubiquitous Services*, Artech House optoelectronics library, 2006.
- [2] T. S. Yu. Francis and Y. Shizhuo, *Fibre Optic Sensors*, Marcel and Dekker, New York, 2002.
- [3] E. Udd, *Fibre Optic Sensors*, Wiley Interscience, New York, 2002.

- [4] K. T. V. Grattan and T. Sun, "Fibre optic sensor technology: an overview," *Sensors and Actuators*, vol. 82, pp. 40–61, 2000.
- [5] B. Lee, "Review of present status of optical fibre sensors", *Optical Fibre Technology*, vol. 9, pp. 57–79, 2003.
- [6] O. S. Wolfbeis, "Fibre-Optic Chemical Sensors and Biosensors," *Anal. Chem.*, vol. 76, pp. 3269-3284, 2004.
- [7] A. Messica, A. Greenstein, and A. Katzir, "Theory of fibre-optic, evanescent-wave spectroscopy and sensors," *App. Opt.*, vol. 35, pp. 2274-2284, 1996.
- [8] Y. C. Kim, W. Peng, S. Banerji, and K. S. Booksh, "Tapered fibre optic surface plasmon resonance sensor for analyses of vapour and liquid phases," *Opt. Lett.*, vol. 30, pp. 2218-2220, 2005.
- [9] A. D. Kersey, M. A. Davis, H. J. Patrick, M. Leblanc, K. P. Koo, C. G. Askin, M. A. Putnam, and E. J. Friebele, "Fibre grating sensors," *J. Lightw. Technol.*, vol. 15, pp. 1442–1463, 1997.
- [10] Q. Wang and G. Farrell, "All-fibre multimode-interference-based refractometer sensor: proposal and design," *Opt. Lett.*, vol. 31, pp. 317–319, 2006.
- [11] Y. J. Rao, "In-fibre Bragg grating sensors", *Meas. Sci. Technol.*, vol. 8, pp. 355–375, 1997.
- [12] Y. Zhao and Y. Liao, "Discrimination methods and demodulation techniques for fibre Bragg grating sensors," *Optics and Lasers in Eng.*, vol. 41, pp. 1-18, 2004.
- [13] E. Li and G. D. Peng, "Wavelength-encoded fibre-optic temperature sensor with ultra-high sensitivity," *Opt. Commun.*, vol. 281, pp. 5768-5770, 2008.
- [14] W. S. Mohammed, P. W. E. Smith, and X. Gu, "All-fibre multimode interference bandpass filter," *Opt. Lett.*, vol. 31, pp. 2547-2549, 2006.
- [15] S. M. Tripathi, A. Kumar, R. K. Varshney, Y. B. P. Kumar, E. Marin, and J. P. Meunier, "Strain and temperature sensing characteristics of single-mode–multimode–single-mode structures," *J. Lightw. Technol.*, vol. 27, pp. 2348-2356, 2009.

- [16] S. Nagai, G. Morishima, H. Inayoshi, and K. Utaka, "Multimode Interference Photonic Switches (MIPS)," *J. Lightw. Technol.*, vol. 20, pp. 675-681, 2002.
- [17] M. R. Paiam and R. I. MacDonald, "A 12-channel phased-array wavelength multiplexer with multimode interference couplers," *Photon. Technol. Lett.*, vol. 10, pp. 241-243, 1998.
- [18] A. Cleary, S. G. Blanco, A. Glidle, J. S. Aitchison, P. Laybourn, and J. M. Cooper, "An integrated fluorescence array as a platform for lab-on-a-chip technology using multimode interference splitters," *Sensors Journal*, vol. 5, pp. 1315-1320, 2005.
- [19] K. R. Kribich, R. Copperwhite, H. Barry, B. Kolodziejczyk, J.-M. Sabattié, K. O'Dwyer, and B.D. MacCraith, "Novel chemical sensor/biosensor platform based on optical multimode interference (MMI) couplers," *Sensors and Actuators B: Chemical*, vol. 107, pp. 188-192, 2005.
- [20] L.B. Soldano and E.C.M. Pennings, "Optical multi-mode interference devices based on self-imaging: principles and applications", *J. Lightw. Technol.*, vol.13, pp. 615-627, 1995.
- [21] D. C. Chang and E. F. Kuester, "A hybrid method for paraxial beam propagation in multimode optical waveguides," *Trans. Microwave Theory Tech.*, vol. 29, pp. 923-933, 1981.
- [22] J. Yamauchi, *Propagating Beam Analysis of Optical Waveguides*, Research Studies Press, 2003.
- [23] Q. Wang, G. Farrell, and W. Yan, "Investigation on singlemode-multimode-singlemode fibre structure," *J. Lightw. Technol.*, vol. 26, pp. 512-519, 2008.
- [24] D. Donlagic and M. Završnik, "Fibre-optic microbend sensor structure," *Opt. Lett.*, vol. 22, pp. 837-839, 1997.
- [25] A. Kumar, R. K. Varshney, S. Antony C., and P. Sharma, "Transmission characteristics of SMS fibre optic sensor structures," *Opt. Commun.*, vol. 219, pp. 215-219, 2003.
- [26] A. Kumar, R. K. Varshney, and R. Kumar, "SMS fibre optic microbend sensor structures: effect of the modal interference," *Opt. Commun.*, vol. 232, pp. 239-244, 2004.

- [27] J. Bures, *Guided Optics: Optical Fibres and All-fibre Components*, Wiley-CVH, 2009.
- [28] http://www.fiberoptic.com/catalog/AFL_Catalog.pdf
- [29] G. Rajan, A macro-bend fibre-based wavelength demodulation system for optical fibre sensing applications, Thesis, Dublin Institute of Technology, 2008.
- [30] S. M. Melle, K. Liu, and R. M. Measures, "Practical fibre optic Bragg grating strain gauge system", *App. Opt.*, vol. 32, pp. 3601–3609, 1993.
- [31] Y. Liu, L. Zhang, and I. Bennion, "Fabricating fibre edge filters with arbitrary spectral response based on tilted chirped grating structures," *Meas. Sci. Technol.*, vol. 10, pp. L1–L3, 1999.
- [32] A. B. L. Ribeiro, L. A. Ferreira, M. Tsvekov, and J. L. Santos, "All-fibre interrogation technique for fibre Bragg sensors using a biconical fibre filter," *Electron. Lett.*, vol. 32, pp. 382–383, 1996.
- [33] M. A. Davis and A. D. Kersey, "All fibre Bragg grating sensor demodulation technique using a wavelength division coupler," *Electron. Lett.*, vol. 30, pp. 75-77, 1994.
- [34] Q. Wang, G. Farrell, T. Freir, G. Rajan, and P. Wang, "Low-cost wavelength measurement based on a macrobending single-mode fibre," *Opt. Lett.*, vol. 31, pp. 1785-1787, 2006.
- [35] Q. Wang, G. Farrell, and T. Freir, "Study of transmission response of edge filters employed in wavelength measurements," *App. Opt.*, vol. 44, pp. 7789-7792, 2005.
- [36] Q. Wang, G. Rajan, P. Wang, and G. Farrell, "Resolution investigation of a ratiometric wavelength measurement system," *App. Opt.*, vol. 46, pp. 6362-6367, 2007.
- [37] G. Rajan, Q. Wang, Y. Semenova, G. Farrell, and P. Wang, "Effect of polarization dependent loss on the performance accuracy of a ratiometric wavelength measurement system," *IET Optoelectronics*, vol. 2, pp. 63-68, 2008.

- [38] G. Rajan, Y. Semenova, P. Wang, and G. Farrell, "Temperature-induced instabilities in macro-bend fibre-based wavelength measurement systems," *J. Lightw. Technol.*, vol. 27, pp. 1355-1361, 2009.
- [39] G. Rajan, Y. Semenova, G. Farrell, Q. Wang, and P. Wang, "A low polarization sensitivity all-fibre wavelength measurement system," *Photon. Technol. Lett.*, vol. 20, pp. 1464-1466, 2008.
- [40] E. Li, "Temperature compensation of multimode-interference-based fibre devices," *Opt. Lett.*, vol. 32, pp. 2064-2066, 2007.
- [41] E. Li, "Sensitivity-enhanced fibre-optic strain sensor based on interference of higher order modes in circular fibres," *Photon. Technol. Lett.*, vol. 19, pp. 1266-1268, 2007.
- [42] D. P. Zhou, L. Wei, W. K. Liu, Y. Liu, and J. W. Y. Lit, "Simultaneous measurement for strain and temperature using fibre Bragg gratings and multimode fibres," *App. Opt.*, vol. 47, pp. 1668-1672, 2008.

Chapter 2

Multimode interference in an SMS fibre structure for an edge filter application

The core aim of this research is to investigate all-fibre multimode interference (MMI) devices based on a step index singlemode-multimode-singlemode (SMS) fibre structure for use as (1) a new type of edge filter for a ratiometric wavelength measurement system and as (2) novel standalone sensors.

This chapter presents a new type of edge filter based on an SMS fibre structure and introduces this novel fibre filter type into a wavelength ratiometric measurement system. Firstly, the numerical design for edge filter is presented. The use of two edge filters based on SMS fibre structures with opposite slope spectral responses, a so called X-type edge filters, is proposed and demonstrated for a ratiometric wavelength measurement system. Two SMS fibre structures are optimized to provide X-type edge filters spectral response as an alternative to a conventional single filter ratiometric wavelength measurement scheme. The experimental results are presented and ratiometric wavelength measurement is demonstrated. This chapter is also supported by a comparison of performance

between the use of single edge filter and the X-type edge filters in a ratiometric wavelength measurement system presented in Appendix B.

Ratiometric wavelength monitor based on singlemode-multimode-singlemode fibre structure^a

Keywords: multimode interference; fibre optics; wavelength monitor

Abstract: An all-fibre ratiometric wavelength monitor for optical wavelength measurement is proposed and is investigated theoretically and experimentally. Two edge filters with opposite slope spectral responses based on singlemode-multimode-singlemode (SMS) fibre structures are developed. A ratiometric wavelength measurement system employing the developed SMS edge filters demonstrates a high discrimination range of 20.41 dB and a potential wavelength measurement resolution of 10 pm over a wavelength range from 1530 to 1560 nm.

2.1 Introduction

A wavelength monitor is a key component for many optical systems such as multichannel dense wavelength-division multiplexing (DWDM) optical communication systems and fibre Bragg grating-based (FBG) optical sensing systems. A FBG-based optical sensing system requires a wavelength

^a A. M. Hatta, G. Farrell, Q. Wang, G. Rajan, P. Wang, and Y. Semenova, "Ratiometric wavelength monitor based on singlemode-multimode-singlemode fibre structure," *Microwave and Optical Technology Letters*, vol. 50, no. 12, pp. 3036-3039, 2008.

demodulation system which is capable of accurately estimating the wavelength shift in the reflected light from an FBG element induced by strain or temperature changes.

Wavelength measurement or monitoring can be implemented using a ratiometric power measurement technique. A ratiometric wavelength monitor usually consists of a splitter with two outputs to which are attached an edge filter arm with a well defined spectral response and a reference arm. Alternatively, two edge filters arms with opposite slope spectral responses can be used. The use of two opposite slope edge filters can increase resolution^a of the ratiometric system [43]. Such a ratiometric wavelength monitor scheme converts the input wavelength shifts into a signal intensity measurement. When compared with a wavelength-scanning-based active measurement scheme, it has the advantages of having a simple configuration, the potential for high-speed measurement, and the absence of mechanical movement. The main element of the ratiometric scheme, the edge filter, can be implemented by either a bulk thin filter [43], a fibre grating [44], biconical fibre couplers [45], or a bending fibre [46], [47]. An all-fibre edge filter has several advantages by comparison to bulk filters, for example, ease of interconnection, mechanical stability, and low polarization sensitivity [48].

Singlemode-multimode and singlemode-multimode-singlemode (SMS) fibre structures have been investigated for use in several applications e.g. a fibre lens, a displacement sensor, a refractometer, a bandpass filter, and an edge filter [49]-[53]. On the basis of our previous investigation [53], this article proposes and demonstrates a ratiometric wavelength monitor using two edge filters consisting

^a That is the resolution at a fixed wavelength, with the assumption of a linear response for the edge filter.

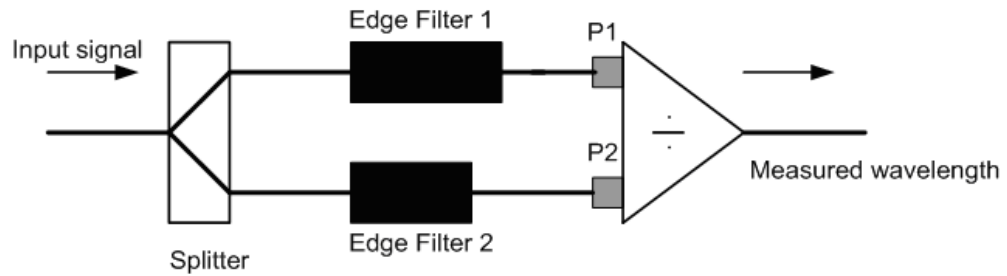
of SMS fibre structures with opposite slope spectral responses. This configuration has the advantage that it can achieve opposite slope spectral responses with a high discrimination range compared to a fibre bend loss edge filter [46], [47] which can only provide a single slope spectral response. In addition, the discrimination range achievable for a fibre bend loss edge filter is limited by the minimum practical bend radius.

2.2 Proposed configuration and its design

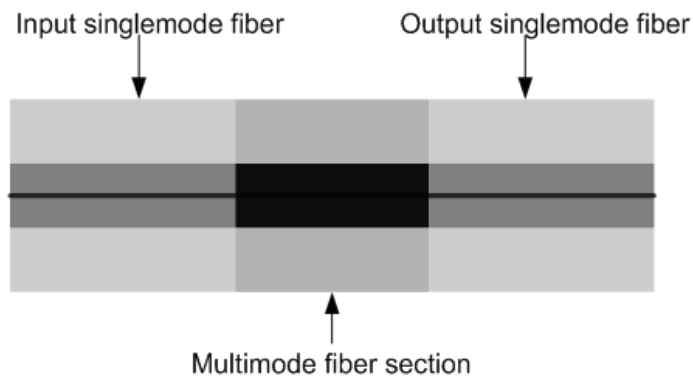
Fig. 8(a) shows the schematic configuration of a ratiometric wavelength monitor. It contains a splitter and two edge filter arms based on a pair of SMS fibre structures. The SMS edge filter structure is shown in Fig. 8(b). It is formed by splicing a step-index multimode fibre (MMF) between two standard singlemode fibres (SMF). The target spectral responses of the two arms are shown in Fig. 8(c) and the corresponding ratio of the two outputs over the wavelength range is presented in Fig. 8(d). The wavelength of an unknown input signal can be determined by measuring the power ratio between the two arms, assuming a suitable calibration has taken place.

The operating principle of the edge filter can be described as follows: the light field propagating along the input SMF enters the MMF section and excites a number of guided modes in the MMF. Interference between the different modes occurs while the light field propagates through the MMF section. By choosing a suitable length for the MMF section, light is coupled into the output SMF in a wavelength dependent manner because of interference. The input-to-output

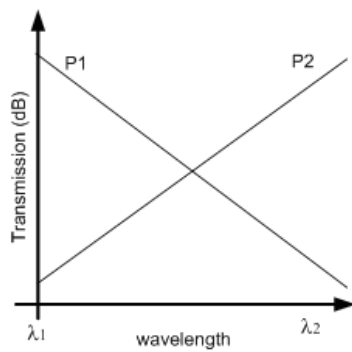
transmission loss is expected to increase/decrease monotonically, as the wavelength of the propagating light increases in a certain wavelength range.



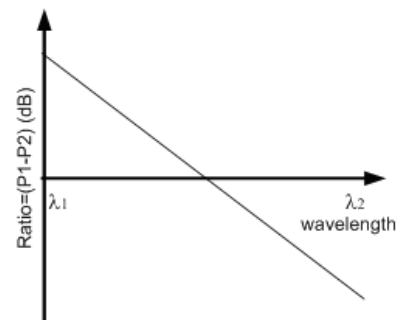
(a)



(b)



(c)



(d)

Figure 8 Schematic structure of (a) a ratiometric wavelength measurement system (b) an SMS fibre-based edge filter (c) the desired spectral response of the two edge filter arms and (d) the output ratio between the two arms

A modal propagation analysis (MPA) using cylindrical coordinates as in [49], [50], [54] is employed to investigate the propagation of light in the MMF section. The input light is assumed to have a field distribution $E(r,0)$ because of the circular symmetry characteristic of the fundamental mode of the SMF. The input field can be decomposed into the eigenmodes $\{LP_{nm}\}$ of the MMF when the light enters the MMF section. Only the $LP_{0\nu}$ modes can be excited because of the circular symmetry of the input field and assuming ideal alignment of the fibre axes of the SMF and the MMF [49], [50], [54]. Defining the field profile of $LP_{0\nu}$ as $F_\nu(r)$, (the eigenmodes of the multimode fibre are normalized as $\int_0^\infty |E(r,0)|^2 r dr = \int_0^\infty |F_\nu(r)|^2 r dr$, $\nu = 1,2,3,\dots,m$, where m is the number of modes in the

MMF) the input field at the MMF can be written as:

$$E(r,0) = \sum_{\nu=1}^m c_\nu F_\nu(r) \quad (2.1)$$

where c_ν is the excitation coefficient of each mode. The coefficient c_ν can be calculated by an overlap integral between $E(r,0)$ and $F_\nu(r)$

$$c_\nu = \frac{\int_0^\infty E(r,0)F_\nu(r)rdr}{\int_0^\infty F_\nu(r,0)F_\nu(r)rdr} \quad (2.2)$$

As the light propagates in the MMF section, the field at a propagation distance z can be calculated by

$$E(r,z) = \sum_{\nu=1}^m c_\nu F_\nu(r) \exp(j\beta_\nu z) \quad (2.3)$$

where β_ν is the propagation constant of each eigenmode of the MMF. The transmission loss in dB can be calculated by using overlap integral method between $E(r,z)$ and the eigenmode of the output SMF $E_0(r)$ as in [51]

$$L_s(z) = 10 \cdot \log_{10} \left(\frac{\left| \int_0^\infty E(r, z) E_0(r) r dr \right|^2}{\int_0^\infty |E(r, z)|^2 r dr \int_0^\infty |E_0(r)|^2 r dr} \right). \quad (2.4)$$

To design the SMS-based edge filter, the MMF length needs to be determined. Our study shows that at a re-imaging distance (the transmission loss will reach a peak at a self image of the input) is highly wavelength dependent. If re-coupling into the SMF takes place at the re-imaging distance, then the MMF section of the SMS structure has by definition a length equal to the re-coupling distance and operates as a bandpass filter as in [52], [54]. However, for the purpose of designing an edge filter, the bandpass response can be considered as two spectral responses, on either side of a centre wavelength. Consequently, the device can behave as an edge filter for a selected wavelength range. Two SMS edge filters with opposite slope spectral responses within a given wavelength range (Fig. 8(c)) can be obtained by choosing two bandpass filters with appropriate centre wavelengths.

To investigate the wavelength dependence at the re-imaging distance, a numerical calculation was carried out. A standard SMF28 was chosen as the SMF, for which the parameters are: the refractive index for the core and cladding is 1.4504 and 1.4447, respectively (at a wavelength of 1550 nm), and the radius of core is 4.15 μm . Furthermore, to illustrate the dependence of the transmission response on the MMF core radius, we used MMFs with core radii of 25, 52.5, 75, and 100 μm . Fig. 9 presents the wavelength dependence of the transmission loss at the re-imaging distance for the different MMF cores radii. It can be seen as expected that the overall response is a bandpass response centred on 1550 nm. On either side of the centre wavelength each bandpass response can be viewed as

consisting of a combination of two spectral responses with opposite slopes over a limited wavelength range. For example from Fig. 9, for a MMF radius of $52.5\ \mu\text{m}$ and a length of $42.87\ \text{mm}$, a positive slope edge filter response exists between 1530 and $1550\ \text{nm}$ and a negative slope edge filter response exists between 1550 and $1580\ \text{nm}$.

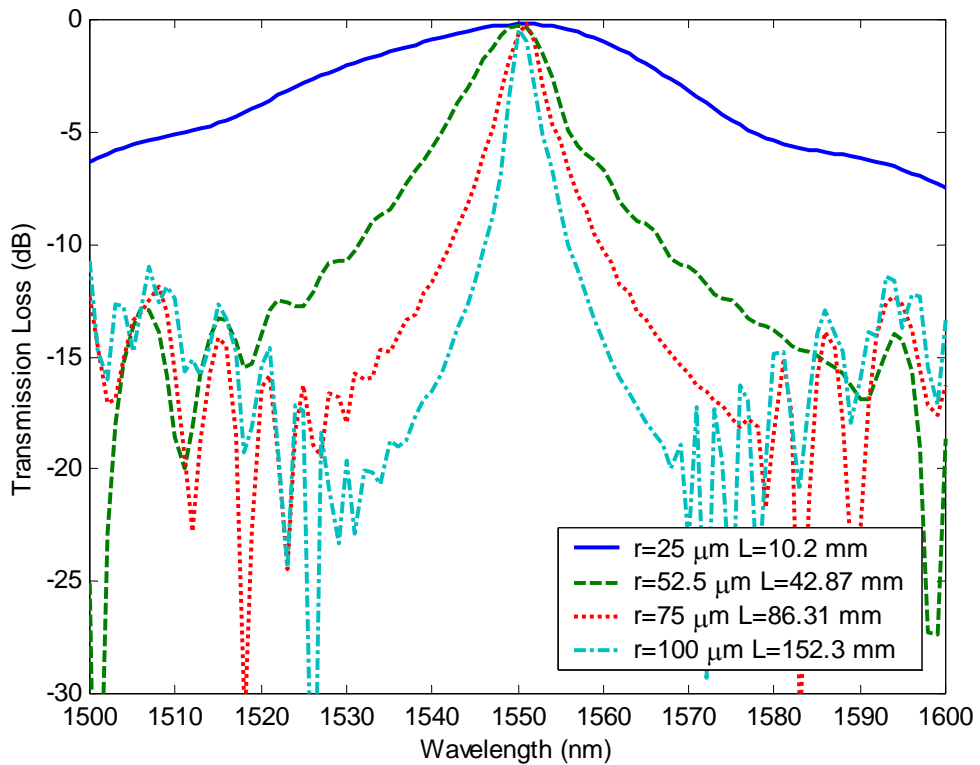


Figure 9 Spectral responses at re-imaging distance for different core radii and MMF section lengths

The peak wavelength of the bandpass filter can be tuned by changing the MMF length as mentioned in [52], [54], and by doing so the range of wavelengths over which an edge filter response exists is also altered. By choosing two bandpass filters with appropriate center wavelengths, it is possible to arrange for an intersection of two edge filters with opposite slopes within a given wavelength

range. Also from Fig. 9, the discrimination range of the edge filters created by appropriate choice of centre wavelengths can be controlled by changing the MMF core size. The discrimination range in dB increases as the core size of the MMF increases, but the usable wavelength range decreases. As an example for $r = 25 \mu\text{m}$, the discrimination range of the positive slope of edge filter is about 7 dB from 1500 to 1550 nm by comparison to $r = 100 \mu\text{m}$, where the discrimination range is about 20 dB from 1538 to 1550 nm.

2.3 Design and experimental results

As an example to illustrate the design process, a target wavelength range for wavelength measurement from 1530 to 1560 nm was chosen. This range was chosen as it corresponds to the typical centre wavelengths for many FBG sensors. On the basis of the proposed configuration in Fig. 8(a) and the design approach abovementioned, the two SMS edge filters are designed. An MMF type AFS105/125Y was chosen, for which the parameters are as follows: refractive index for the core and cladding is 1.4446 and 1.4271, respectively, a core radius $r = 52.5 \mu\text{m}$. This fibre type was chosen based on the results from the previous section where it was shown that there is a trade-off between the slope of the edge filter response and the usable wavelength range. A core radius $r = 52.5 \mu\text{m}$ (in Fig. 9) can provide an edge filter response 30 nm wide with a reasonable discrimination range^a. As mentioned earlier, for the specified wavelength range, two opposite response slope edge filters (SMS-1 and SMS-2) could be obtained by designing two bandpass filters with peak wavelengths: $\leq 1530 \text{ nm}$ and ≥ 1560

^a That is, a discrimination range of $> 8 \text{ dB}$ as in [29].

nm, respectively. On the basis of on our calculation for SMS-1, peak wavelengths from 1520 to 1530 nm correspond with the MMF length $L = 43.7$ to 43.4 mm, respectively. For SMS-2, peak wavelengths from 1560 to 1570 correspond with the MMF length $L = 46.625$ to 42.42 mm. It was founded, suitable peak wavelengths for the targeted wavelength range are 1523 nm and 1560 nm with the corresponding MMF lengths are $L = 43.6$ mm and $L = 42.625$ mm for the SMS-1 and SMS-2, respectively. Peak wavelength values of 1523 nm and 1560 nm were chosen for the two SMS edge filters because their transmission loss spectral responses were suitably linear over the targeted wavelength range of 1530 to 1560 nm. The calculated transmission loss by using (2.4) for the designed SMS edge filters is shown in Fig. 10. As shown in Fig. 10, the calculated negative slope response of the SMS-1 structure 1530 to 1560 nm has a transmission loss from -5.73 to -15.76 dB, respectively. The calculated positive slope response of the SMS-2 structure from 1530 to 1560 nm is -13.22 to -0.29 dB, respectively^a.

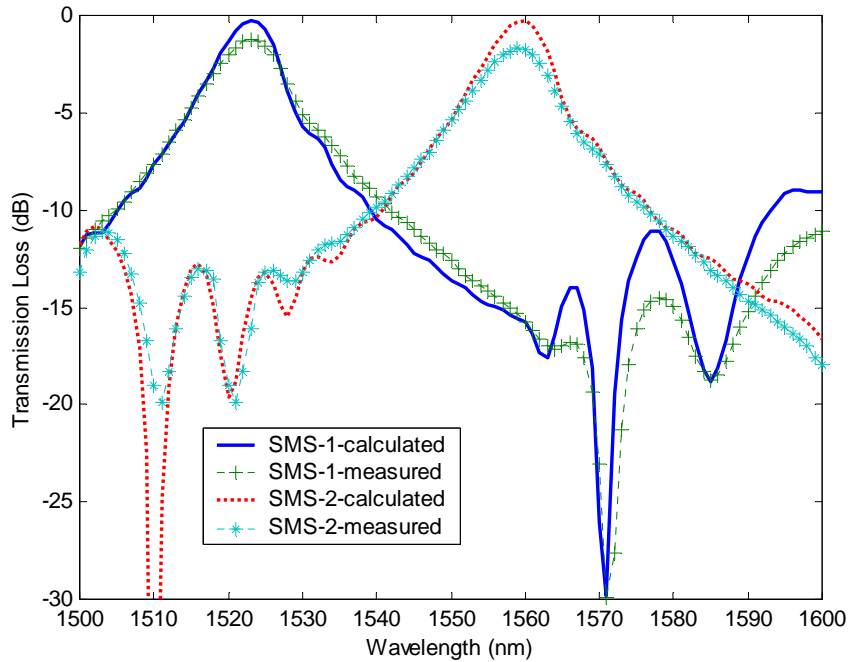
For the purpose of experimental verification of the performance of the edge filters the SMS structures were fabricated by using a Fujikura CT-07 cleaver and a Sumitomo type-36 fusion splicer. For each SMS structure the process was the same. First, the input SMF and the input end of the MMF were cleaved and spliced together. The cleaver was used again to cleave the unterminated end of the MMF fibre so that its length was set to the desired value. Finally, the output end of MMF section was spliced to the cleaved end of the output SMF.

The spectral response of each fabricated filter was measured using a tunable laser and optical spectrum analyzer (OSA). The measured results are

^a The calculated positive slope of SMS-2 showed a monotonically increasing response from 1534 to 1560 nm. The measured positive slope and overall measured ratio also showed a monotonically increasing response within the wavelength range of 1530-1560 nm.

shown in Fig. 10 and show a good agreement with calculated results. For operation as edge filters over the wavelength range 1530 to 1560 nm the measured negative slope of SMS-1 and positive slope of SMS-2 are -5.09 to -15.71 dB and -13.16 to -1.75 dB.

To demonstrate the use of the edge filters in a functioning wavelength measurement system, a ratiometric measurement system was built as shown in Fig. 8(a). The input signal was split into two equal intensity signals using a 3 dB fibre splitter^a. One light signal passes through SMS-1 and the other passes through SMS-2. A high speed dual channel power meter was placed at the ends of both arms. Fig. 11 shows the measured ratio of the optical power. The ratio measured between 1530 to 1560 nm has a linear slope with a discrimination range of 20.41 dB from 7.72 to -12.69 dB which is suitable for wavelength measurement.



^a 10202A-50 - 2x2 SM Coupler

Figure 10 Calculated and measured spectral responses of the SMS edge filters

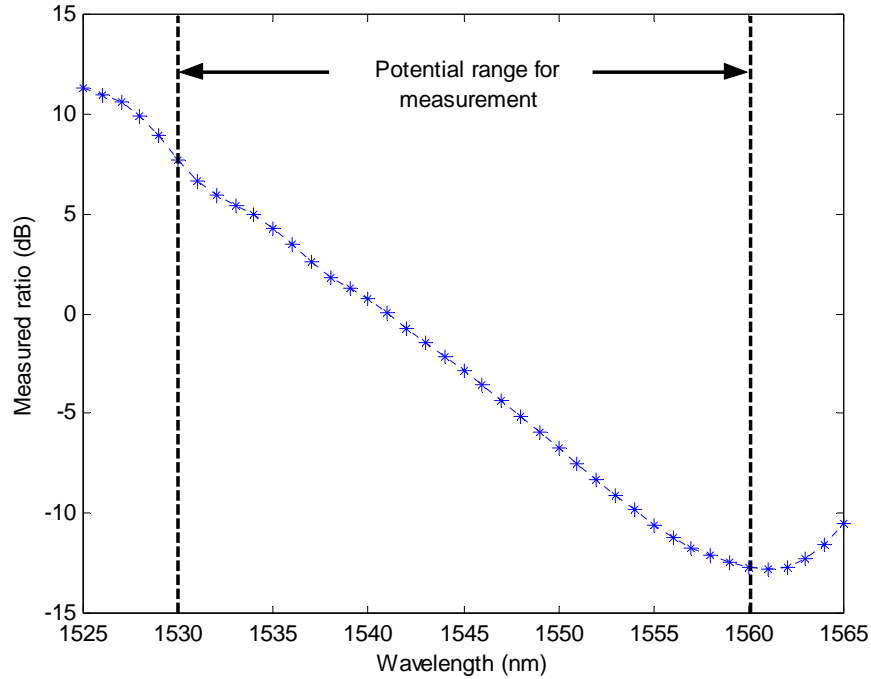


Figure 11 Measured ratio

Finally, the minimum detectable wavelength shift or resolution of the developed ratiometric system was also investigated. To investigate the resolution, the tunable laser was used to provide an input signal and the corresponding output ratio also recorded. The minimum tuning step for the laser used is 10 pm. The source wavelength was set to 1540 nm and was tuned by successively increasing increments of 10, 20 and 30 pm. The dual channel power meter was used to sample the SMS outputs for 6-7 s without averaging and the ratio in dB of the power levels is determined for each sample with a sampling rate of 50 measurements/second. Fig. 12 shows the complete time series of the measured ratio values as a function of sample time and the wavelength increments. From

Fig. 12, it is clear that the minimum detectable change in the wavelength is better (lower) than 10 pm^a.

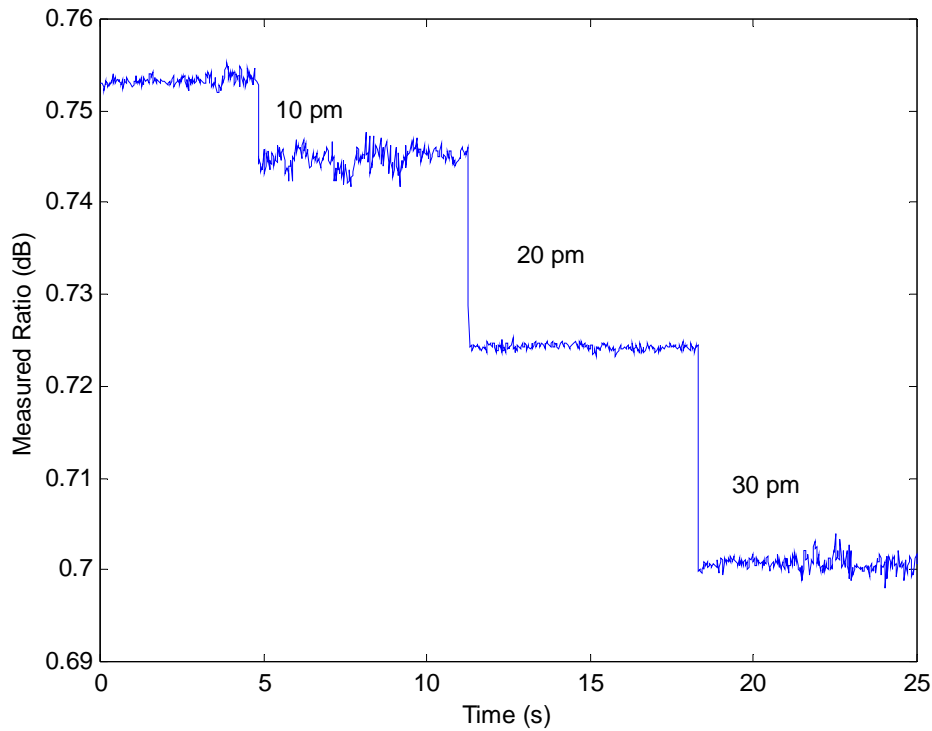


Figure 12 Measured ratio as the wavelength is tuned

2.4 Conclusion

In this article, it has been proposed and demonstrated a ratiometric wavelength monitoring scheme based on a pair of SMS-fibre structures. The two opposite spectral response edge filters used are realised by a pair of SMS-fibre structures. When applied in a ratiometric wavelength measurement, a discrimination range of

^aThe observed fluctuation in the measured ratio is 0.003 dB, peak-to-peak.

20.41 dB in the wavelength range 1530 to 1560 nm and a resolution better than 10 pm have been demonstrated.^a

2.5 References

- [43] S. M. Melle, K. Liu, and R. M. Measures, "Practical fibre-optic Bragg grating strain gauge system," *App. Opt.*, vol. 32, pp. 3601-3609, 1993.
- [44] J. Yates, J. Lacey, and D. Everitt, "Blocking in multiwavelength TDM networks," *Telecomm. System*, vol. 12, pp. 1-19, 1999.
- [45] E. Karasan and E. Ayanoglu, "Performance of WDM transport networks," *J. Select. Areas Commun.*, vol. 16, pp. 1081-1096, 1998.
- [46] Q. Wang, G. Farrell, T. Freir, G. Rajan, and P. Wang, "Low-cost wavelength measurement based on a macrobending single-mode fibre," *Opt. Lett.*, vol. 31, pp. 1785-1787, 2006.
- [47] P. Wang, G. Farrell, Q. Wang, and G. Rajan, "An optimized macrobending-fibre-based edge filter," *IEEE Photon. Technol. Lett.*, vol. 19, pp. 1136-1138, 2007.
- [48] M.C. Cardakli et. al., "Tunable all-optical time slot-interchange and wavelength conversion using difference-frequency-generation and optical buffers," *IEEE Photon. Technol. Lett.*, vol. 14, pp. 200-202, 2002.
- [49] W. S. Mohammed, A. Mehta, and E. G. Johnson, "Wavelength tunable fibre lens based on multimode interference," *J. Lightw. Technol.*, vol. 22, pp. 469-477, 2004.
- [50] A. Mehta, W. S. Mohammed, and E. G. Johnson, "Multimode interference-based fibre optic displacement sensor," *IEEE Photon. Technol. Lett.*, vol. 15, pp. 1129-1131, 2003.
- [51] Q. Wang and G. Farrell, "All-fibre multimode-interference-based refractometer sensor: proposal and design," *Opt. Lett.*, vol. 31, pp. 317-319, 2006.

^a This system provides a greater sensitivity of 0.68 dB/nm compared to the sensitivity of 0.16 dB/nm achieved by the macrobending fibre edge filter reported in [46].

- [52] W. S. Mohammed, P. W. E. Smith, and X. Gu, "All-fibre multimode interference bandpass filter," *Opt. Lett.*, vol. 31, pp. 2547-2549, 2006.
- [53] Q. Wang and G. Farrell, "Multimode-fibre-based edge filter for optical wavelength measurement application and its design," *Microw. Opt. Technol. Lett.*, vol. 48, pp. 900-902, 2006.
- [54] Q. Wang, G. Farrell, and W. Yan, "Investigation on singlemode-multimode-singlemode fibre structure," *J. Lightw. Technol.*, vol. 26, pp. 512-519, 2008.

Chapter 3

Effect of misalignment on an SMS fibre structure-based edge filter

In Chapter 2, the demonstration of X-type edge filters based on SMS fibre structures and their implementation in a ratiometric wavelength measurement was described. The application of SMS fibre structures as edge filters for wavelength measurement requires further study of several issues relating to SMS structure design and performance, including the effect of misalignment of SMS fibre cores, polarization dependence and temperature dependence.

In this chapter, the effect of misalignment of the SMS fibre cores, due to the fabrication process, on the spectral responses of X-type edge filters is investigated. Commercial fibre fusion splicers are normally used to splice SMF to SMF or MMF to MMF with very low lateral core offsets and therefore, very low loss. However, fusion splicers are not pre-programmed to deal with splicing SMF to MMF so that during the splicing process for SMF to MMF or vice-versa, significant lateral core offset errors may arise.

In Chapter 2, an SMS fibre structure-based edge filter was analyzed by using the MPA based on LP_{0m} under the assumption of an ideal core alignment. However, in the presence of lateral core offsets, the MPA based on LP_{0m} cannot

be used. Thus, to investigate the effect of misalignment of SMS fibre cores, all possible modes in the MMF section, not only the LP_{0m} modes should be taken into account in the MPA. This chapter analyzes misalignment effect of SMS fibre cores on the edge filter spectral response. A numerical model based on the MPA with a set of calculated guided modes using the finite difference method (FDM) was developed to investigate the effect of misalignment of SMS fibre cores. It was found that a limit of tolerable misalignment of SMS fibre cores exists beyond which the spectral performance of the edge filter-based SMS fibre structure degrades unacceptably. The experimental verification of this result is also presented.

Misalignment limits for a singlemode-multimode-singlemode fibre-based edge filter^a

Keywords : optical fibres, multimode interference, edge filter

Abstract: Misalignment effects on the spectral characteristics of edge filters based on singlemode-multimode-singlemode (SMS) fibre structures are investigated numerically and experimentally. A modal propagation analysis is used with a set of guided modes calculated using the finite difference method (FDM) to determine the transmission loss of the SMS-based edge filters. A limit

^a A. M. Hatta, G. Farrell, P. Wang, G. Rajan, and Y. Semenova, "Misalignment limits for a singlemode-multimode-singlemode fibre-based edge filter," *Journal of Lightwave Technology*, vol. 27, no. 13, pp. 2482-2488, 2009.

for the tolerable misalignment of the SMS fibre-based edge filter is proposed, beyond which the spectral performance of the SMS structure degrades unacceptably. The numerical results are verified experimentally with good agreement.

3.1 Introduction

Singlemode-multimode-singlemode (SMS) fibre structures have been investigated for use in several applications e.g. as a refractometer, a bandpass filter, and an edge filter [55]-[58]. An optical device based on the SMS fibre structure offers an all-fibre solution for optical communications and optical sensing applications with the advantages of simplicity of packaging and ease of inter-connection to other optical fibres.

The SMS structure is fabricated by splicing a precisely dimensioned multimode fibre (MMF) section between two singlemode fibres (SMFs). Ideally, the centre axes of all the fibre cores are precisely aligned. However, in practice the splicing process itself, along with the manufacturing variations in core-cladding concentricity can introduce lateral misalignment between the centres of the SMF-MMF-SMF cores.

In the ref. [56], [58], and [59], the SMS fibre structure is analyzed using a modal propagation analysis (MPA) for the linearly polarized (LP) (or scalar) modes. The input light can be assumed to have the field distribution of the fundamental mode of the SMF [59]. When the light launches into the MMF, the input field can be decomposed into the eigenmodes (LP_m) of the MMF. Due to the circular symmetric nature of the input field and an ideal alignment assumption,

the number of guided modes of the MMF used in the modal propagation analysis is greatly reduced from LP_{nm} to LP_{0m} or the circular symmetry modes. This reduced number of modes means the calculation can be performed efficiently. In [55] and [57], the SMS structure is investigated using the beam propagation method, where it is assumed that only the circular symmetry modes exist. With this assumption the optical field is simplified so that it is independent of the angular coordinate in a cylindrical coordinate system. However, if the centre (or meridional) axes of the SMS cores are misaligned relative to one another, it cannot be assumed circularly symmetrical modes. Thus, both approaches published so far cannot be used to study the effect of misalignment in an SMS structure.

An MPA using a complete set of hybrid modes or vectorial form guided modes in the MMF has been proposed to analyze the misalignment effect [60]. In this approach, a complete set of guided modes in the MMF is calculated and an adaptive algorithm is developed to perform mode expansion of the optical field in the MMF. However, the complete set of guided modes in the MMF can also be solved with an alternative numerical method, the finite difference method (FDM) [61]. The numerical approach using FDM offers simplicity of its implementation. In this paper, the FDM is used to calculate the complete set of guided modes in the MMF and then the MPA was performed to analyze the misalignment effect. Building on previous research on an SMS-based edge filter [57], [58], in this paper, the effect of fibre misalignment within an SMS-based edge filter was investigated both numerically and experimentally, so as to establish an upper limit on tolerable misalignment above which the performance of SMS structure has

degraded significantly.

To put the misalignment induced performance degradation in context, the application chosen here for the SMS was that of an edge filter used within a ratiometric wavelength measurement system. A ratiometric wavelength measurement usually consists of a 3 dB coupler^a with the two outputs connected to an edge filter arm with a well defined spectral response and a reference arm, or alternatively two edge filters arms with opposite slope spectral responses can be used. The use of two opposite slope edge filters can increase the usable resolution of the ratiometric system [62]. A ratiometric wavelength measurement-based system on two opposite slope SMS-based edge filters was built and demonstrated in this paper.

3.2 SMS-based edge filters

A schematic structure for a ratiometric wavelength measurement consisting of two SMS-based edge filters is shown in Fig. 13(a). The target spectral responses in dB of the SMS-based edge filters are shown in the Fig. 13(b), and can have either a negative (P1) or a positive (P2) slope. Two key parameters for an edge filter are baseline loss and discrimination range. The SMS-based edge filter operates over a wavelength range from λ_1 to λ_2 with a progressively larger or smaller transmission loss as the wavelength increases from λ_1 to λ_2 , for the negative or positive slope, respectively. The baseline loss is defined as the transmission loss of the filter at λ_1 or λ_2 , for the negative and the positive slope, respectively, while the discrimination range is the difference between the transmission loss at λ_1 and

^a 10202A-50 - 2x2 SM Coupler

λ_2 . The corresponding ratio (P2-P1) of the two outputs over the wavelength range is presented in the Fig. 13(c). The wavelength of an input signal can be determined through measuring the power ratio of the output ports at the outputs of the two arms, assuming a suitable calibration has taken place.

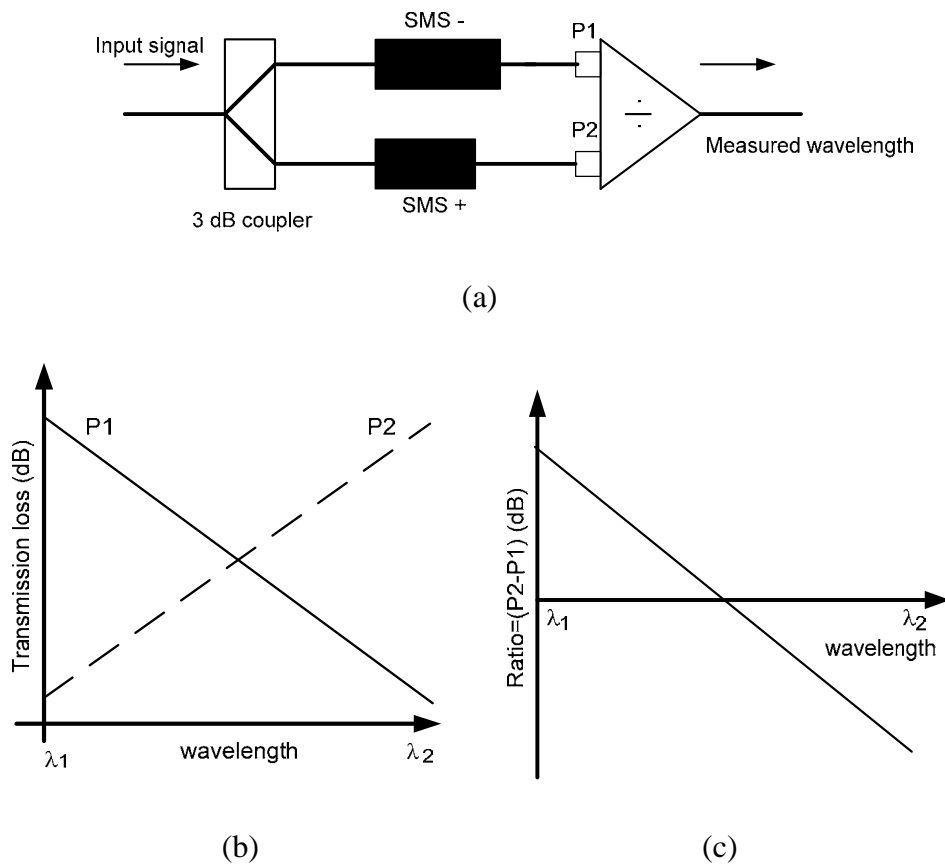


Figure 13 (a) Schematic configuration of a ratiometric wavelength measurement (b) desired spectral responses of the SMS-based edge filter, negative (solid line) and positive (dash line) slope versions, and (c) the output ratio between two output SMS-based edge filters

The fibre structure under consideration consists of an input SMF, a sandwiched MMF section, and an output SMF, as shown in Fig. 14(a). The

concentric alignment and misalignment conditions in the Cartesian coordinate system, between the input SMF, MMF section, and output SMF cores, are shown in Fig. 14(b) and 14(c), respectively. The radii of SMF and MMF are denoted as R_s and R_m , respectively. The input SMF and output SMF positions are denoted by the coordinates $I[x, y]$ and $O[x, y]$, respectively, where x and y are in μm .

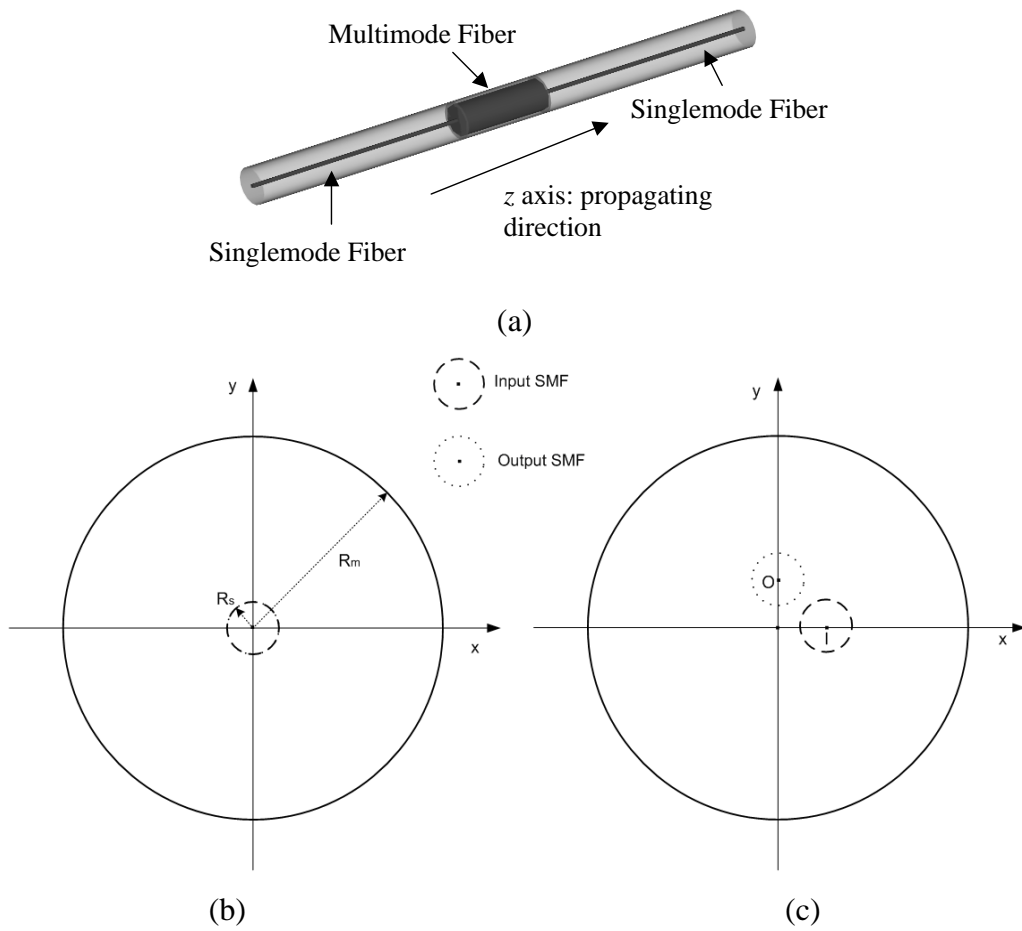


Figure 14 (a) Schematic configuration of the SMS fibre structure (b) concentric alignment (c) misalignment condition

3.3 Modal propagation analysis

The MMF section can support many guided modes and the input field is reproduced as single image at periodic intervals along the propagation direction due to the interference between these guided modes. This is the so-called self-imaging principle and the distance at which self-imaging occurs is called the re-imaging distance. The approach used here to analyze the field distribution in the MMF section is a modal propagation analysis [63]. In the MMF, an MPA using a cylindrical coordinate system has been employed in [56], [58], and [59] based on a scalar approximation of the LP_{0m} modes. The LP_{0m} modes could not be used to investigate misalignment effects because it only consists of circularly symmetrical modes. To analyze misalignment it is necessary to calculate a complete set of guided modes in the MMF [60]. In the approach used here, the MPA is performed in the Cartesian coordinate system with a set of calculated guided modes using FDM to allow investigation of misalignment effects.

The MPA procedure is as follows: the input light is assumed to have the field distribution $\psi(x, y, 0)$ of the fundamental mode of the SMF. The input field can be decomposed into the eigenmodes of the MMF, $\varphi_v(x, y)$, when the light enters the MMF section. The input field at the MMF can be written as:

$$\psi(x, y, 0) = \sum_v c_v \varphi_v(x, y) \quad (3.1)$$

where c_v is the excitation coefficient of each mode. The coefficient c_v can be calculated by an overlap integral between $\psi(x, y, 0)$ and $\varphi_v(x, y)$,

$$c_v = \frac{\int \psi(x, y, 0) \varphi_v(x, y) dx dy}{\sqrt{\int \varphi_v^2(x, y) dx dy}}. \quad (3.2)$$

As the light propagates in the MMF section, the field at a propagation distance z can be calculated by

$$\psi(x, y, z) = \sum_v c_v \varphi_v(x, y) \exp[j\beta_v z] \quad (3.3)$$

where β_v is the propagation constant of each eigenmode of the MMF. The transmission loss in dB can be determined by using the overlap integral method between $\psi(x, y, z)$ and the eigenmode of the output SMF $\psi_o(x, y)$

$$L_s(z) = 10 \cdot \log_{10} \left(\frac{\left| \int \psi(x, y, z) \psi_o(x, y) dx dy \right|^2}{\int |\psi(x, y, z)|^2 dx dy \int |\psi_o(x, y)|^2 dx dy} \right). \quad (3.4)$$

Here $\varphi_v(x, y)$ and β_v can be obtained by using a semi-vectorial FDM. It should be noted that FDM calculates a set of all possible guided modes in the MMF section, not just concentric circular modes, allowing the transmission loss due to misalignment to be calculated. Using the above equations, the light propagation in the whole structure can be analyzed.

3.4 Design example and spectral response

To investigate the effect of misalignment, in the first instance it is necessary to present a typical SMS structure designed to meet a target spectral response and calculate its ideal, perfectly aligned, spectral response.

To design the SMS-based edge filter, the MMF length needs to be determined. It has been shown that the re-imaging distance is wavelength dependent [56], [59]. If re-coupling into the output SMF takes place at the re-imaging distance, then the MMF section of the SMS structure has by definition a length equal to the re-coupling distance and operates as a bandpass filter as in [56]

and [59]. However, for the purpose of designing an edge filter, the bandpass response can be considered as two spectral responses, on the either side of a centre wavelength. Consequently, the device can behave as an edge filter for a selected wavelength range. Two SMS-based edge filters with opposite slope spectral responses within a given wavelength range can be obtained by choosing two bandpass filters with appropriate centre wavelengths [58].

As an example, to illustrate the design process, a target wavelength range for wavelength measurement from $\lambda_1 = 1520$ nm to $\lambda_2 = 1545$ nm was chosen. This range is chosen as it corresponds to the typical centre wavelengths for many fibre Bragg grating (FBG) sensors. Based on the target spectral responses as in Fig. 13(b), the SMS-based edge filters are designed with the baseline loss > -8 dB and the desired discrimination range > 8 dB. A standard SMF28 fibre was chosen as the SMF, for which the parameters are: the refractive indices for the core and cladding are 1.4504 and 1.4447 respectively (at a wavelength of 1550 nm), and the radius of the core $R_s = 4.15$ μm . An MMF type AFS105/125Y was chosen as the MMF section for which the parameters are: refractive indices for the core and cladding are 1.4446 and 1.4271, respectively, with a core radius $R_m = 52.5$ μm . The small difference between the refractive indices of the SMF and MMF means that the Fresnel reflection occurring at their interface is negligible (the level of reflection is -54 dB or lower relative to the injected light level) and a one-way modal propagation analysis can be used [59]. As mentioned above, for the specified wavelength range, two opposite response slope edge filters (negative and positive slopes) can be obtained by designing two bandpass filters with peak wavelengths: ≤ 1520 nm and ≥ 1545 nm, respectively. From (10) in ref [59], the

peak wavelengths from 1500 to 1520 nm correspond to the MMF lengths $L = 44.25$ to 43.66 mm, and from 1545 to 1560 nm correspond to $L = 43.00$ to 42.58 mm. Suitable peak wavelengths for the targeted wavelength range are 1510 and 1547 nm and the corresponding MMF lengths are $L = 43.96$ mm and $L = 42.95$ mm, for the negative and positive slope edge filters, respectively. The peak wavelengths at 1510 and 1547 nm were chosen for the SMS-based edge filters because their transmission loss responses have a suitable spectral response over the targeted wavelength range from 1520 to 1545 nm. The transmission loss responses, calculated using (3.4) for the designed SMS-based edge filter, are shown in Fig. 15. These responses represent the performance of the design example for the case of perfect alignment. It can be seen that the two opposite edge filter responses within the targeted wavelength range can be achieved using two bandpass filters. The calculated negative and positive slope responses of the SMS-based edge filters from 1520 to 1545 nm have a transmission loss from -7.20 to -15.53 dB and -11.84 to -0.77 dB, respectively, and the corresponding discrimination ranges are 8.33 dB and 11.06 dB, respectively, suitable for use as edge filters.

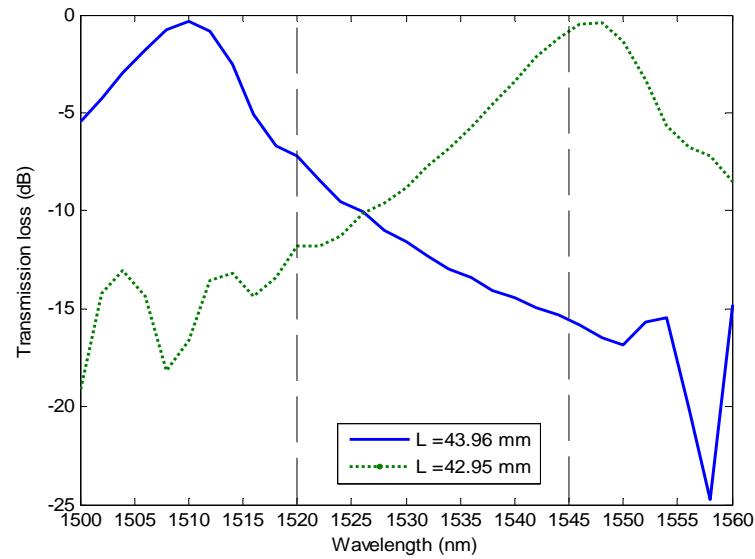


Figure 15 Transmission loss responses of the two SMS-based edge filters

3.5 Investigation of misalignment effects for the design example

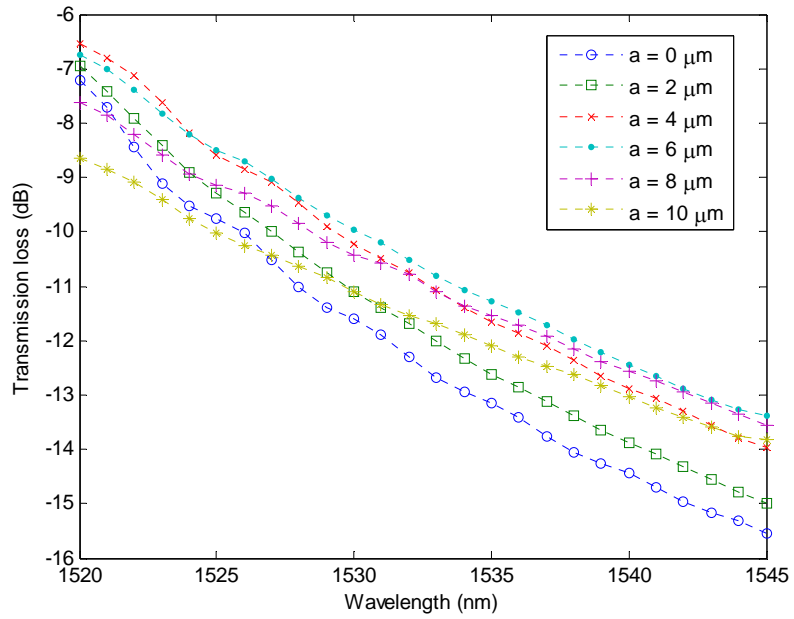
To investigate the misalignment effect, the transmission loss of several positions of the input SMF and output SMF are calculated using (3.4). The transmission loss was calculated within the wavelength range 1520-1545 nm of the offset positions, $I[a,0]$, $O[0,a]$, where $a = 0-10 \mu\text{m}$ with an increment $2 \mu\text{m}$. Given the need to undertake experimental verification, these misalignment values are chosen based on the deliberate offset that can be produced by the fusion splicer used in the experiments described later. The calculated transmission loss responses are shown in Fig. 16(a) and 16(b), for the negative and positive slope edge filters, respectively. From Fig. 16(a), for the negative slope, it can be seen that, even with misalignment, the response retains a monotonically decreasing characteristic over the wavelength range and thus, is still suitable for use as the edge filter response. However, the discrimination range decreases as the offset increases, from 8.33 dB

without an offset to 8.03, 7.41, 6.64, 5.93, and 5.15 dB for an offset equal to 2, 4, 6, 8, and 10 μm , respectively. A reduced discrimination range will have a negative impact on measurement accuracy where the edge filter is used within a ratiometric wavelength measurement system. For the positive slope filter, as shown in Fig. 16(b), the response slope changes very significantly when the offset increases. For an offset $a = 2$, and 4 μm the spectral responses are still suitable as the edge filter, but for larger offset values the transmission loss responses do not monotonically increase across the wavelength range and therefore are not suitable for use as an edge filter.

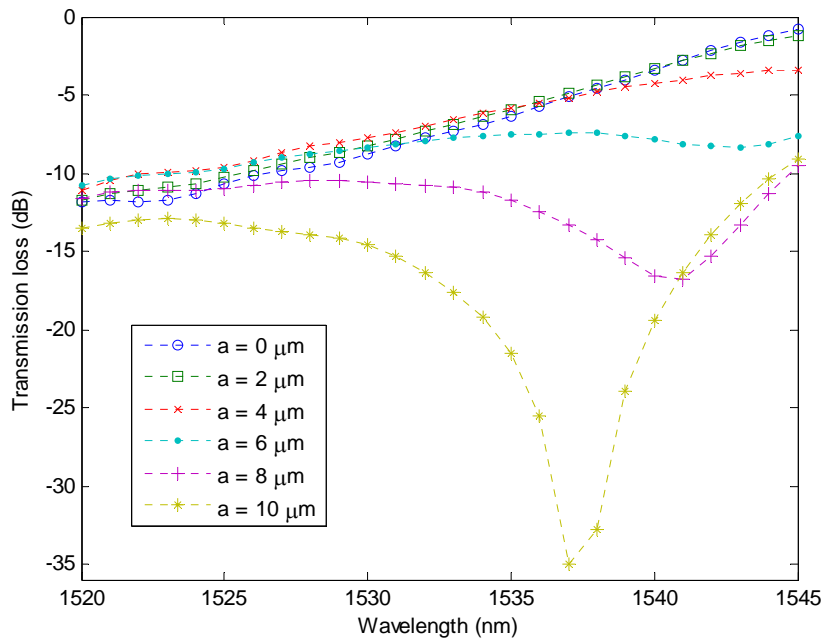
The change in the negative and positive slopes due to an offset needs to be considered in the context of changes to the overall bandpass responses. The consequences of an increase in the offset on the bandpass response are a shift of the self-imaging position and a reduction in the maximum transmission loss at the peak wavelength of the bandpass filter. Such changes in the overall bandpass response will clearly also change the positive and negative slope responses.

In practice, there is a significant difference between the negative and positive slope responses in terms of the change in the response that is induced by an offset. This difference can be explained as follows. From the MPA above and as described in [60], the presence of an offset for the input SMF increases the number of excitation modes (circularly symmetrical modes and azimuthal modes) compared to the case without an offset (circularly symmetrical modes only). Increasing the number of excitation modes changes the MMF field pattern resulting from interference in the MMF. In turn, the transmission loss which is a function of the overlap between the MMF field and the eigenmode of the output

SMF, varies with changes in the offset of the output SMF.



(a)



(b)

Figure 16 Calculated transmission loss response due to misalignment effect of the SMS-based edge filter (a) negative slope (b) positive slope

To better understand the difference in the manner on which an offset affects the negative and positive slopes, the MMF field amplitude profiles for the cases of $a = 0 \mu\text{m}$ and $a = 10 \mu\text{m}$ are shown in Fig. 17 for a wavelength of 1537 nm. This wavelength is chosen as it corresponds to the wavelength at which the changes in the positive slope are most pronounced, as shown in Fig. 16. The MMF field amplitude profiles for the negative slope response for the case of $a = 0 \mu\text{m}$ and $a = 10 \mu\text{m}$ are shown in Fig. 17(a) and 17(b), respectively. The overlap between the MMF field amplitude profile and the eigenmode of the output SMF is located at $O[0,0]$ and $O[0,10]$ in μm , for the case of $a = 0 \mu\text{m}$ and $a = 10 \mu\text{m}$, respectively. Comparing Fig. 17(a) and 17(b), there is only a relatively small difference in the amplitude of the MMF field in the MMF overlap region when an offset is introduced. As the result, the transmission losses are not strongly influenced by offset^a.

For the positive slope response, the MMF field amplitude profile for the case of $a = 0 \mu\text{m}$ and $a = 10 \mu\text{m}$ is shown in Fig. 17(c) and 17(d), respectively. Comparing these figures it can be seen that when an offset is introduced, that is $a = 10 \mu\text{m}$, the eigenmode of the output SMF located at $O[0,10]$ overlaps a portion of the MMF field amplitude profile which has a very low value. The result is a very high transmission loss when an offset is introduced and thus, there is a strong dependence of the transmission loss on offset.

To further analyze the spectral quality of the edge filter, it is necessary to examine the linearity of the transmission loss when misalignment occurs. Linearity is important for an edge filter used in wavelength measurement

^a As shown in Fig. 16(a)

application for two reasons. First, a linear response by definition monotonically increases or decreases, so there can be no ambiguity in wavelength measurements. Second, a linear response will ensure the resolution for wavelength measurement is the same for all measured wavelengths.

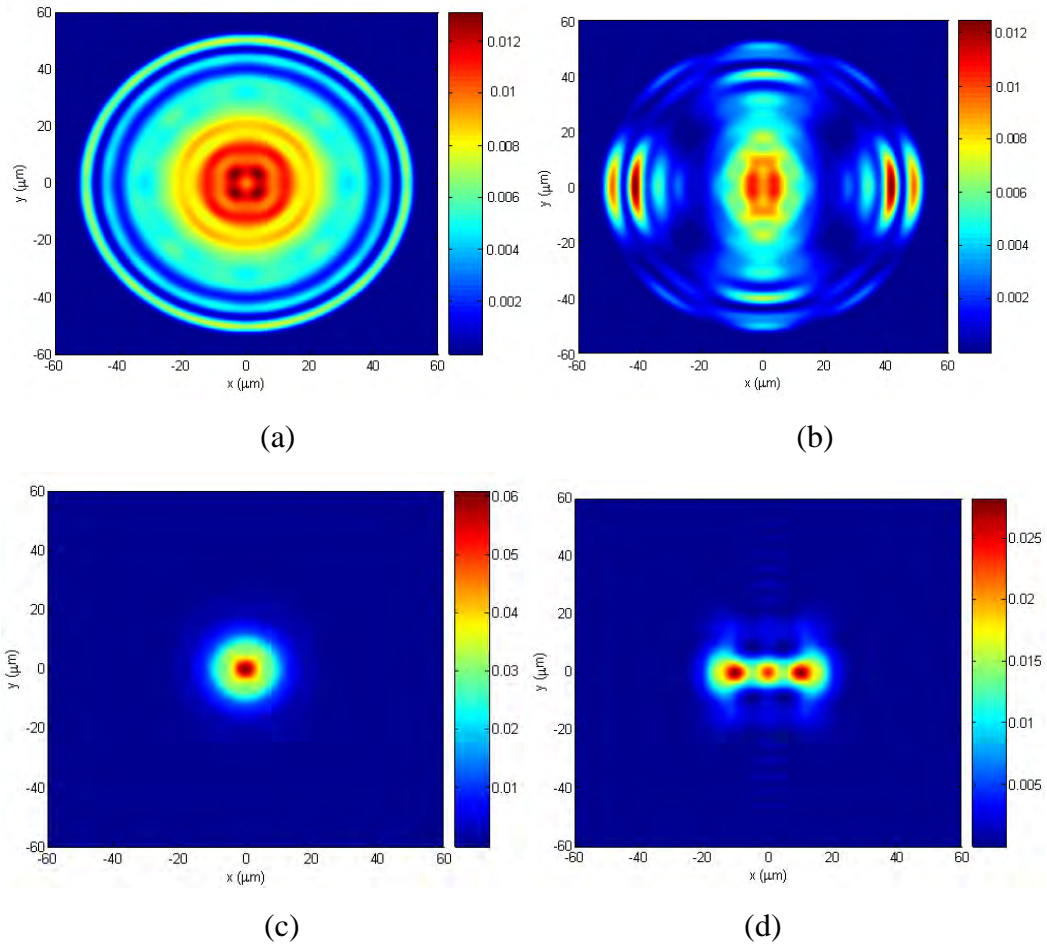


Figure 17 The MMF field amplitude profile at $\lambda = 1537$ nm for the negative slope (a) $a = 0$ μm , (b) $a = 10$ μm ; for the positive slope (c) $a = 0$ μm , (d) $a = 10$ μm

The linearity can be examined by using the correlation coefficient (R^2) of the linear regression analysis. An ideal spectral response has $R^2 = 1$, and a lower $R^2 < 1$ indicates a lower quality for the spectral response linearity. Fig. 18 shows

the correlation coefficient for the different offsets from 0 to 10 μm with an increment of 1 μm . It is shown that for the negative slope, the R^2 maintains a high value and is almost constant with $R^2 = 0.98, 0.98, 0.99, 0.99, 0.99,$ and 0.99 for the offset $a = 0, 2, 4, 6, 8,$ and $10 \mu\text{m}$, respectively. This means that the offset has little effect on the slope quality for the negative slope spectral response, but does reduce the discrimination range as mentioned above. For the positive slope, it is clear that the offset effects the slope quality. The R^2 are $0.98, 0.99, 0.99, 0.67, 0.28,$ and 0.07 for the offset of $0, 2, 4, 6, 8,$ and $10 \mu\text{m}$, respectively. The R^2 value degrades beyond an offset value of $a = 5 \mu\text{m}$, with $R^2 = 0.95$, and such spectral responses are not suitable for use in an edge filter. Based on the calculation of the R^2 value, it is suggested as a conservative guiding principle that the misalignment should be less than the core radius of the SMF ($4.15 \mu\text{m}$ in this case) to maintain the slope quality for the two SMS-based edge filters with opposite spectral responses.

For the purpose of experimental verification, the two SMS-based edge filters were fabricated using a precision Fujikura CT-07 cleaver and a Sumitomo type-36 three-axis fusion splicer. For each SMS structure the process is the same. Firstly, the input SMF and the input end of the MMF are cleaved and spliced together. To deliberately introduce an offset (and thus misalignment) in this splice, an attenuation splicing mode, available as an option on the fusion splicer, is used. This splicing mode allows for the creation of a fibre splice with a preset optical power loss. Given a preset power loss, the fusion splicer will automatically perform the splice with an appropriate axial offset.

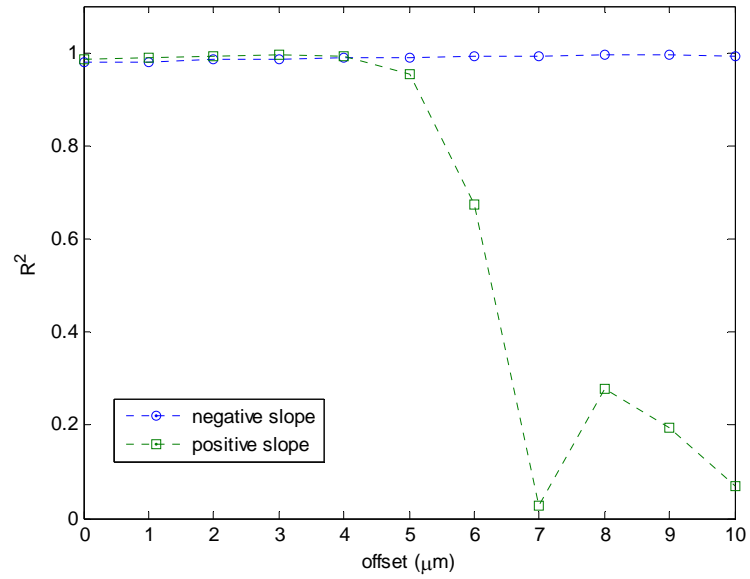


Figure 18 Correlation coefficient of the spectral response for different offsets

The cleaver is again used to precisely cleave the un-terminated end of the MMF fibre so that its length is set to the desired value. Finally, the output end of MMF section is spliced to the cleaved end of the output SMF, again with the attenuation splicing option. The desired power loss is set to that corresponding to an offset of 3.3 μm .

The transmission loss response of each fabricated filter was measured using a tunable laser and optical spectrum analyzer (OSA). The measured results are shown in Fig. 19 for the negative and the positive slope SMS-based edge filters. The calculation of transmission loss using (2.4) is also shown in the Fig. 19. The calculated and measured results show a good agreement. The discrepancy between the calculated and measured results due to a result of: 1) residual splicing insertion losses and 2) errors in the exact length of the MMF section. MMF section length errors, which arise during fabrication of the SMS structure, shift the

peak wavelength of the bandpass filter response, which in turn alters the measured transmission loss values over a fixed wavelength range.

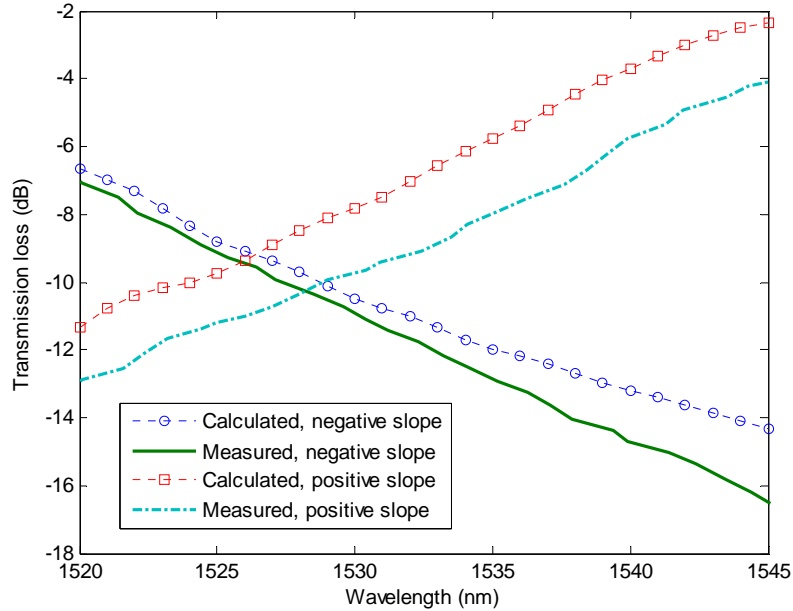


Figure 19 Measured and calculated transmission loss with misalignment of the SMS-based edge filters

Experimentally, the two edge filters with their deliberate misalignment, while they possess a higher insertion loss, demonstrate response slopes with an acceptable discrimination range of 9.47 and 8.89 dB for the negative and positive slopes, respectively. The misaligned edge filters are therefore still suitable for use as edge filters. This result verifies our assertion that as long as the misalignment between SMF and MMF cores is less than an offset misalignment limit equal to the SMF core radius then there is no significant effect on the slope quality.

To provide confirmation a misaligned SMS-based edge filter will work as long as lateral misalignment in an SMS structure is less than the limit proposed, the edge filter described above with a 3.3 μm lateral misalignment was employed

in a functioning wavelength measurement system, based on the scheme described in Fig. 13(a). The input signal is split into two equal intensity signals using a 3 dB fibre splitter^a. One of the signals passes through the negative slope SMS-based edge filter and the other passes through the positive slope SMS-based edge filter. A dual channel power meter is placed at the ends of both arms. Fig. 20 shows the measured ratio of the optical power. The measured ratio between 1520 to 1545 nm has a linear slope with a discrimination range of 18.14 dB from 7.17 to -10.97 dB, which is suitable for wavelength measurement^b.

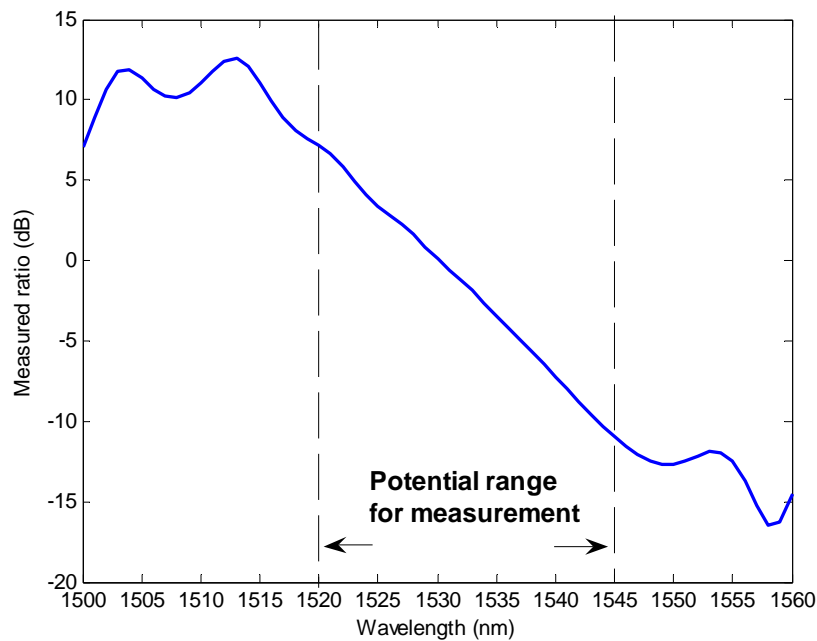


Figure 20 Measured ratio

It should be noted that for the fabrication of an SMS, it is preferable to use a fusion splicing machine with the capability of three-axis adjustment rather than a single-axis (also called a fixed V-groove) fusion splicer. Lateral misalignment

^a 10202A-50 - 2x2 SM Coupler

^b The correlation coefficient using a linear regression analysis for the discrimination range is 0.999, confirming the linearity of the slope.

arises in an SMS structure for two reasons. First, there is the lateral misalignment introduced by the fusion splicer itself, and second, there is the misalignment that results from the limited manufacturing tolerance of core-cladding concentricity of the fibres used. Using a fusion splicer with three-axis adjustment can negate the effect of the limited core-cladding concentricity of the fibres. This means that the only significant source of misalignment is the inherent alignment accuracy of the fusion splicer itself. Typical three-axis adjustment splicers can maintain inherent misalignment to less than 0.5 μm in the case of identical SMF or MMF splicing and thus can allow the fabrication of SMS structures with repeatably low lateral misalignment. The use of a single-axis fusion splicer is less advisable for SMS fabrication as it is not possible to overcome misalignment due to limited core concentricity and furthermore a single-axis splicer typically has an inherent misalignment that is higher than a three-axis adjustment splice machine.

3.6 Conclusion

The effect of misalignment on the spectral response of an SMS-based edge filter has been investigated. An MPA with a calculated set of guided modes using FDM is employed to analyze the misalignment effect. It is shown that the performance of the SMS-based edge filter degrades when the lateral misalignment is larger than a misalignment limit equal to the core radius of the SMF used. The measured transmission loss responses show a good agreement with the numerical results. The SMS-based edge filter used in the experiment is found to be suitable for use in a wavelength measurement system. Overall, it was shown that an SMS structure fabricated using a fusion splicer with three axis adjustment has the

advantage of a useful fabrication tolerance, within which the lateral misalignment has no significant effect on the slope of edge filter.

3.7 References

- [55] Q. Wang and G. Farrell, "All-fibre multimode-interference-based refractometer sensor: proposal and design," *Opt. Lett.*, vol. 31, pp. 317-319, 2006.
- [56] W. S. Mohammed, P. W. E. Smith, and X. Gu, "All-fibre multimode interference bandpass filter," *Opt. Lett.*, vol. 31, pp. 2547-2549, 2006.
- [57] Q. Wang and G. Farrell, "Multimode-fibre-based edge filter for optical wavelength measurement application and its design," *Microw. Opt. Technol. Lett.*, vol. 48, pp. 900-902, 2006.
- [58] A. M. Hatta, G. Farrell, Q. Wang, G. Rajan, P. Wang, and Y. Semenova, "Ratiometric wavelength monitor based on singlemode-multimode-singlemode fibre structure", *Microw. Opt. Technol. Lett.*, vol. 50, pp. 3036-3039, 2008.
- [59] Q. Wang, G. Farrell, and W. Yan, "Investigation on singlemode-multimode-singlemode fibre structure," *J. Lightw. Technol.*, vol. 26, pp. 512-519, 2008.
- [60] H. Li, M. Brio, L. Li, A. Schülzgen, N. Peyghambarian, and J. V. Moloney, "Multimode interference in circular step-index fibres studied with the mode expansion approach", *J. Opt. Soc. Am. B, Opt. Phys.*, vol. 24, pp. 2707-2720, 2007.
- [61] K. Kawano and T. Kitoh, *Introduction to Optical Waveguide Analysis: Solving the Maxwell Equations and the Schrödinger Equation*, Hoboken, NJ: Wiley, 2001, pp. 117-160.
- [62] S. M. Melle, K. Liu, and R. M. Measures, "Practical fibre-optic Bragg grating strain gauge system," *App. Opt.*, vol. 32, pp. 3601-3609, 1993.
- [63] L.B. Soldano and E.C.M. Pennings, "Optical multi-mode interference devices based on self-imaging: principles and applications," *J. Lightw. Technol.*, vol.13, pp. 615-627, 1995.

Chapter 4

Polarization dependence of an SMS fibre structure-based edge filter

In the previous chapter, the effect of misalignment of SMS fibre cores due to the fabrication process on the edge filter spectral response was investigated using the MPA with a set of calculated guided modes using the FDM. In this chapter, polarization dependence loss (PDL) of the SMS-based edge filter is investigated. By using the modelling platform described in Chapter 3, the PDL due to lateral and rotational SMS fibre cores offsets is investigated. It is shown that core offset must be minimised to achieve low PDL for an SMS fibre structure-based edge filter. It is also proposed and demonstrated that when lateral core offsets are unavoidable, the PDL of an SMS fibre structure-based edge filter can still be minimized by introducing a rotational core offset of 90^0 during the splicing process. Supporting experimental results are also presented.

Polarization dependence of an edge filter based on singlemode-multimode-singlemode fibre^a

Keywords: multimode fibre, polarization dependent loss, edge filter

Abstract: The polarization dependent loss (PDL) of a singlemode-multimode-singlemode (SMS) fibre structure used as an edge filter is presented. Minor errors in the fabrication process for the SMS fibre structure can introduce SMS fibre core offsets. The PDL due to lateral and rotational core offsets is investigated numerically and experimentally. It is shown that small core offsets are necessary to achieve low PDL for an SMS fibre-based edge filter. It is also demonstrated that when lateral core offsets are unavoidable, the PDL of an SMS edge filter can still be minimized by introducing a rotational core offset of 90°.

4.1 Introduction

One approach to measuring optical wavelength is the use of a ratiometric all-fibre scheme, with the advantages of low cost, simple configuration, simple interconnections, and the potential for high speed measurement. An all-fibre ratiometric wavelength measurement scheme consists of a 3 dB coupler with the two coupler outputs connected to a fibre edge filter arm, with a well defined spectral response, and a reference arm. Alternatively, two fibre edge filters arms with overlapping and opposite slope spectral responses, a so-called X-type

^a A. M. Hatta, Y. Semenova, G. Rajan and G. Farrell, "Polarization dependence of an edge filter based on singlemode-multimode-singlemode fibre," *Optics & Laser Technology*, in press, accepted on 19th January 2010.

spectral response, can be used. The use of an X-type spectral response can increase the measurement resolution of the ratiometric system [64]. Two edge filters for an X-type spectral response can be implemented by using step index singlemode-multimode-singlemode (SMS) fibre structures [65].

An SMS fibre structure also has been demonstrated for applications such as a bandpass filter, strain and temperature sensors, a wavelength encoded temperature sensor, and an intensity-based temperature sensor [66]-[69]. The SMS fibre structure is fabricated by splicing a specified length of a multimode fibre (MMF) between two singlemode fibres (SMF). A commercial fibre fusion splicer is normally used to splice SMF to SMF or MMF to MMF with a very low loss, which means very low lateral core offsets. However, fusion splicers are not pre-programmed to deal with splicing SMF to MMF so that during the splicing process for SMF to MMF or vice-versa, significant lateral core offset errors may arise. In a previous study [70], it was shown that an upper limit to lateral core offset is needed to ensure the edge filter spectral response stays within specification.

It is well known, that individually SMF or MMF has a low polarization dependent loss (PDL)^a, but for an SMS fibre structure, the PDL for an edge filter application has not been investigated. It has been previously shown that the polarization dependence of the edge filter based on a macro bend fibre in the all-fibre ratiometric system has a significant effect, specifically that high PDL for an edge filter can significantly decrease the accuracy of wavelength measurement

^a As in [27].

[71]. In this paper, the PDL of an SMS edge filter is investigated numerically and experimentally, in particular the PDL induced by lateral core offsets.

4.2 Calculation of PDL for an SMS fibre structure

The SMS fibre structure is shown in the inset figure in Fig. 21. It is formed by splicing a step-index multimode fibre (MMF) between two standard singlemode fibres (SMF). A brief review of the design, fabrication, and characterisation of an SMS edge filter can be found in [65]. For a MMF length of 44.44 mm, with a core/cladding diameter of 9/125 μm for the SMF and 105/125 μm for the MMF, the calculated spectral response is shown in Fig. 21. A negative slope edge filter response can be obtained in a wavelength range of about 20 nm from 1505 to 1525 nm.

To investigate polarization dependent effects, a modal propagation analysis (MPA) was performed in the Cartesian coordinate system with a set of calculated guided modes using the finite difference method (FDM) [70]. It should be noted that FDM calculates a set of all possible guided modes and can be calculated for quasi TE (E_x) and quasi TM (E_y) modes, allowing investigation of polarization effects. The PDL is defined as the difference in the transmission loss (L_s) between the quasi TE and quasi TM modes in dB as

$$PDL = |L_{s_{TE}} - L_{s_{TM}}|. \quad (4.1)$$

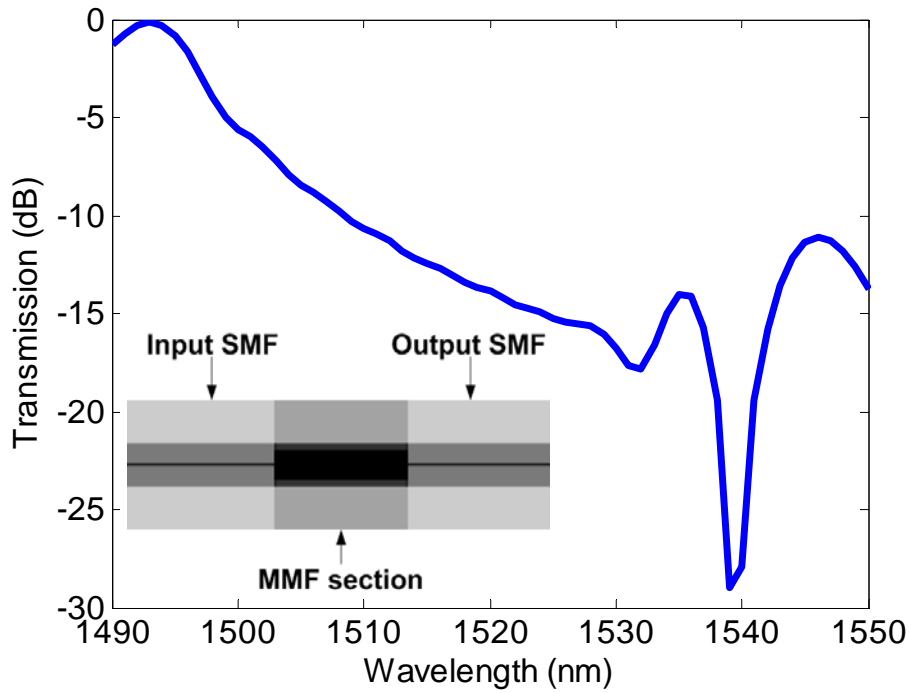


Figure 21 Schematic structure of an SMS fibre structure (inset). Calculated spectral response of SMS fibre structure

The splicing process can introduce lateral core offsets between the SMS fibre cores, that is the input/output SMFs may have lateral core offsets relative to the centre of the MMF core. In addition the two lateral core offsets at each end of the MMF may also have a different orientation relative to each other, which will henceforth be referred to as a rotational offset. To analyze the PDL of an SMS fibre structure, a means to precisely describe lateral and rotational offsets is needed. Fig. 22(a) and 22(b) show the interfaces between the input SMF and the MMF section cores and the MMF section and the output SMF cores, respectively. Where the lateral core offsets of the input and output SMF have the same orientation, the rotational core offset is defined as 0° . Rotational core offsets of

90° and 180° are also shown in Fig. 22(b).

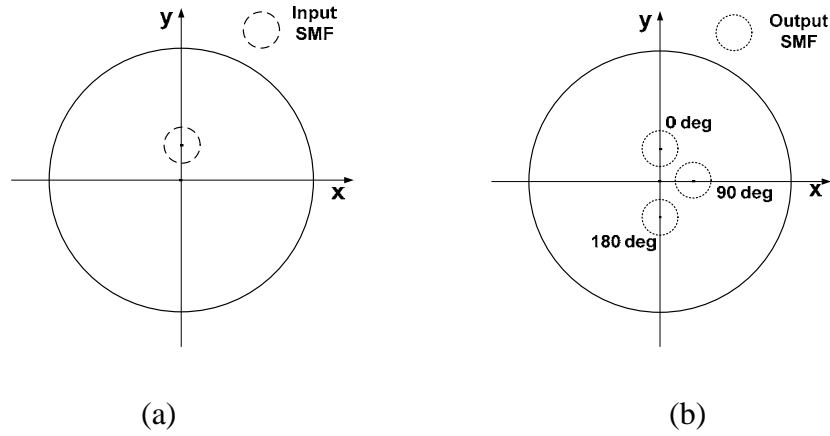


Figure 22 Interfaces of input/output SMF core to the MMF core (a) position of input SMF core, and (b) position of output SMF core

The PDL of an SMS edge filter due to the lateral and rotational core offset was calculated using (4.1). Fig. 23 shows the PDL at a wavelength of 1510 nm for a rotational core offset from 0 to 180° for lateral core offset values of 1, 2, 3, and 4 μm . The limit of 4 μm is chosen because in [70] it was shown that the spectral responses of an SMS edge filter degrades significantly when the lateral core offsets exceeds the SMF core radius. The PDL depends on the lateral and rotational core offsets. Generally, a larger lateral core offset induces a higher PDL. However, it is clear that the PDL at the rotational core offset of 90° has the lowest PDL for the lateral core offsets from 1 to 4 μm .

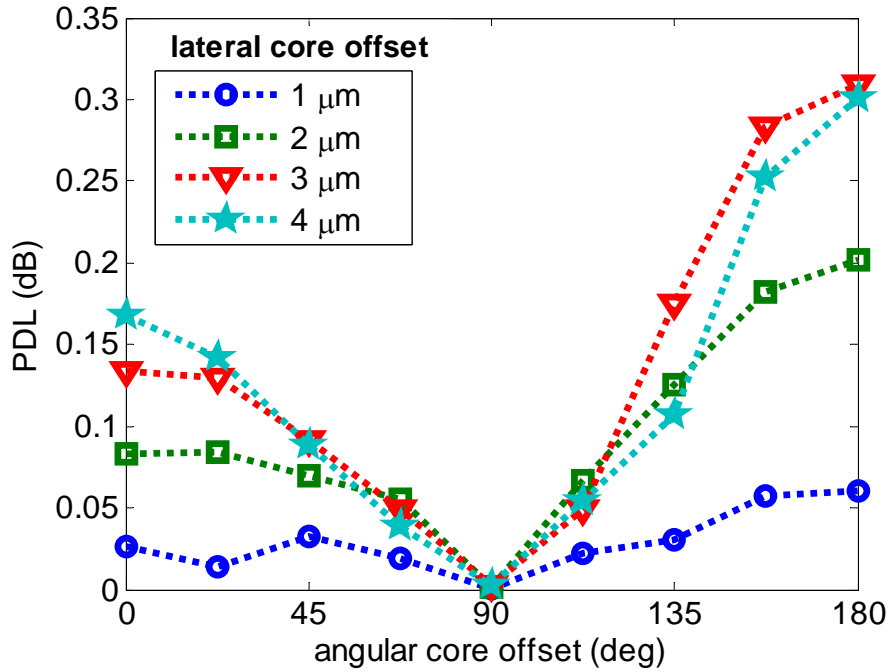


Figure 23 Calculated PDL for several lateral core offsets at the rotational core offset from 0 to 180°

The physical insight into the results in Fig. 23 is as follows. Assuming some lateral core offset of the input SMF is as in Fig. 22(a), the field profile at the output end of the MMF section depends on the input field polarization state of the quasi TE mode (x -directed) or quasi TM mode (y -directed). In turn, the transmission loss for each mode depends on the overlap between the field profile at the output end of the MMF section and the eigen-mode profile of the output SMF. A low PDL occurs when the overlap profiles for the TE and TM modes are similar. At a rotational core offset of 90°, the orientation between the input/output SMF and the input field direction of TE/TM are parallelized. Thus, the overlap between the field profile at the output end of the MMF section and the eigen-

mode profile of the output SMF for both TE and TM modes are similar and the PDL is minimized.

To illustrate this further, the field amplitude profiles at the output end of the MMF section when the input SMF has a lateral core offset of $4\ \mu\text{m}$ are shown in Fig. 24(a) and 24(b) for TE and TM modes, respectively. Fig. 24(c) and 24(d) are the same profiles but with greater magnification, in the vicinity of the output SMF position. It can be seen from the magnified images that the amplitude profiles for the TE and TM modes are slightly different, and this difference in the amplitude profiles is presented in Fig. 24(e). It is clear that the difference in the amplitude for TE and TM modes varies significantly with the co-ordinates within the cross-section of the output end of the MMF. In the regions corresponding to 90° or 270° rotational offsets the difference between TE and TM amplitudes is lower compared to the positions corresponding to 0 and 180° rotational offsets as in Fig. 23. Thus, when the output SMF is positioned so that its core centre is at the point of minimal difference thus, has a rotational core offset of 90° , the PDL is minimized. Therefore, during the fabrication of an SMS edge filter it is desirable to have a low lateral core offsets but should lateral offsets occur, rotating the output SMF relative to the input SMF by 90° can mitigate the effect on PDL of lateral offset. The resultant PDL of the SMS structure is minimized.

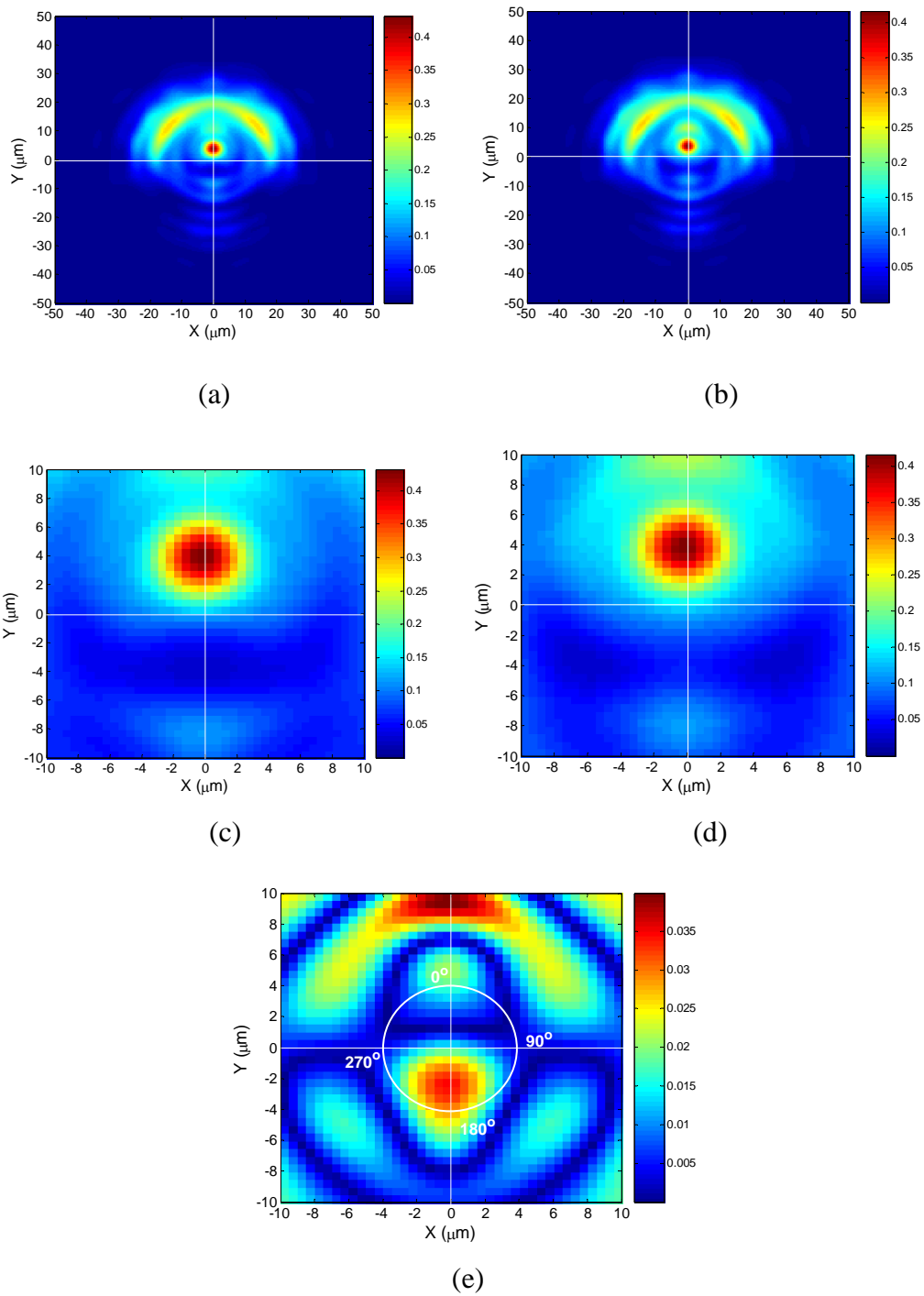


Figure 24 Field amplitude profile at the output end of the MMF section (a) TE mode, (b) TM mode; close up images: (c) TE mode, (d) TM mode, and (e) the difference in the amplitude profiles between TE and TM modes

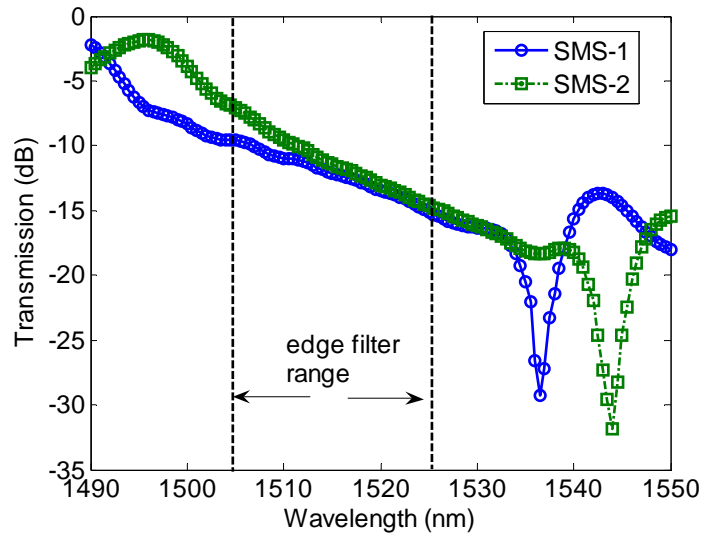
4.3 Experimental results

The SMS edge filter described above was fabricated using a precision Fujikura CT-07 cleaver and a Sumitomo type-36 three-axis fusion splicer. Four edge filters based on SMS structures were fabricated to investigate the PDL due to the lateral and rotational core offsets.

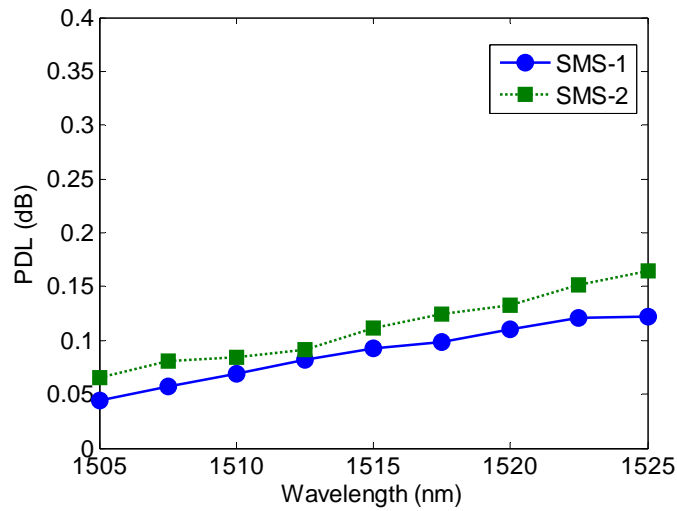
Firstly, two edge filters, SMS-1 and SMS-2 were fabricated using an automatic splicing mode where there is no user control of lateral and rotational cores offsets. The transmission responses of the fabricated SMS edge filters were measured using a tunable laser TUNIC PLUS and a power meter and these results are shown in Fig. 25(a). It is clear that the wavelength range of 1505 to 1525 nm is suitable for an edge filter application. The MMF length of SMS-1 and SMS-2 is circa $44.4 \text{ mm} \pm 0.2 \text{ mm}$, corresponding to $\mp 8 \text{ nm}$ shifts in the spectral response [72]. The lateral core offsets are circa 0.5 to 1 μm according to the fusion splicer's post splicing report.

To measure the PDL of the SMS edge filters, a fibre polarization controller was used to change the polarization state of the input signal. The SMS fibre structures were fixed to a rigid base using super glue, to prevent bending, twisting and strain effects of the SMS structure. The transmission response was measured and the difference between the maximum and minimum transmission response was calculated as the PDL. The PDL of the fabricated SMS edge filters were measured within the wavelength range with an increment of 2.5 nm as shown in Fig. 25(b). The PDL of SMS-1 and SMS-2 produced using the automatic splicing mode shows an average PDL of 0.088 and 0.112 dB, respectively. A standard deviation of the average PDL within the wavelength

range is $\pm 1.685 \times 10^{-3}$ and $\pm 1.886 \times 10^{-3}$ for SMS-1 and SMS-2, respectively. The measured PDL results include the inherent PDL of the system which is about 0.03 dB.



(a)



(b)

Figure 25 Measured results of SMS edge filters using the automatic splicing mode (a) spectral responses, (b) PDL

Secondly, SMS-3 and SMS-4, with MMF lengths of about 44.4 mm were fabricated using an attenuation splicing mode with the same lateral core offsets as in the case of the auto mode, that is 3.31 μm , but with different rotational core offsets of 90° and 180° , respectively. A given lateral offset can be achieved using the splice attenuation setting of the fusion splicer. A splicing attenuation of 1 dB, which is the minimum value, corresponds to a lateral core offset of 3.31 μm . Fig. 26 shows a screenshot in the vicinity of the output splice, using the attenuation splicing setting. The screenshot shows the MMF and the SMF (M-S structure) on the left and right side, respectively.

To achieve different rotational offsets in our experiments the input splice for the SMS has a lateral core offset applied prior to fusion such that the input SMF is shifted in the y-axis by 3.31 μm as in Fig. 22(a). Fusion is then carried out but before the spliced fibres are removed from the splicing machine the top of the input SMF is carefully marked. To splice the other end of the MMF, the S-M structure is again placed in the splicing machine, with a y-axis shift of 3.31 μm . However, the rotational position is controlled by rotating the S-M structure from the reference marker to the desired rotational core offset.

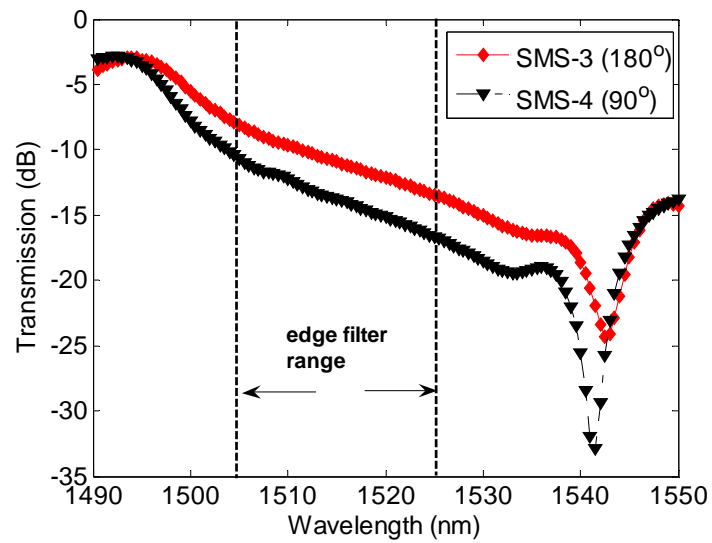
The transmission responses of SMS-3 and SMS-4 were measured as shown in Fig. 27(a). The wavelength range of 1505 to 1525 is suitable for an edge filter application. The measured PDL of SMS-3 and SMS-4 is shown in Fig. 27(b). The average PDL of SMS-3 and SMS-4 for the rotational core offset of 180° and 90° are 0.215 and 0.092 dB, respectively. The standard deviation of the average PDL within the wavelength range is $\pm 1.733 \times 10^{-3}$ and $\pm 1.423 \times 10^{-3}$ for SMS-3 and SMS-4, respectively. It is clear from Fig. 27(b) that the average PDL

of SMS edge filter decreases noticeably for the case of a rotational core offset of 90° . It is also clear from Fig. 25(b) and Fig. 27(b), that the average PDL depends on the lateral offsets, where a lower lateral core offset exhibits a lower PDL.

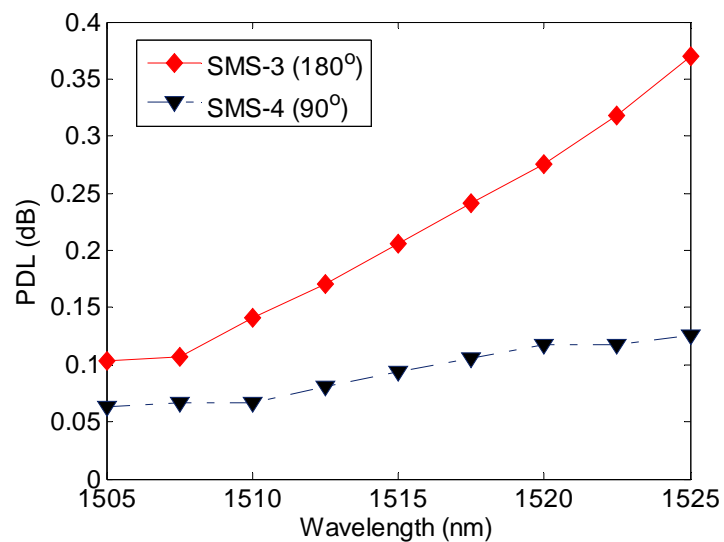


Figure 26 Screenshot of the splicing process using attenuation splicing mode

It can be concluded that the main source of PDL for an SMS edge filter is lateral core offset. Where lateral core offsets do exist, the value of the rotational core offset can either increase or decrease the net PDL. Therefore, to minimize the PDL, it is necessary to ensure low lateral core offsets but if lateral offsets cannot be avoided then control of the rotational core offset is needed during the fabrication of an SMS edge filter. It is also preferable to use a three axis adjustment fibre fusion splicer instead of a single axis adjustment (a fixed V-grove) fibre fusion splicer. Using a three axis adjustment splicer can minimize the lateral offsets that arise because of the limited core-cladding concentricity of the fibres and in turn can minimize both the overall loss and the PDL.



(a)



(b)

Figure 27 Measured results of SMS edge filters with the rotational core offsets of 180° and 90° (a) spectral responses, (b) PDL

4.4 Conclusion

The PDL of an SMS fibre-based edge filter has been investigated. An MPA based on FDM was used to analyze the PDL of SMS edge filter with core offsets. It was

demonstrated that the PDL of the SMS edge filter depends on its lateral and rotational core offsets. Lateral core offsets are undesirable as they will increase the PDL for the SMS edge filter. However, if lateral offsets do occur, then by introducing a rotational core offset of 90° , the PDL can be reduced considerably.

4.5 References

- [64] S. M. Melle, K. Liu, and R. M. Measures, "Practical fibre-optic Bragg grating strain gauge system," *App. Opt.*, vol. 32, pp. 3601-3609, 1993.
- [65] A. M. Hatta, G. Farrell, Q. Wang, G. Rajan, P. Wang, and Y. Semenova, "Ratiometric wavelength monitor based on singlemode-multimode-singlemode fibre structure", *Microw. Opt. Technol. Lett.*, vol. 50, pp. 3036-3039, 2008.
- [66] W. S. Mohammed, P. W. E. Smith, and X. Gu, "All-fibre multimode interference bandpass filter," *Opt. Lett.*, vol. 31, pp. 2547-2549, 2006.
- [67] D. P. Zhou, L. Wei, W. K. Liu, Y. Liu, and J. W. Y. Lit, "Simultaneous measurement for strain and temperature using fibre Bragg gratings and multimode fibres," *App. Opt.*, vol. 47, pp. 1668-1672, 2008.
- [68] E. Li, G.-D. Peng, "Wavelength-encoded fibre-optic temperature sensor with ultra-high sensitivity," *Opt. Commun.*, vol. 281, pp. 5768-5770, 2008.
- [69] A. M. Hatta, G. Rajan, Y. Semenova, and G. Farrell, "SMS fibre structure for temperature measurement using a simple intensity-based interrogation system," *Electron. Lett.*, vol. 45, pp. 1069-1071, 2009.
- [70] A. M. Hatta, G. Farrell, P. Wang, G. Rajan, and Y. Semenova, "Misalignment limits for a singlemode-multimode-singlemode fibre-based edge filter," *J. Lightw. Technol.*, vol. 27, pp. 2482-2488, 2009.
- [71] G. Rajan, Q. Wang, Y. Semenova, G. Farrell, and P. Wang, "Effect of polarization dependent loss on the performance accuracy of a ratiometric wavelength measurement system," *IET Optoelectronics*, vol. 2, pp. 63-68, 2008.

- [72] Q. Wang, G. Farrell, and W. Yan, "Investigation on singlemode-multimode-singlemode fibre structure," *J. Lightw. Technol.*, vol. 26, pp. 512-519, 2008.

Chapter 5

Temperature dependence of an SMS fibre structure-based edge filter

The effect of temperature on the optical and mechanical properties of silica means that the temperature changes do affect the spectral performance of edge filter fibre-based devices. This chapter analyzes the temperature dependence of an edge filter based on an SMS fibre structure numerically and experimentally. The MPA presented in Chapter 2 is used to investigate the temperature dependence of the SMS fibre structure-based edge filter. The influence of two parameters – the thermo optic coefficient (TOC) and the thermal expansion coefficient (TEC) on the temperature dependence of an SMS edge filter is investigated numerically. It is shown the TOC makes more significant contribution to the temperature dependence compared to the TEC. Experimental studies of temperature dependence for X-type edge filters in the ratiometric system are presented. It is shown that a small temperature variation can still induce a ratio variation significant enough to induce a wavelength measurement error. However, the linear relation between the ratio and temperature means that it is feasible to apply

calibration correction. By knowing the operating temperature, the correction required to the calibrated ratio response over the whole wavelength range can be determined. It is proposed and demonstrated that self-monitoring of temperature can be carried out using an expanded ratiometric scheme.

Analysis of temperature dependence for a ratiometric wavelength measurement system using SMS fibre structure-based edge filters^a

Keywords: temperature dependence, edge filter, multimode fibre

Abstract Temperature dependence of an edge filter based on singlemode-multimode-singlemode (SMS) fibre structure is investigated numerically and experimentally. The experimental results and numerical results are in good agreement within an operational temperature range from 10 to 40 °C. It is found that the thermo-optic coefficient (TOC) has a more significant effect on the temperature dependence of an SMS edge filter compared to the thermal expansion coefficient (TEC). In the ratiometric wavelength measurement using two SMS edge filters, a small temperature variation can induce the ratio variation and in turn the wavelength measurement error. It is found the SMS edge filter's response to both wavelength and temperature is linear. It is proposed that self monitoring of temperature can be carried out using an updated ratiometric scheme. Self-

^a A. M. Hatta, Y. Semenova, G. Rajan, P. Wang, J. Zheng and G. Farrell, "Analysis of temperature dependence for a ratiometric wavelength measurement system using SMS fibre structure-based edge filters" *Optics Communications*, accepted for publication on 4th November 2009.

monitoring of the temperature reduces temperature induced wavelength error to ± 10.7 pm at 1545 nm, regardless of the ambient temperature variation.

5.1 Introduction

Singlemode-multimode-singlemode (SMS) fibre structures have been demonstrated experimentally as an all-fibre implementation of a bandpass filter, an edge filter, a wavelength encoded temperature sensor, and a strain and temperature sensor [73]-[77]. An SMS fibre structure is fabricated by splicing a specified length of a multimode fibre (MMF) with two singlemode fibres (SMF) at the ends of MMF. This configuration offers simplicity, an all fibre configuration, and low cost.

Recently, the application of SMS fibre structures as edge filters for wavelength monitoring [74] and on the effect of misalignment of the SMF-MMF-SMF cores [75] were reported. Wavelength measurement is essential for a fibre-Bragg-grating (FBG)-based sensing system. Among the available schemes, an all-fibre ratiometric power measurement technique offers a simple configuration, competitive resolution, and high speed measurement compared to an active scanning method. A ratiometric scheme converts the input wavelength shift into a signal intensity measurement. An all-fibre ratiometric wavelength monitor consists of a 3 dB fibre coupler^a with two outputs to which a fibre edge filter arm with a well defined spectral response and a reference arm are attached. Alternatively, two fibre edge filter arms with overlapping opposite slope spectral responses can be used. The use of two edge filters can increase the resolution of the measurement system [78]. Two fibre edge filters with overlapping and

^a 10202A-50 - 2x2 SM Coupler

opposite slope spectral responses, a so-called “X-type spectral response” based on SMS fibre structure have been investigated numerically and experimentally [74].

The effect of temperature on the optical and mechanical properties of silica means that temperature changes could affect the spectral performance of devices based on an SMS fibre structure. An investigation has been carried out previously [79] on the peak wavelength shift of the transmission spectral response of an SMS structure due to temperature change and the reduction of this peak shift to a low value by temperature compensation. However, in an edge filter-based ratiometric wavelength measurement scheme, even low values of peak wavelength shift can still induce sufficient ratio variation to degrade wavelength measurement accuracy [80]. In this paper, it is presented an analysis verified by experimental results of the effect of temperature on the overall transmission response of an SMS structure used as an edge filter. In Section 5.2, it is investigated the temperature dependence of an SMS-based edge filter and find that there is a linear relationship between temperature and wavelength. Importantly there is also a linear response to temperature and this suggests that self monitoring of temperature is possible to reduce wavelength measurement error to a minimum, using an updated ratiometric system. This is presented in Section 5.3.

5.2 Temperature dependence in an SMS edge filter

It is useful to initially consider the design of the X-type spectral response SMS edge filters. In order to design an SMS fibre edge filter, a modal propagation analysis (MPA) for linearly polarized (LP) modes was used [73], [81]. A brief review of the design, fabrication and measurement of the X-type SMS edge filters

can be found in [74]. A standard SMF type SMF28 and an MMF type AFS105/125Y were used with core/cladding diameters of 8.3/125 μm and 105/125 μm , respectively. Two lengths of MMF were chosen to provide the X-type SMS edge filters within a wavelength range 1530 to 1560 nm (typical for an FBG sensing), $L_1 = 43.57$ mm and $L_2 = 42.63$ mm for SMS-1 and SMS-2, respectively. The calculated and measured results for SMS edge filters are shown in Fig. 28. The measured results show a good agreement with the numerical results. The discrepancy between the calculated and measured results is most likely a consequence of splice insertion losses.

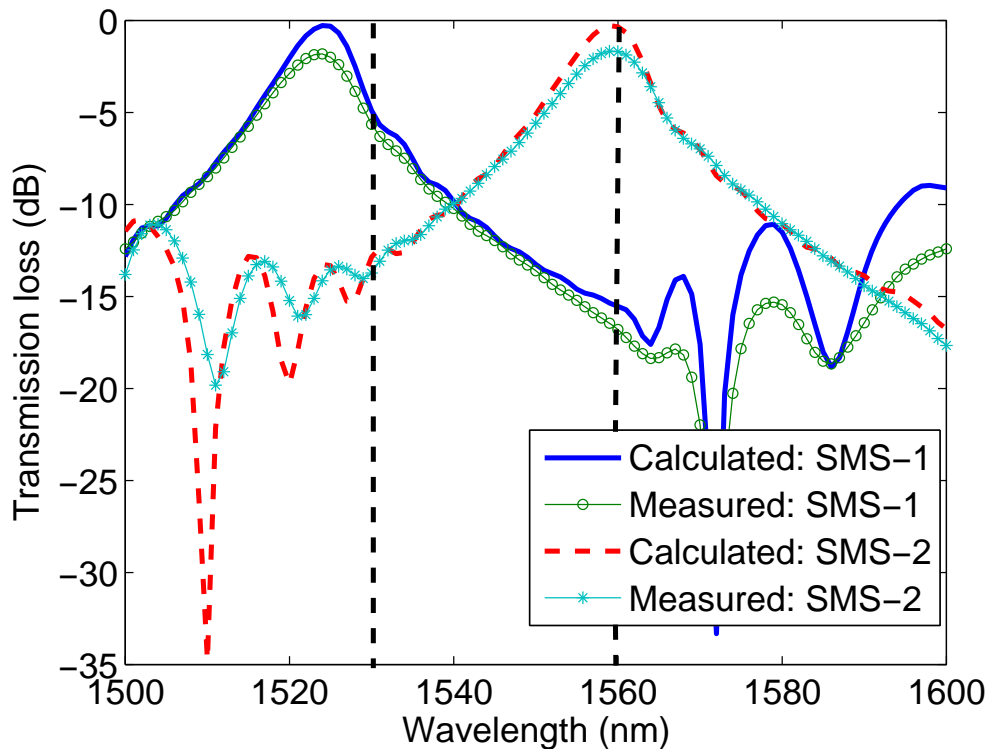


Figure 28 Calculated and measured two edge filters X-type spectral response

It is well known that there are two parameters which characterize the effect of temperature on the fibre, the thermal expansion coefficient (TEC) and the thermo-optic coefficient (TOC). The TEC characterizes the physical expansion or contraction of the material's vol., while the TOC characterizes refractive index change in response to temperature change. Using the TEC and TOC, the change in core radius (R), MMF length (L), and the refractive index (n) due to a temperature variation (ΔT), can be expressed, respectively, as

$$R_{(smf,mmf)T} = R_{(smf,mmf)0} + \alpha \cdot R_{(smf,mmf)0} \cdot \Delta T \quad (5.1a)$$

$$L_{(1,2)T} = L_{(1,2)0} + \alpha \cdot L_{(1,2)0} \cdot \Delta T \quad (5.1b)$$

$$n_{(core,clad)T} = n_{(core,clad)0} + \xi \cdot n_{(core,clad)0} \cdot \Delta T \quad (5.1c)$$

where α and ξ are the TEC and the TOC, respectively.

To gain an insight into the effect of temperature changes on the transmission loss of an SMS-based edge filter, it was investigated experimentally and numerically the effect of temperature at a single wavelength. The experimental setup was built as shown in Fig. 29. The SMS edge filter was attached to a thermoelectric Peltier cooler, which was controlled by a precision digital temperature controller (ITC 510, Thorlabs), while a digital resistance thermometer sensor probe was also attached to accurately measure the temperature.

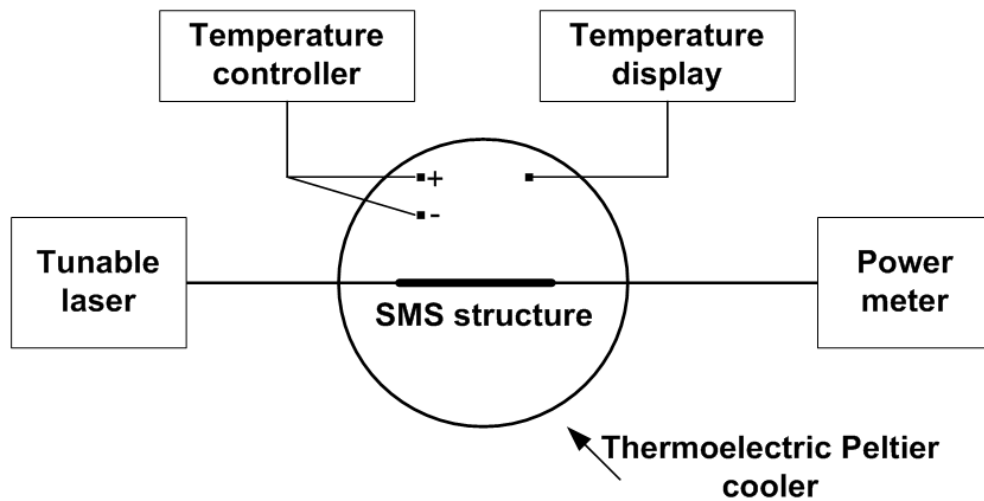
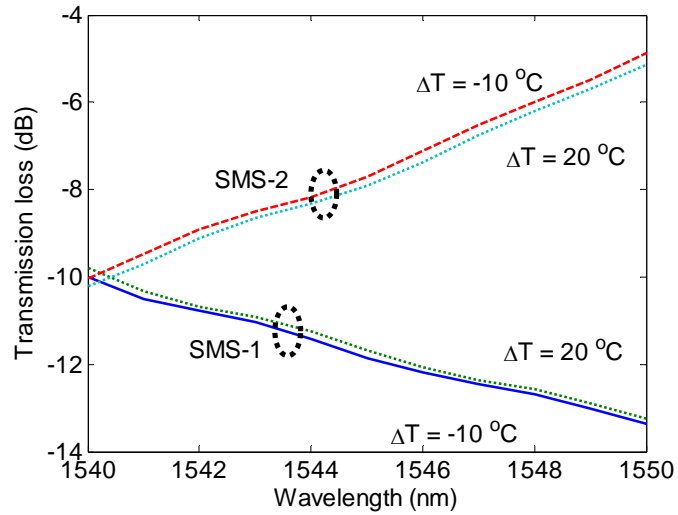


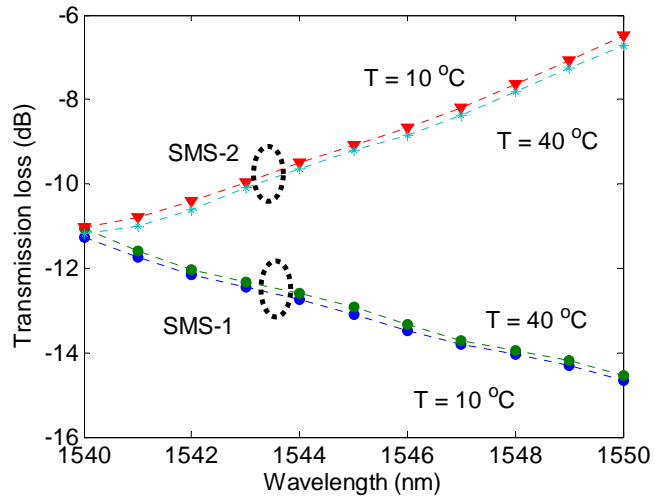
Figure 29 Schematic set-up for measuring the temperature dependence on the SMS edge filter transmission loss

To calculate the temperature dependence of the transmission loss, on the basis of parameters in [79], it is assumed $\alpha = 5 \times 10^{-7} / ^\circ\text{C}$ and $\xi = 6.9 \times 10^{-6} / ^\circ\text{C}$ for both the SMF and MMF [79]. By using an MPA the transmission loss from 1540 to 1550 nm for the temperature of 10 and 40 °C was calculated and presented in Fig. 30(a). The measured results are also shown in Fig. 30(b). One can see both calculated and measured results for SMS-1 and SMS-2 show that an increase in temperature results in a spectral response shift to the higher wavelength as in [82], [83]. The change in transmission loss from the value at 20 °C is calculated for temperatures from 10 to 40 °C, at a wavelength of 1545 nm. The calculated and measured results for the transmission loss change over the temperature range for SMS-1 and SMS-2 are shown in Fig. 31. The calculated and measured results are in good agreement. From Fig. 31, it is also clear that the change in transmission loss for both SMS-1 and SMS-2 has a linear response with temperature. The

transmission loss difference between 10 to 40 °C is 0.171 dB for SMS-1 and 0.134 dB for SMS-2.



(a)



(b)

Figure 30 Transmission loss response at the temperature of 10 and 40 °C: (a) calculation results (b) measurement results

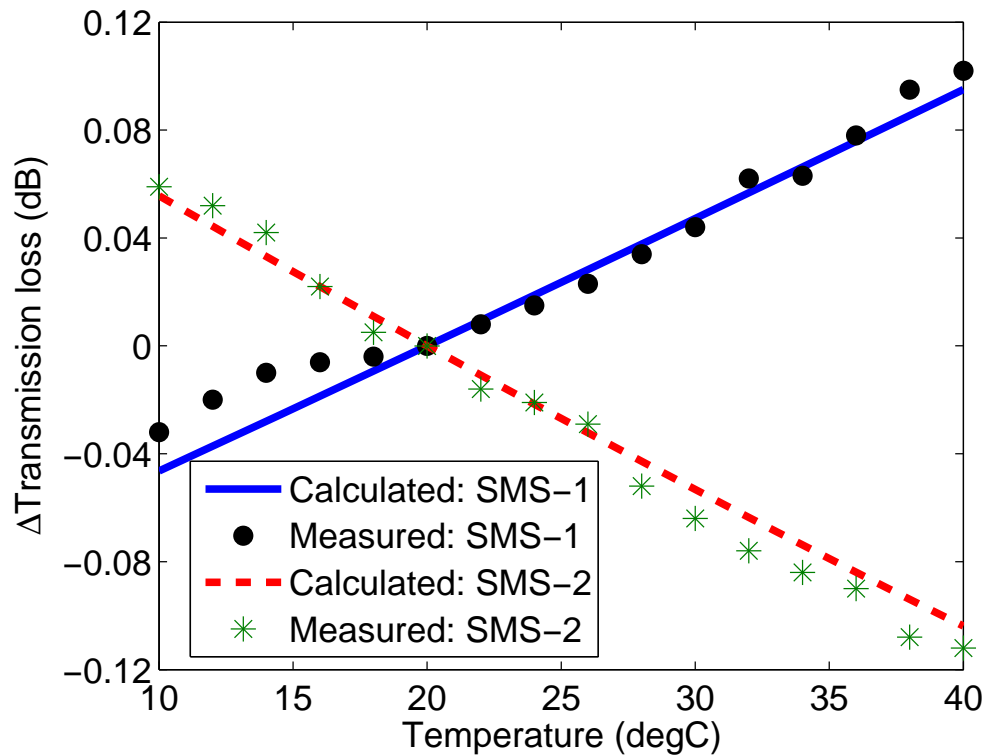


Figure 31 Transmission loss change as a function of temperature at a wavelength of 1545 nm for a reference temperature of 20 °C

It is useful to analyze the separate contributions to temperature dependent effects of the TEC and TOC. The transmission loss change, relative to 20 °C, due to an increase in temperature is calculated for TEC only and then for TOC only and is compared to the contribution of both TEC and TOC taken together. As an example for SMS-1 at a wavelength of 1545 nm, the calculated transmission loss change due to a change in temperature for the contribution of TEC and TOC individually, and for the contribution of TEC and TOC together are shown in Fig. 32. It can be seen, with a change in temperature, the transmission losses for the TEC and TOC parameters have opposite slopes and thus induce opposite transmission spectral response shifts. However, the TEC has a significantly lower

contribution to the temperature dependence of the edge filter transmission loss compared to the TOC.

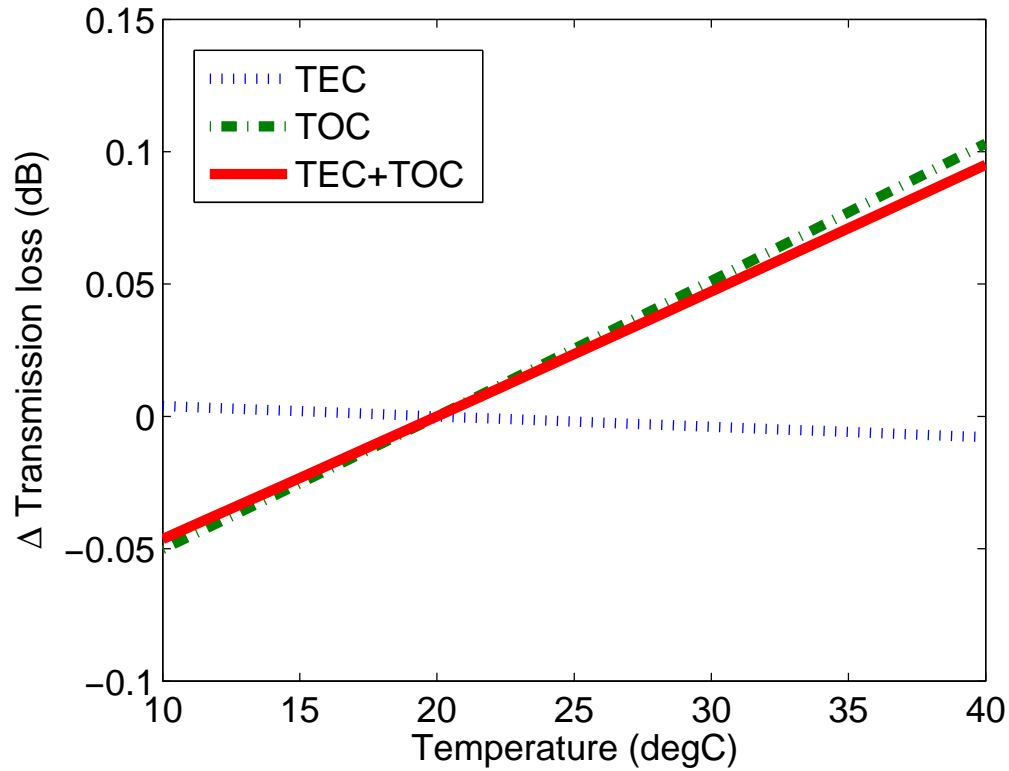


Figure 32 Calculated transmission loss change due to temperature change for TEC, TOC separately and also for TEC and TOC together

5.3 Temperature dependence in the ratiometric wavelength measurement system

To investigate the effect of temperature on the accuracy of wavelength measurement, the temperature dependence for a ratiometric wavelength measurement system, similar to that described in [74] using a pair of SMS structures as X-type filters, was studied. The input signal from a tunable laser was

split into two equal intensity signals using a 3 dB fibre coupler^a (see inset figure in Fig. 33). One of the signals was transmitted through SMS-1 and the other through SMS-2. A dual channel power meter was placed at the ends of both arms. The two SMS edge filters were attached to the thermoelectric Peltier cooler. The ratio spectral response was measured from 10 to 40 °C within the wavelength range 1530-1560 nm. Fig. 33 shows the measured optical power ratio spectrum for several temperatures. The ratio response difference between 10 and 40 °C is 0.306 dB at a wavelength of 1545 nm (see inset graph in Fig. 33). The ratio change for a ± 5 °C temperature change is ± 0.051 dB. While this is a small change in ratio, the impact on wavelength accuracy is still significant. From the measured results it is estimated that a temperature variation of ± 5 °C at 20 °C induces a wavelength error of ± 67.4 pm at 1545 nm. This error is very significant as the inherent error in a ratiometric system due to noise and other non-temperature related effects can be less than 10 pm [74].

Therefore in order to maintain accuracy when utilizing such SMS structures as edge filters, there are two possible solutions: (i) use a packaging material for the SMS structure with a suitable TEC value which compensates for temperature induced changes in the SMS structure [79] or (ii) actively monitor the filter temperature and correct the calibration as required (active temperature stabilization of the filter is possible but is more complex than monitoring). For the solution involving the use of a packaging material, a small un-compensated temperature drift due to a small mismatch in the TEC value of packaging material and the SMS can lead to a significant wavelength measurement error. For the

^a 10202A-50 - 2x2 SM Coupler

temperature monitoring solution, from the inset graph in Fig. 33, the linear relation between the ratio and temperature shows that it is feasible to apply a calibration correction. By knowing the operating temperature, the correction required to the calibrated ratio response over the whole wavelength range can be determined.

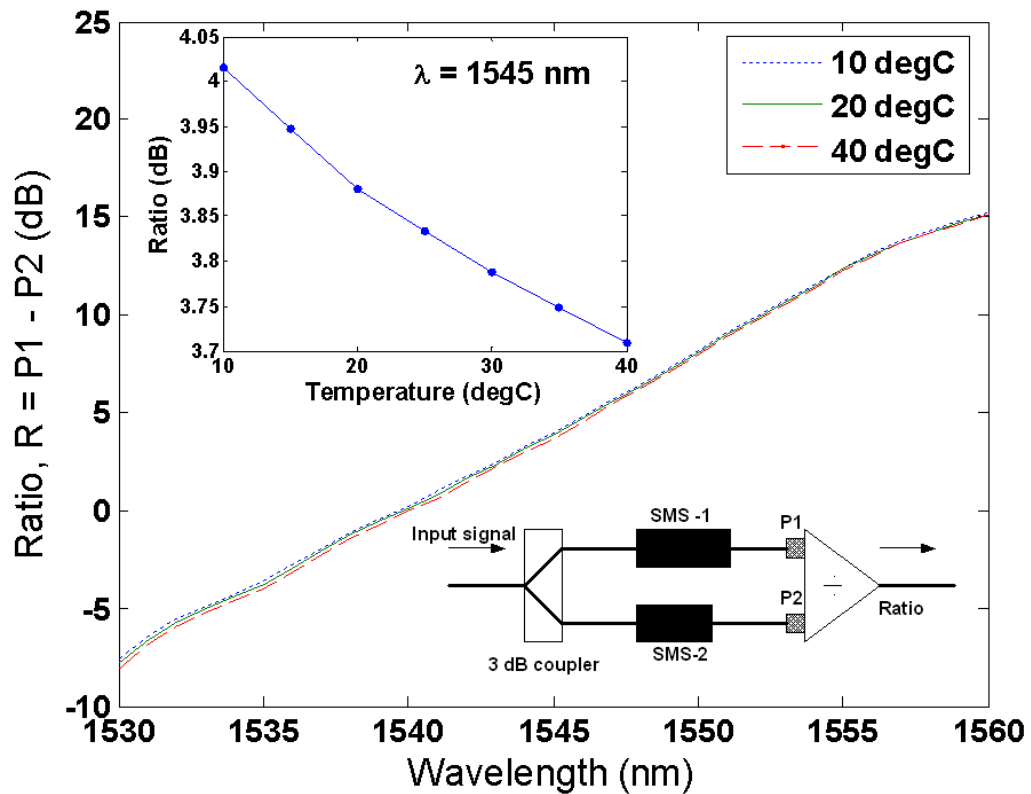


Figure 33 Measured ratio at different temperatures within the wavelength range. Schematic configuration of ratiometric wavelength measurement (inset figure). Temperature response at 1545 nm (inset graph)

The linearity of the SMS edge filter's response to both wavelength and temperature potentially allows one to use the SMS structure to monitor its own temperature, with the added advantage that simultaneous measurement of the

wavelength and temperature is possible if required. To implement a self-monitoring approach an updated ratiometric scheme is proposed as in Fig. 34. A 3 dB coupler and a power meter are added to the existing ratiometric scheme as in the inset figure in Fig. 33. The ratio $R_1 = P_{ref} - P_1$ and $R_2 = P_{ref} - P_2$ in dB are measured. The wavelength change, $\Delta\lambda$, and temperature change, ΔT , to the ratio change ΔR_1 and ΔR_2 can be expressed as:

$$\begin{bmatrix} \Delta R_1 \\ \Delta R_2 \end{bmatrix} = \begin{bmatrix} \alpha_1 & \beta_1 \\ \alpha_2 & \beta_2 \end{bmatrix} \begin{bmatrix} \Delta\lambda \\ \Delta T \end{bmatrix} = M \begin{bmatrix} \Delta\lambda \\ \Delta T \end{bmatrix}, \quad (5.2)$$

where $\alpha_{1,2}$ and $\beta_{1,2}$ are the matrix coefficients of M that correspond to the wavelength and temperature slopes respectively, which can be determined experimentally. Thus, the wavelength and temperature changes can be determined simultaneously from

$$\begin{bmatrix} \Delta\lambda \\ \Delta T \end{bmatrix} = M^{-1} \begin{bmatrix} \Delta R_1 \\ \Delta R_2 \end{bmatrix}, \quad (5.3)$$

where M^{-1} is the inverse matrix of M . The resolution of wavelength and temperature measurement can be determined from:

$$\begin{bmatrix} \delta(\Delta\lambda) \\ \delta(\Delta T) \end{bmatrix} = abs(M^{-1}) \begin{bmatrix} \delta(\Delta R_1) \\ \delta(\Delta R_2) \end{bmatrix} \quad (5.4)$$

where $\delta(\Delta R_{1,2})$ is the uncertainty in ratio measurement.

To determine the wavelength and temperature coefficients, pre-determined wavelength and temperature changes were applied separately to the ratiometric system. It was measured, the ratio R_1 and R_2 in the wavelength range of 1540 to 1550 nm at a fixed temperature of 10 °C as shown in Fig. 35(a). A smaller wavelength range is chosen to ensure a piece-wise linear response. The wavelength was then fixed at 1540 nm and the temperature was changed. Fig.

35(b) shows the ratio R_1 and R_2 with the respect to temperature changes at the wavelength 1540 nm. The measured ratios R_1 and R_2 have a good linear response^a with variations in wavelength and temperature. The coefficients $\alpha_{1,2}$ and $\beta_{1,2}$ can be obtained as a ratio slope with $\alpha_1 = -0.4588$ dB/nm, $\alpha_2 = 0.331$ dB/nm, $\beta_1 = 0.0016$ dB/°C, and $\beta_2 = -0.0076$ dB/°C. Assuming an uncertainty in ratio measurement of 0.003 dB, the estimated measurement resolution for wavelength and temperature are 9.8 pm and 0.8 °C, respectively. Without temperature self monitoring the temperature induced wavelength error will be high, eg. ± 67.4 pm for a 5 °C temperature variation. In practice much higher worst case ambient temperature variations could occur and induce even larger errors. Self monitoring of the temperature reduces the worst case temperature induced wavelength error to ± 10.7 pm at 1545 nm, regardless of ambient temperature variations, a value comparable to errors induced by noise and other sources.

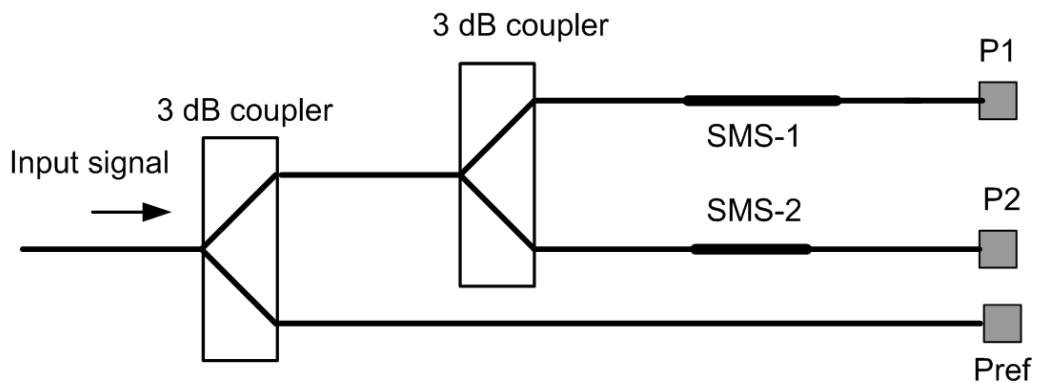
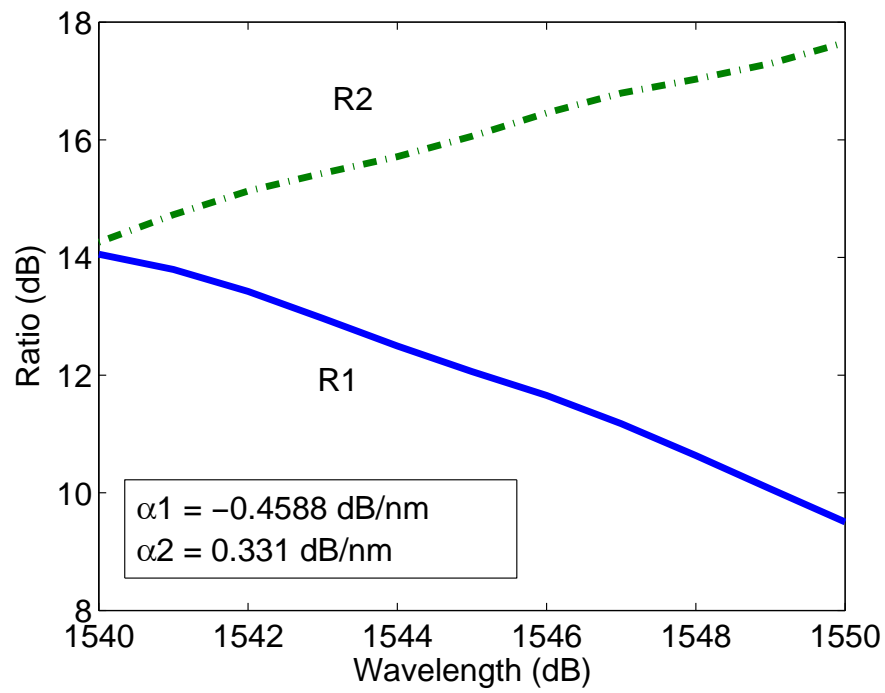
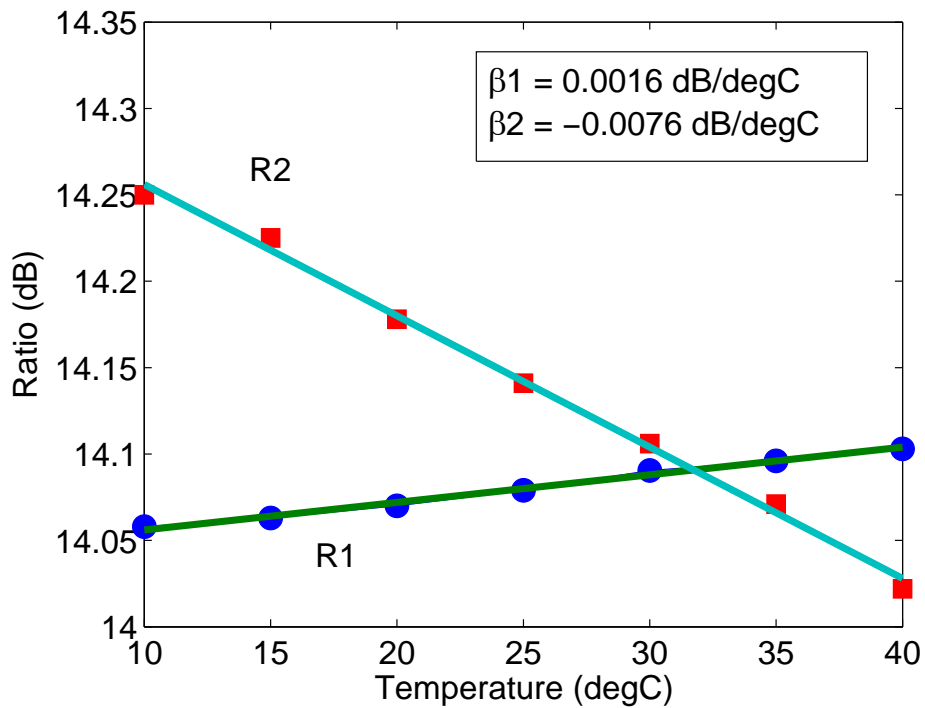


Figure 34 Updated schematic ratiometric system to allow self-monitoring of temperature

^a The correlation coefficients from a linear regression analysis of the wavelength responses (shown in Fig. 35(a)) are 0.994 and 0.996, and for the temperature responses (shown in Fig. 35(b)) are 0.99 and 0.996, for the ratios R_1 and R_2 , respectively.



(a)



(b)

Figure 35 (a) wavelength coefficients at the temperature of 10 °C, and (b) temperature coefficients at the wavelength of 1540 nm

It should be noted that the estimated wavelength error above is based on the matrix coefficients α and β at a fixed temperature of 10 °C and a fixed wavelength of 1540 nm, respectively. However, detailed experimental results have shown that there is a variation of matrix coefficients α and β with temperature and wavelength. For the temperature range from 10 to 40 °C and a wavelength range from 1540 to 1550 nm the measured matrix coefficients variations are $\alpha_1 = -0.46 \pm 3.19 \times 10^{-4}$ dB/nm, $\alpha_2 = 0.33 \pm 1.42 \times 10^{-3}$ dB/nm, $\beta_1 = 1.68 \times 10^{-3} \pm 1.42 \times 10^{-4}$ dB/°C, and $\beta_2 = -7.63 \times 10^{-3} \pm 7.48 \times 10^{-4}$ dB/°C. The calculated results are comparable with matrix coefficient variations thus: $\alpha_1 = -0.51 \pm 1.66 \times 10^{-3}$ dB/nm, $\alpha_2 = 0.34 \pm 2.16 \times 10^{-3}$ dB/nm, $\beta_1 = 3.24 \times 10^{-3} \pm 9.77 \times 10^{-4}$ dB/°C, and $\beta_2 = -5.08 \times 10^{-3} \pm 9.74 \times 10^{-4}$ dB/°C. The measured and calculated matrix coefficients show a good agreement^a. Discrepancies could be attributed to the small wavelength dependent response of the 3 dB couplers used in the measurement and the accuracy of TEC and TOC coefficients used in the calculation. These matrix coefficients variations can increase the error measurement as described in [84]. Self temperature monitoring is still feasible if an artificial neural network (ANN) approach as in [85]-[87] is used rather than the inverse matrix approach above. The ANN can model the nonlinear or linear relationship between the input and output data using several neurons with nonlinear transfer functions. By using sufficient neurons, the ANN can learn the relationship between the input and output data. Therefore, the relationship between $\{\Delta\lambda, \Delta T\}$ and $\{R_1, R_2\}$ can be modelled more accurately by using an ANN

^a The agreement between the measured and calculated values is 90.2%, 97.1%, 51.8%, and 66.6 % for the matrix coefficients α_1 , α_2 , β_1 , and β_2 , respectively.

and it has been reported that the use of ANN can increase the measurement accuracy compared to the inverse matrix approach above [85]-[87].

5.4 Conclusion

An analysis of the temperature dependence of a ratiometric wavelength measurement scheme using SMS fibre structure-based edge filters has been carried out. It has been investigated numerically and experimentally, the effects of temperature on the transmission loss of a dual SMS edge filter. The experimental results are in good agreement with the numerical results^a. It is found that the TOC makes a more significant contribution to the temperature dependence of an SMS edge filter compared to the TEC. The linearity of the SMS edge filter's response to both wavelength and temperature potentially allows one to use the SMS structure to monitor its own temperature using an updated ratiometric scheme, with the additional advantage of simultaneous measurement of the wavelength and temperature if required. It was demonstrated a self-monitoring of the temperature reduces temperature induced wavelength error to ± 10.7 pm regardless of the ambient temperature variation^b. It was also noted that using an artificial neural network could improve accuracy still further^c.

Acknowledgment

The valuable assistance of the National Natural Science Foundation of China (NSFC 60777038) is acknowledged in supporting this research.

^a As in Fig. 31, the measured and calculated discrimination ranges for SMS-1 are 0.141 and 0.134 dB and for SMS-2 are 0.171 and 0.172 dB, respectively.

^b Over a temperature range from 10 to 40 °C.

^c According to [85], the use of ANN model can improve accuracy by a factor of 12-13 times compared to the use of an inverse matrix approach.

5.5 References

- [73] W. S. Mohammed, P. W. E. Smith, and X. Gu, "All-fibre multimode interference bandpass filter," *Opt. Lett.*, vol. 31, pp. 2547-2549, 2006.
- [74] A. M. Hatta, G. Farrell, Q. Wang, G. Rajan, P. Wang, and Y. Semenova, "Ratiometric wavelength monitor based on singlemode-multimode-singlemode fibre structure", *Microw. Opt. Technol. Lett.*, vol. 50, pp. 3036-3039, 2008.
- [75] A. M. Hatta, G. Farrell, P. Wang, G. Rajan, and Y. Semenova, "Misalignment limits for a singlemode-multimode-singlemode fibre-based edge filter," *J. Lightw. Technol.*, vol. 27, pp. 2482-2488, 2009.
- [76] E. Li, G.-D. Peng, "Wavelength-encoded fibre-optic temperature sensor with ultra-high sensitivity," *Opt. Commun.*, vol. 281, pp. 5768-5770, 2008.
- [77] D. P. Zhou, L. Wei, W. K. Liu, Y. Liu, and J. W. Y. Lit, "Simultaneous measurement for strain and temperature using fibre Bragg gratings and multimode fibres," *App. Opt.*, vol. 47, pp. 1668-1672, 2008.
- [78] S. M. Melle, K. Liu, and R. M. Measures, "Practical fibre-optic Bragg grating strain gauge system," *App. Opt.*, vol. 32, pp. 3601-3609, 1993.
- [79] E. Li, "Temperature compensation of multimode-interference-based fibre devices," *Opt. Lett.*, vol. 32, pp. 2064-2066, 2007.
- [80] G. Rajan, Y. Semenova, P. Wang, and G. Farrell, "Temperature-induced instabilities in macro-bend fibre-based wavelength measurement systems," *J. Lightw. Technol.*, vol. 27, pp. 1355-1361, 2009.
- [81] Q. Wang, G. Farrell, and W. Yan, "Investigation on singlemode-multimode-singlemode fibre structure," *J. Lightw. Technol.*, vol. 26, pp. 512-519, 2008.
- [82] S. M. Tripathi, A. Kumar, R. K. Varshney, Y. B. P. Kumar, E. Marin, and J. P. Meunier, "Strain and temperature sensing characteristics of single-mode-multimode-single-mode structures," *J. Lightw. Technol.*, vol. 27, pp. 2348-2356, 2009.

- [83] E. Li, X. Wang and C. Zhang, "Fibre-optic temperature sensor based on interference of selective higher-order modes," *App. Phys. Lett.*, vol. 89, pp. 091119, 2006.
- [84] W. Jin, W. C. Michie, G. Thursby, M. Konstantaki, and B. Culshaw, "Simultaneous measurement of strain and temperature: error analysis," *Opt. Eng.*, vol. 36, pp. 598–609, 1997.
- [85] C. C. Chan, W. Jin, A. B. Rad, and M. S. Demokan, "Simultaneous measurement of temperature and strain: an artificial neural network approach," *IEEE Photon. Technol. Lett.*, vol. 10, pp. 854-856, 1998.
- [86] J. Sun, C. C. Chan, K. M. Tan, X. Y. Dong, and P. Shum, "Application of an artificial neural network for simultaneous measurement of bending curvature and temperature with long period fibre gratings," *Sensors and Actuators A*, vol. 137, pp. 262–267, 2007.
- [87] J. Sun, C. C. Chan, X. Y. Dong, and P. Shum, "Application of an artificial neural network for simultaneous measurement of temperature and strain by using a photonic crystal fibre long-period grating," *Meas. Sci. Technol.*, vol. 18, pp. 2943–2948, 2007.

Chapter 6

New standalone sensors based on an SMS fibre structure

In the previous chapters SMS fibre structures have been implemented as a new type of edge filter for ratiometric wavelength measurement. Several aspects of SMS fibre-based edge filters have been investigated including the effect of misalignment of SMS fibre cores, polarization dependence and temperature dependence.

The second primary objective of this research is to investigate the use of SMS fibre structures as novel standalone optical fibre sensors. As an alternative to FBG-based sensors, SMS fibre structures can be used as sensors with the advantages of low cost and simple fabrication by comparison to FBGs or other optical fibre sensors. In this chapter, SMS fibre structure sensors are interrogated using an intensity-based measurement system, offering low cost, simple configuration, and the potential for high speed measurement compared to an interrogation technique that tracks a peak or a dip in a spectral response using an OSA.

In Chapter 5, the temperature dependence of the SMS fibre structure-based edge filter was described. The existence of strong temperature dependence for the

SMS spectrum and the linear nature suggests that an SMS fibre structure can be utilized as a temperature sensor. In this chapter, the new application of an SMS fibre structure as a standalone sensor of temperature using interrogation based on intensity measurement is investigated numerically and experimentally. The SMS fibre structure is optimized to provide a strong temperature dependence that can be utilized as a temperature sensor. A temperature measurement range of 50 to 200 °C with a potential resolution of better than 0.2 °C is demonstrated. The sensor is simpler and can provide a competitive resolution when compared to an FBG-based temperature sensor. As a demonstration of the competitive resolution, an equivalent FBG-based temperature sensor can resolve a temperature change of ~ 0.1 °C, but requires high wavelength resolution measurement of ~ 1 pm [12]. The proposed sensor can be used for temperature monitoring in industrial process, automotive and aeronautical engines, and other applications.

Another potential application of an SMS fibre structure presented in this chapter is a voltage measurement based on utilizing the strain effect. As a starting point the strain effect in an SMS fibre structure is investigated. For use as a voltage sensor, to transfer the voltage into the strain, a piezoelectric transducer (PZT) is proposed. The SMS fibre structure, attached to the PZT, is utilized in a ratiometric power measurement scheme and is investigated and demonstrated both numerically and experimentally. A DC voltage measurement range from 0 to 100 V with a resolution of about 0.5 V or 0.5% of full scale measurement is demonstrated. The proposed sensor offers a simple configuration, a fast measurement capability, and the potential for kilovolt measurements with a suitable choice of PZT. As a comparison using an FBG alternative, a voltage

measurement range from 0 to 5 kV using an FBG and a suitable PZT can provide a measurement resolution of 3% of full scale^a, significantly worse than that which can be achieved by the proposed SMS sensor.

6.1 SMS fibre structure for temperature measurement using a simple intensity-based interrogation system^b

Keywords: fibre optic sensor, temperature measurement

Abstract: A singlemode-multimode-singlemode (SMS) fibre structure for temperature measurement that utilises a simple intensity-based interrogation system is proposed. The temperature dependence of the SMS fibre structure utilised as a sensor is investigated numerically and experimentally. It is found that a strong temperature dependence for the SMS fibre structure exists at selected wavelengths. The temperature characteristic at such wavelengths is linear in nature and can be used for temperature measurements. The proposed temperature sensor offers a high resolution and accuracy and also benefits from a simple configuration and low cost when compared to other fibre-optic temperature sensors.

^a M. Pacheco, F. M. Santoyo, A. M´endez, and L. A. Zenteno, “Piezoelectric-modulated optical fibre Bragg grating high-voltage sensor,” *Meas. Sci. Technol.*, vol. 10, pp. 777–782, 1999.

^b A. M. Hatta, G. Rajan, Y. Semenova and G. Farrell, “SMS fibre structure for temperature measurement using a simple intensity-based interrogation system,” *Electronics Letters*, vol. 45, no. 21, pp. 1069-1071, 2009.

6.1.1 Introduction

Singlemode-multimode-singlemode (SMS) fibre structures have been demonstrated for use as a bandpass filter, an edge filter, and a wavelength encoded temperature sensor [88]-[90]. Multimode interference (MMI) is the basic operating mechanism of such SMS fibre devices, where interference between modes in the multimode fibre (MMF) occurs along the MMF length. The SMS structure can generate minimum or maximum interference at specific MMF lengths. By precisely optimising the MMF length, different device functions can be implemented.

SMS structures demonstrate temperature dependence and previous investigations have shown that the effect of temperature on the wavelength response of an SMS fibre device can be compensated for by using a suitable packaging material [91]. It is also possible to exploit this temperature dependence to implement a temperature sensor. However, to date the temperature information has been extracted by measuring the temperature-induced shift in the peak wavelength of the SMS spectrum [90], which will involve a complex and expensive interrogation system. Other established methods to measure temperature using fibre optic sensors include a singlemode-multimode (SM) fibre structure [92], FBG sensors, interferometric sensors, etc. However, these techniques also require complex interrogation units to extract the temperature information. Therefore, a simple and reliable fibre temperature sensor is needed, which can be interrogated using a simple intensity-based system. Our recent studies demonstrated that SMS structures can be used for intensity-based wavelength measurements in a ratiometric scheme with very low temperature

dependency. However, by properly utilising the temperature properties of an SMS fibre structure used as an edge filter it is possible to implement a temperature sensor that utilises a simple intensity-based interrogation technique. In this Letter, we propose such a temperature sensor based on an SMS fibre structure, which has high temperature dependence at selected wavelengths. Theoretical simulation of the temperature dependence of the SMS structure is presented together with experimental validation.

6.1.2 SMS fibre structure

A schematic of an SMS fibre structure is shown in the inset in Fig. 36. The SMS fibre structure is fabricated by splicing a specified length of MMF between two singlemode fibres (SMF). To design an SMS fibre structure device, a modal propagation analysis (MPA) for linearly polarized (LP) modes was used [88], [93]. It was shown that at a re-imaging distance, the SMS fibre structure is highly wavelength dependent and operates as a bandpass filter [88], [93]. The peak wavelength of the bandpass filter response can be tuned by varying the MMF length [93]. For example, based on the fibre parameters in [88], [93], an SMS structure with the length of MMF $L = 44.12$ mm has a bandpass response with a peak wavelength at 1502 nm, as shown in Fig. 36. To investigate the application of this SMS structure as a temperature sensor, the structure was fabricated and the impact of temperature on the spectral response was studied to determine which portion of the response is most sensitive to temperature.

The SMS fibre structure was fabricated using a Fujikura CT-07 cleaver and a Sumitomo type-36 fusion splicer. The spectral response of the SMS fibre structure was measured using a tunable laser and an optical power meter. The

measured result is presented in Fig. 36. The measured result shows a good agreement with the calculated results^a. The discrepancy between the calculated and measured results due to a consequence of splice insertion losses and a result from small fibre core offsets [94].

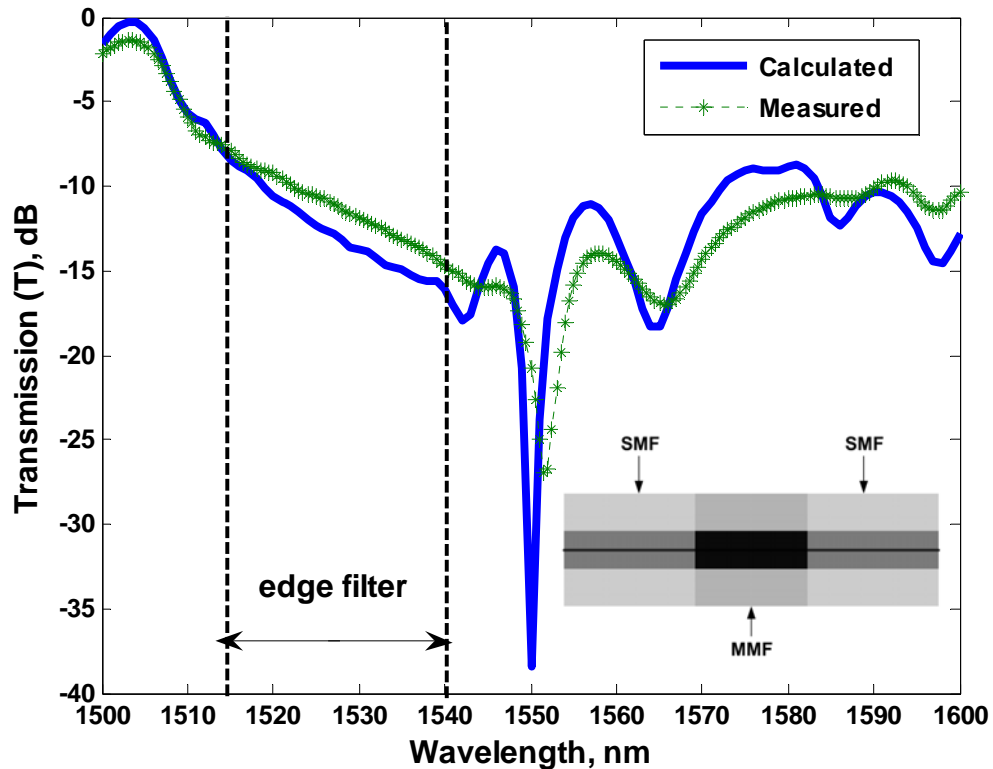


Figure 36 Calculated and measured of SMS fibre structure spectral response (Inset: a schematic structure of an SMS fibre structure)

6.1.3 Temperature dependence

It is well known that the effect of temperature on the fibre can be expressed using two parameters: the thermal expansion coefficient (TEC) and the thermo-optic

^a For the calculated and measured responses the peak wavelength of the bandpass response is 1503 and 1503.5 nm with corresponding transmission values of -0.266 and -1.381 dB, respectively.

coefficient (TOC)^a. The TEC characterises the physical expansion or contraction of the material's vol., while the TOC characterises refractive index change in response to temperature change. Using the TEC and TOC it is possible to determine the change in the core diameter of fibres, MMF length, and refractive indices due to a temperature variation.

To calculate the temperature dependence (TD) of the transmission (T) response, we assumed $TEC = 5 \times 10^{-7} / ^\circ C$ and $TOC = 6.9 \times 10^{-6} / ^\circ C$ for both the SMF and MMF [90], [92]. For example, within a temperature range 50-200 °C, a TD can be defined as $TD = T(200 \text{ } ^\circ C) - T(50 \text{ } ^\circ C)$ in dB. Fig. 37 presents the TD of the designed SMS fibre structure. It can be seen from the Figure that within the edge filter wavelength range TD is low. For example, at the wavelength of 1530 nm the TD is 0.62 dB over 150 °C temperature range. However, significantly higher TDs can be obtained outside the edge filter wavelength range. For example, at the wavelength $A = 1509.5 \text{ nm}$ and $B = 1554 \text{ nm}$, the TD is 1.79 and -7.43 dB, respectively.

For experimental verification the SMS fibre structure was attached to an integrated temperature controller IKA RCT. A tunable laser and optical power meter were used to measure the TD. A schematic of the measurement set-up is shown in inset Fig. 37. The measured TD shows a good agreement with the calculated result and is shown in Fig. 37.

The temperature dependence of the transmission at the wavelengths A and B are presented in Fig. 38. The transmission values were measured in the temperature range 50-200 °C with an increment of 10 °C. The measured and

^a As in [90], [92].

calculated results show a good agreement^a. Discrepancies are most likely a result of fusion splice loss, core offset errors and marginal differences between the designed length of the MMF section (used in the calculations) and the actual fabricated length. The slopes of the temperature dependencies were measured approximately as 0.0122 dB/°C and -0.0508 dB/°C for the wavelength A = 1509.5 and B = 1554 nm, respectively, providing potential temperature sensor resolutions of ~1°C and ~0.2 °C (assuming the accuracy of a typical commercial optical power meter is 0.01 dB). This confirms that the high TD of an SMS fibre structure at selected wavelengths can be utilised as an intensity-based temperature sensor.

To avoid the effect of source signal power variation, an all-fibre ratiometric power measurement technique can be used. A ratiometric system consists of an optical source, a fibre splitter the two arms of which are connected to the SMS fibre structure (temperature sensor arm) and a reference arm. The output powers of the two arms are monitored by two optical power meters. The temperature can be determined by measuring the ratio of two output powers, assuming a suitable calibration has taken place.

^a The calculated and measured discrimination range for the temperature range 50 to 200 °C for wavelength A is 1.787 and 1.835 dB, while for wavelength B it is 7.434 and 7.558 dB, respectively.

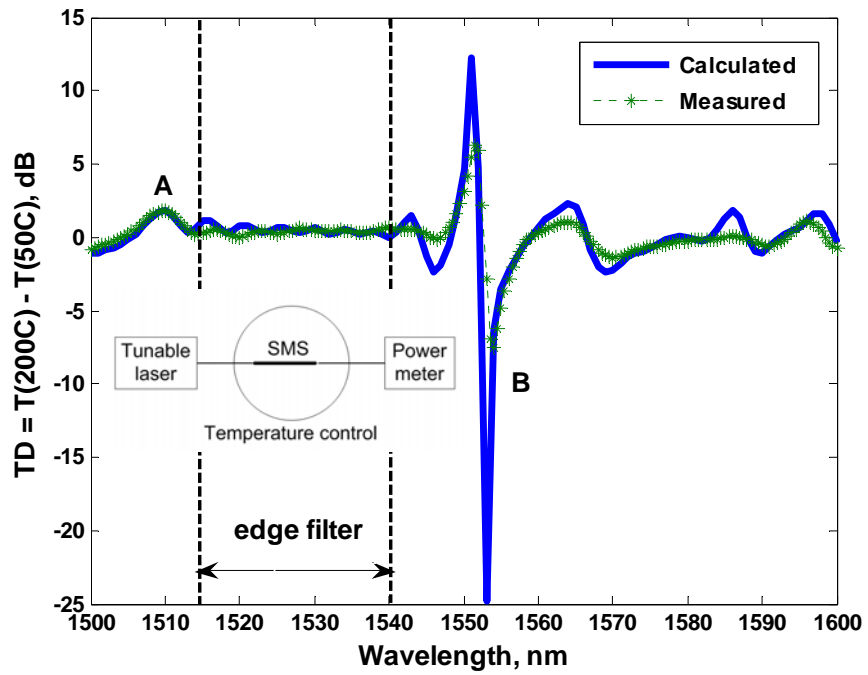


Figure 37 Temperature dependence of SMS fibre structure (Inset: schematic of the measurement set-up)

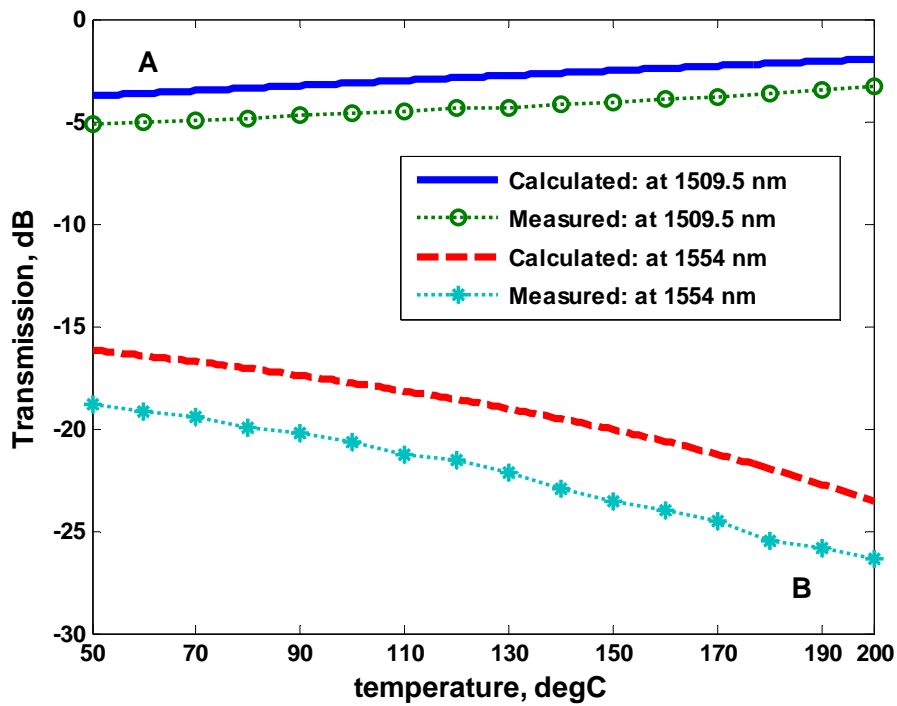


Figure 38 Transmission of the SMS structure against temperature at the wavelengths of 1509.5 nm and 1554 nm

6.1.4 Conclusion

The temperature dependence of an SMS fibre structure has been investigated and proposed as an intensity-based temperature sensor at selected wavelengths. The sensor has a temperature range 50-200 °C and a high temperature resolution of 0.2 °C^a. The proposed sensor can utilise a simple interrogation technique and can provide high speed measurement^b for a range of temperature sensor applications^c.

6.1.5 References

- [88] W. S. Mohammed, P. W. E. Smith, and X. Gu, "All-fibre multimode interference bandpass filter," *Opt. Lett.*, vol. 31, pp. 2547-2549, 2006.
- [89] A. M. Hatta, G. Farrell, Q. Wang, G. Rajan, P. Wang, and Y. Semenova, "Ratiometric wavelength monitor based on singlemode-multimode-singlemode fibre structure", *Microw. Opt. Technol. Lett.*, vol. 50, pp. 3036-3039, 2008.
- [90] E. Li, G.-D. Peng, "Wavelength-encoded fibre-optic temperature sensor with ultra-high sensitivity," *Opt. Commun.*, vol. 281, pp. 5768-5770, 2008.
- [91] E. Li, "Temperature compensation of multimode-interference-based fibre devices," *Opt. Lett.*, vol. 32, pp. 2064–2066, 2007.
- [92] E. Li, X. Wang, and C. Zhang, "Fibre-optic temperature sensor based on interference of selective higher-order modes," *App. Phys. Lett.*, vol. 89, pp. 091119, 2006.
- [93] Q. Wang, G. Farrell, and W. Yan, "Investigation on singlemode-multimode-singlemode fibre structure," *J. Lightw. Technol.*, vol. 26, pp. 512-519, 2008.
- [94] A. M. Hatta, G. Farrell, P. Wang, G. Rajan, and Y. Semenova, "Misalignment limits for a singlemode-multimode-singlemode fibre-based edge filter," *J. Lightw. Technol.*, vol. 27, pp. 2482-2488, 2009.

^a Assuming the uncertainty in the measured power is 0.01 dB.

^b Ratiometric power measurement system is faster and less complex than other techniques based on a tunable laser or an OSA and also is independent of power fluctuations.

^c Such as the measurement of temperature in an industrial process or automotive engines.

6.2 A voltage sensor based on a Singlemode-Multimode-Singlemode fibre structure^a

Keywords: multimode interference, fibre optic sensor, voltage measurement

Abstract: A voltage sensor based on a singlemode-multimode-singlemode (SMS) fibre structure, attached to a piezoelectric (PZT), utilized in a ratiometric optical power measurement scheme is proposed. The elongation of the PZT due to an applied voltage induces a strain on the SMS fibre structure and in turn results in a change in the transmission loss response of the SMS fibre structure. It is found that at selected wavelengths, a strong voltage dependence for the transmission loss of the SMS fibre structure can be achieved. The voltage information can be obtained from the power ratio of the system, assuming the system is calibrated. The proposed voltage sensor offers a simpler configuration when compared to other fibre optic voltage sensors.

6.2.1 Introduction

Optical fibre voltage sensors have a number of advantages over conventional voltage sensors such as resistance to electromagnetic interference, low weight, compactness, fast response, and are also suitable for remote operation [95]. In some optical fibre voltage sensors, piezoelectric (PZT) devices have been utilized as transducers. The optical fibre sensor is securely attached to the PZT so that a

^a A. M. Hatta, G. Rajan, Y. Semenova and G. Farrell, "A voltage sensor based on a singlemode-multimode-singlemode fibre structure," *Microwave and Optical Technology Letters*, (under review).

voltage applied to the PZT induces a strain in the PZT and thus, in the optical fibre sensor. By using the fibre to sense the strain, voltage can be measured. The fibre sensor could be a singlemode fibre [96], a hollow fibre [97], or a fibre-Bragg grating (FBG) [98]. Depending on the fibre sensor used, the measurement of strain and thus, voltage can be carried out using an interferometric measurement system [96], [97] or by measuring reflected wavelength [98]. Both of these measurement schemes are complex and expensive to implement.

A singlemode-multimode-singlemode (SMS) fibre structure has been used to sense strain [99]. The characteristics of the wavelength shift of the SMS spectral response due to the strain applied to SMS fibre structure have been investigated previously in [99], [100]. In this paper, by utilizing the effect of strain on the SMS fibre structure, we present for the first time a simple method to measure DC voltage using an SMS fibre structure attached to a PZT stack, while employing a simple ratiometric power measurement scheme. The specific advantages of utilizing an SMS fibre structure over the FBG or hollow fibre PZT-based voltage sensors are ease of fabrication, low cost and simplicity of interrogation. A DC voltage sensor is demonstrated with a range of 0 to 100 V which is suitable for remote voltage monitoring. The sensor is connected to the measurement system only by fibre and thus, has the advantages that the sensor requires no local electrical power source and is furthermore electrically isolated. Possible applications include voltage monitoring in areas with high electrical field strengths. Moreover, it has the potential to be applied to high voltage sensor applications with a suitable choice of PZT.

6.2.2 Strain dependence of SMS fibre structure

Strain and consequent elongation is produced in a PZT when a voltage is applied. The voltage sensor is fabricated by securely bonding an SMS fibre structure to the PZT stack, as shown in Fig. 39. Two ends of the PZT stack are bonded between a solid fixed platform and a light weight bracket. The two ends of the SMS fibre structure are glued to the platform and the bracket. The elongation of the PZT, when voltage is applied, will induce an axial strain in the SMS fibre structure. It is shown in [99], [100] that the spectral response of an SMS fibre structure shifts to a lower wavelength due to applied strain. As a result if the transmission loss of the SMS fibre structure is measured at a fixed wavelength, the loss will be proportional to the strain and thus the voltage.

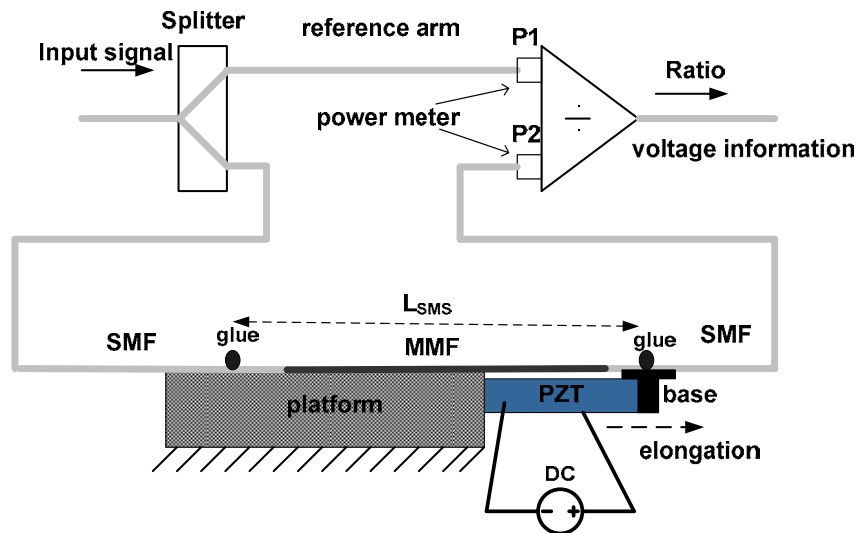


Figure 39 Schematic configuration of SMS fibre structure voltage sensor system

Fig. 39 shows a schematic configuration of the voltage sensor using a ratiometric power measurement system. The optical input signal is divided into two equal power signals, one goes to the reference arm and the other one goes to the SMS fibre structure. Two photodiodes and associated electronics are used to measure the optical output power ratio from the two arms. A ratiometric scheme is used to ensure independence from input signal power variations improving the stability and accuracy of the measurement system. An unknown applied voltage can be measured by measuring the ratio of the photodiode outputs, assuming the system is calibrated.

To optimize an SMS fibre structure and to select an operating wavelength, it is useful to initially investigate the strain dependence of the spectral response of an SMS fibre structure. A modal propagation analysis (MPA) for linearly polarized (LP) modes can be used to investigate light propagation in the SMS fibre structure [101]. It is known that an applied strain (ε) induces a change in the length (ΔL) and the core radius (Δa) of an SMS fibre structure employing a step index MMF and also change the refractive index (Δn) of the SMF and MMF sections^a. For an applied strain (ε), the change in MMF length, the core radius and refractive index can be expressed as [100]:

$$\Delta L = L\varepsilon \quad (6.1a)$$

$$\Delta a = -va\varepsilon \quad (6.1b)$$

$$\Delta n_i = -\frac{n_i^2}{2}[p_{12} - \nu(p_{11} + p_{12})]\varepsilon = -p_e\varepsilon \quad (6.1c)$$

^a As in [100].

where L is the length of MMF, a is the core radius of SMF/MMF, n_i represents the refractive index of the core and cladding of the SMF/MMF, p_{11} and p_{12} are strain-optic coefficients for fused silica, p_e is the effective strain-optic coefficient, and ν is the Poisson ratio.

In this paper, the core/cladding diameter of the SMF is 9/125 μm and of the MMF is 105/125 μm , while an MMF length of 43.93 mm are used for calculation. MMF lengths from 44.19 to 41.54 mm provide a bandpass spectral response with a peak bandpass wavelength from 1500 to 1600 nm, respectively [101]. The spectral response of the SMS fibre structure is calculated using the MPA and it is shown in Fig. 40 for the case without an applied strain, $\Delta\varepsilon = 0 \mu\varepsilon$. The bandpass spectral response is shown with the peak bandpass wavelength of 1510 nm.

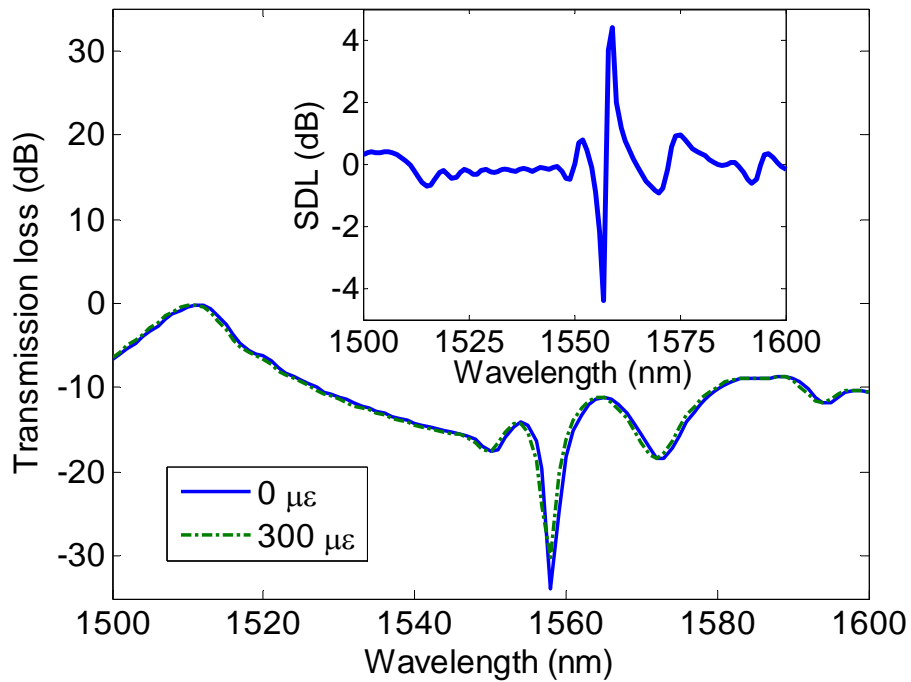


Figure 40 Transmission loss response of the SMS fibre structure. SDL of the SMS fibre structure (inset figure)

To determine which wavelength of the response is most sensitive to strain, a strain dependent loss (SDL) of the response is investigated. The SDL is defined as the transmission loss difference between with- and without- applied strain. A commercial PZT stack AE0505D18 (from Thorlabs) was used as the strain transducer. It has a length of 20 mm and cross sectional dimensions of 5 x 5 mm. The maximum elongation is 15 μm at a maximum DC voltage of 100 V. For the $L_{\text{SMS}} = 50$ mm, the SDL due to the maximum elongation which corresponds to $\Delta\varepsilon = 300$ $\mu\varepsilon$ is calculated. The strain related coefficient of $p_e = 0.22$ and $\nu = 0.16$ were used as in [100]. In Fig. 40, the calculated spectral response is shown at $\Delta\varepsilon = 300$ $\mu\varepsilon$, while the inset figure in Fig. 40 shows the SDL of SMS fibre structure. It is clear that at certain wavelengths, the sensitivity to strain is much higher and such wavelengths are therefore suitable operating wavelengths for voltage measurement. A wavelength of 1556.8 nm, is a good example of a suitable wavelength due to its high SDL value which improves strain sensitivity and thus voltage sensitivity. In Fig. 41, the transmission loss response, at 1556.8 nm, due to the applied strain from 0 to 300 $\mu\varepsilon$ is shown with a monotonically decreasing response and a discrimination range of -4.378 dB. This is equivalent to a strain sensitivity of 0.0146 dB/ $\mu\varepsilon$ and thus a voltage sensitivity of 0.0438 dB/V.

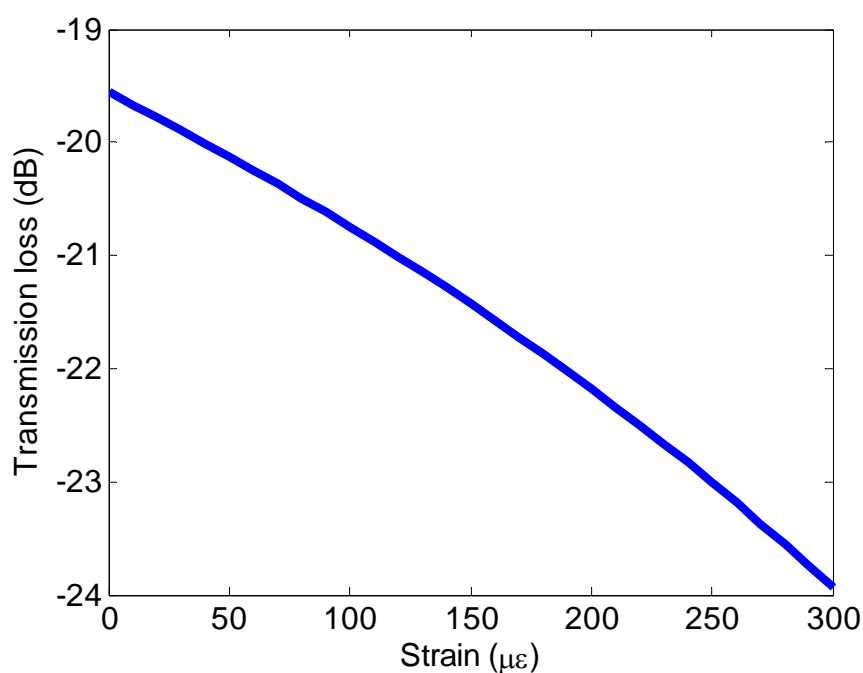


Figure 41 Transmission loss vs applied strain to the SMS fibre structure at a wavelength of 1556.8 nm

6.2.3 Experimental results

The SMS fibre structure described above was fabricated using a Fujikura CT-07 cleaver and a Sumitomo type-36 fusion splicer. As shown in Fig. 39, the SMS fibre structure was glued^a to the platform and the bracket at two fixed points, with a total length between the fixed points of about 50 mm. The PZT stack AE0505D18 was used as the transducer.

A tunable laser TUNICS-PLUS was used as the input signal source. Initially, to select the appropriate wavelength, two spectral ratio responses were measured at voltages of 0 and 100 V. A single channel piezo controller MDT694A (Thorlabs) was used to supply DC voltages from 0 to 100 V. The

^a Using a LOCTITE superglue

measured spectral ratio responses at 0 V and 100 V for a wavelength range of 1500 to 1600 nm with an increment of 0.1 nm are shown in Fig. 42. It can be seen that the spectral response of the SMS fibre structure is shifted to a lower wavelength region when the voltage was applied. This spectral response shift to the lower wavelength region confirms the strain effect on the SMS fibre structure as in [99], [100].

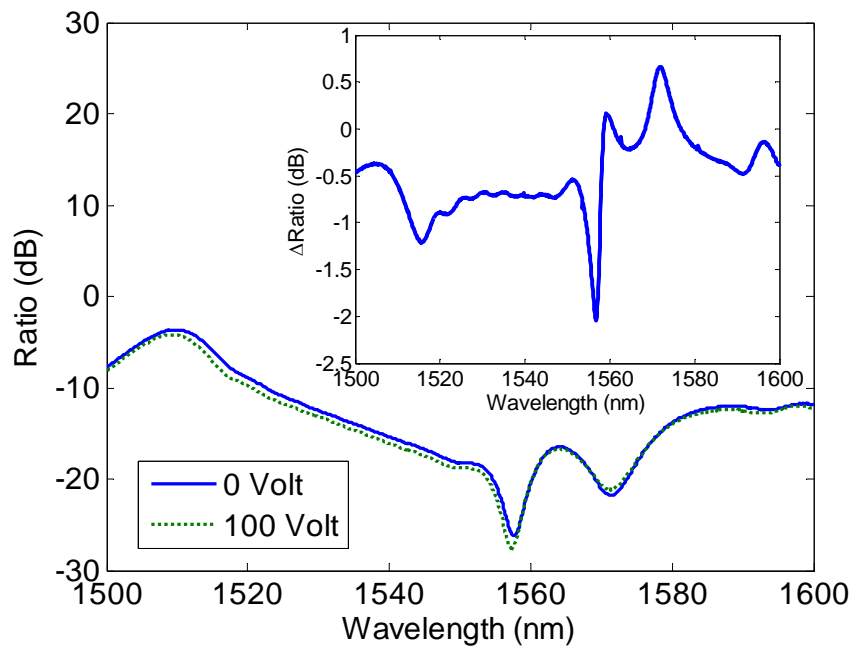


Figure 42 Measured ratio spectral response at 0 V and 100 V (inset: ratio difference)

For the purpose of ratiometric power-based measurement, it is necessary to select the optimal operating wavelength. The ratio difference at 100 V and 0 V is presented in the inset in Fig. 42. A wavelength of 1556.8 nm shows the largest ratio difference of -1.95 dB between 0 V and 100 V and thus is selected as the operational wavelength. The measured ratio response due to an applied voltage

from 0 to 100 V with an increment of 5 V at the operational wavelength of 1556.8 nm is presented in Fig. 43. A monotonic decrease in the ratio response with applied voltage is demonstrated with a sensitivity of 0.0195 dB/V. The experimental sensitivity is lower than that predicted but this discrepancy can be attributed to small length errors in the fabricated SMS structure and the accuracy of the coefficient strain values used in the calculations. Assuming a power measurement resolution of 0.005 dB is possible, then the voltage measurement resolution should be better than 0.5 V.

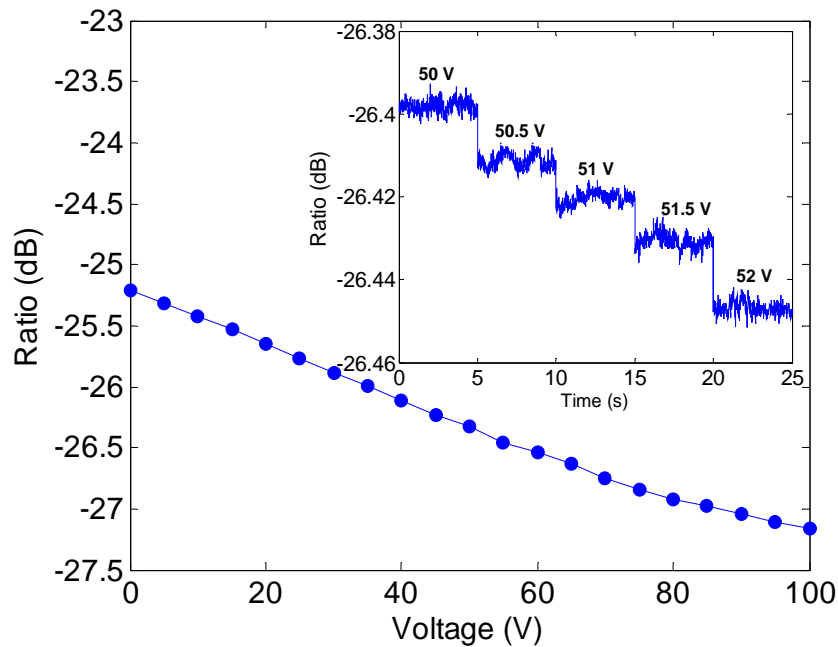


Figure 43 Ratio response of system against voltage at the operational wavelength 1556.8 nm (inset: variation in ratio for a step change of 0.5 V)

To check the voltage measurement resolution of the system, a step change of 0.5 V from 50 to 52 V, with a time interval of 5 seconds was applied to the SMS fibre structure sensor. The measured ratio variation was shown in the inset

of Fig. 43. It is clear that the resolution of the voltage sensing system is better than 0.5 V, confirming that the SMS fibre structure, together with a PZT, is suitable as a voltage sensor for DC voltage measurements from 0 to 100 volts.

It is well known that the PZT exhibits the hysteresis in strain to voltage response and therefore, we also observed the hysteresis in measured ratio response against the voltage. However, hysteresis can be minimized by the selection of an appropriate PZT material [102] or by applying numerical techniques to compensate for the hysteresis [103].

For a given fixed signal source wavelength, the MMF length will need to be optimized to achieve the highest ratio (and thus voltage) dependence. It is shown in [101], that the peak wavelength of a bandpass filter can be tuned by selecting a suitable MMF length. It is also possible to use the SMS fibre structure for high voltage measurements. The operating voltage depends on the PZT's strain-voltage characteristic. In [98], an FBG is attached to a PZT as a high voltage sensor. The PZT in [98] can be operated over a voltage range from 0 to 5 kV with a maximum PZT elongation of about 19 μm which is similar to the maximum PZT elongation used in this paper. The maximum PZT elongation should be within the strength limits of the SMS fibre structure, which is approximately 100 μm in the present case.

6.2.4 Conclusion

The SMS fibre structure attached to the PZT transducer is proposed as a voltage sensor employed in a ratiometric power measurement scheme.^a A DC voltage

^a With $L_{\text{mmf}} = 43.93$ mm at an operating wavelength of 1556.8 nm.

sensor from 0 to 100 V with a resolution about 0.5 V is demonstrated^a. The proposed sensor requires no electrical power source and is electrically isolated. It utilizes a simple ratiometric power measurement system, offering a fast measurement capability^b with the potential for kilovolt measurement with a suitable choice of PZT.

6.2.5 References

- [95] G. Fusiek, P. Niewczas, and J. R. McDonald, "Feasibility study of the application of optical voltage and current sensors and an arrayed waveguide grating for aero-electrical systems," *Sens. and Actuat. A*, vol. 147, pp. 177–182, 2008.
- [96] L. M-Leom, A. Diez, J. L. Cruz, and M. V. Andres, "Frequency-output fibre-optic voltage sensor for high-voltage lines," *IEEE Phot. Technol. Lett.*, vol. 13, pp. 996-998, 2001.
- [97] S. Kim, J. Park and W.-T. Han, "Optical fibre AC voltage sensor," *Microw. Opt. Technol. Lett.*, vol. 51, pp. 1689-1691, 2009.
- [98] P. Niewczas, L. Dziuda, G. Fusiek, and J. R. McDonald, "Design and evaluation of a preprototype hybrid fibre-optic voltage sensor for a remotely interrogated condition monitoring system," *IEEE Trans. Inst. Meas.*, vol. 54, pp. 1560-1564, 2005.
- [99] S. M. Tripathi, A. Kumar, R. K. Varshney, Y. B. P. Kumar, E. Marin, and J. P. Meunier, "Strain and temperature sensing characteristics of single-mode–multimode–single-mode structures," *J. Lightwav. Technol.*, vol. 27, pp. 2348-2356, 2009.
- [100] E. Li, "Temperature compensation of multimode interference-based fibre devices," *Opt. Lett.*, vol. 32, pp. 2064-2066, 2007.

^a The accuracy of system measurement is limited by the polarization dependence of the input light and temperature variation as described in Chapter 4 and 5.

^b It is estimated a measurement speed up to 1 kHz can be achieved.

- [101] Q. Wang, G. Farrell, and W. Yan, "Investigation on singlemode-multimode-singlemode fibre structure," *J. Lightw. Technol.*, vol. 26, pp. 512-519, 2008.
- [102] M. Pacheco, F. M. Santoyo, A Mendez, and L. A Zenteno, "Piezoelectric-modulated optical fibre Bragg grating high-voltage sensor," *Meas. Sci. Technol.*, vol. 10, pp. 777-782, 1999.
- [103] G. Fusiek, P. Niewczas, L. Dziuda, and J. R. McDonald, "Hysteresis compensation for a piezoelectric fibre optic voltage sensor," *Opt. Eng.*, vol. 44, pp. 114402 1-6, 2005.

Chapter 7

Strain sensor based on an SMS fibre structure and its temperature compensation

The previous chapter described the use of an SMS fibre structure as an intensity-based temperature sensor and a voltage sensor based on strain. It is well known that temperature can induce a strain measurement error in fibre optics-based strain sensors [104]-[106]. In this Chapter, strain and temperature effects on an SMS fibre structure configured as a strain sensor are investigated in depth. The application of an SMS fibre structure as a strain sensor with very low temperature induced strain measurement error is investigated. For this purpose two SMS fibre structures are proposed and demonstrated in a ratiometric power measurement scheme, one SMS structure acts as the strain sensor and the other SMS structure acts as the temperature monitor and is not subject to the strain. The use of this configuration can minimize the temperature induced strain measurement error. It is demonstrated that for strain measurement from 0 to 1000 $\mu\epsilon$ within the temperature range from 10 to 40 °C, the proposed configuration can provide a

strain and temperature resolution of $0.34 \mu\epsilon$ and $0.14 ^\circ\text{C}$, respectively, with a temperature induced strain measurement error as low as $0.39 \mu\epsilon$.

Strain sensor based on a pair of singlemode-multimode-singlemode fibre structures in a ratiometric power measurement scheme^a

Keywords: fibre optic sensor, strain sensor, temperature dependence

Abstract: The strain and temperature dependencies of a step index singlemode-multimode-singlemode (SMS) fibre structure are investigated numerically and experimentally. For intensity-based strain measurement using a single SMS fibre structure, at a selected wavelength, it is found that there is a high strain dependence, but also a temperature dependence that will induce strain measurement error. To minimise the temperature induced strain measurement error, two SMS fibre structures are proposed and demonstrated in a ratiometric power measurement scheme, one SMS structure acts as the strain sensor and the other SMS structure acts as the temperature monitor. The extracted temperature information is used to determine a strain value based on a suitable calibration of strain responses with temperature variations. It is demonstrated that for strain measurement from 0 to $1000 \mu\epsilon$ within the temperature range from 10 to $40 ^\circ\text{C}$, the proposed configuration can provide a strain and temperature resolution of 0.34

^a A. M. Hatta, Y. Semenova, Q. Wu and G. Farrell, " Strain sensor based on a pair of singlemode-multimode-singlemode fibre structures in a ratiometric power measurement scheme," *Applied Optics*, vol. 49, no. 3, pp. 536-541.

$\mu\epsilon$ and $0.14\text{ }^{\circ}\text{C}$, respectively, with a temperature-induced strain measurement error as low as $0.39\ \mu\epsilon$.

7.1 Introduction

Fibre optic sensors are widely used for strain measurement in structural health monitoring^a. It is well known that temperature can induce a strain measurement error for fibre optics-based strain sensors^b. Therefore, many techniques have been proposed to compensate for temperature dependence or to simultaneously measure strain and temperature, most commonly based on a fibre Bragg grating (FBG) [104]-[106]. In FBG-based sensor, techniques employing an optical spectrum analyzer (OSA) are commonly used to extract wavelength information due to strain or temperature variation.

Recently, a singlemode-multimode-singlemode (SMS) fibre structure has been investigated for various applications because of its low cost and ease of fabrication. Several applications of an SMS have been demonstrated, including a refractometer, filters, and temperature sensors [106]-[111]. The characteristics of the wavelength shift of the SMS spectral response due to strain and temperature applied to a step index SMS fibre structure were investigated previously in [112]. In [113], an SMS fibre structure employing a graded index MMF was studied in regard to the sensing applications of wavelength shift due to strain and temperature. In [114], an SMS fibre structure combined with a FBG is utilized to enhance the sensitivity of strain measurement. A FBG combined with an SMS fibre structure has also been reported for simultaneous strain and temperature

^a As in [2]-[5]

^b As in [104]-[106]

measurement [115]. However, all of these strain measurement techniques, with or without temperature determination, require the use of an OSA.

In addition to the disadvantage of needing an OSA, in an SMS fibre structure the wavelength shift in the spectral response due to increases in strain or temperature are in opposite directions, shifting to a lower or higher wavelength, respectively, as in [112], [113]. Therefore, when using a single SMS fibre structure as a strain sensor where there are ambient temperature variations, accurate strain measurement can be carried out only when temperature information is known. In this paper, the use of a pair of SMS fibre structures is proposed and demonstrated as a strain sensor with self-temperature monitoring. Additionally, an intensity-based measurement scheme rather than an OSA is used. Two SMS fibre structures are used; one as a strain sensor and the other one as a temperature monitor located in the same thermal environment. A ratiometric power measurement scheme is used which offers low cost, simple configuration and the potential for high speed measurement compared to the techniques which employ an OSA.

7.2 Strain and temperature dependence of a step index

SMS fibre structure

AN SMS fibre structure as shown in Fig. 44(a) is formed by splicing a step-index multimode fibre (MMF) between two standard singlemode fibres (SMFs). Fig. 44(b) shows the schematic of a system utilizing a pair of SMS fibre structures for strain sensor with self-temperature monitoring in a ratiometric power measurement technique. The input signal is divided into two paths and connected

to a pair of SMS fibre structures and a single reference arm. Both of the SMS fibre structures, SMS-1 and SMS-2, are located close together^a and therefore experience the same ambient temperature. The strain is only applied to the SMS-1. At a chosen fixed input wavelength, strain applied to SMS-1 changes the output power ratio R1, where $R1 = P1 - P_{ref}$ in dB. The output power ratio R1 variation tracks the variation in strain. SMS-2 is used as a temperature monitor, so that the variation in the output power ratio R2, where $R2 = P2 - P_{ref}$ in dB, tracks temperature variations. However, the presence of a temperature fluctuation also affects SMS-1 and changes the output power P1 and thus R1. To determine the applied strain accurately with ambient temperature variations, the strain independent temperature information obtained from R2 is used to accurately extract the value of applied strain on its own, even in presence of temperature-induced variations in R1. This assumes that a suitable calibration of R1 to account for the effect of strain and temperature has taken place.

To optimize an SMS fibre structure for the application described here and to select a suitable operating wavelength, it is useful to initially investigate the strain and temperature dependence of the spectral response of a single SMS fibre structure as in Fig. 44(a). A modal propagation analysis for linearly polarized (LP) modes can be used to investigate light propagation in the SMS fibre structure [116]. It is known that an applied strain (ϵ) and a temperature variation (ΔT) induce a change in the length (ΔL) and the core radius (Δa) of the step index MMF section of the SMS fibre structure as well as a change in the refractive index (Δn) of the SMF and MMF sections.

^a The separation distance between SMS-1 and SMS-2 is less than 1 cm.

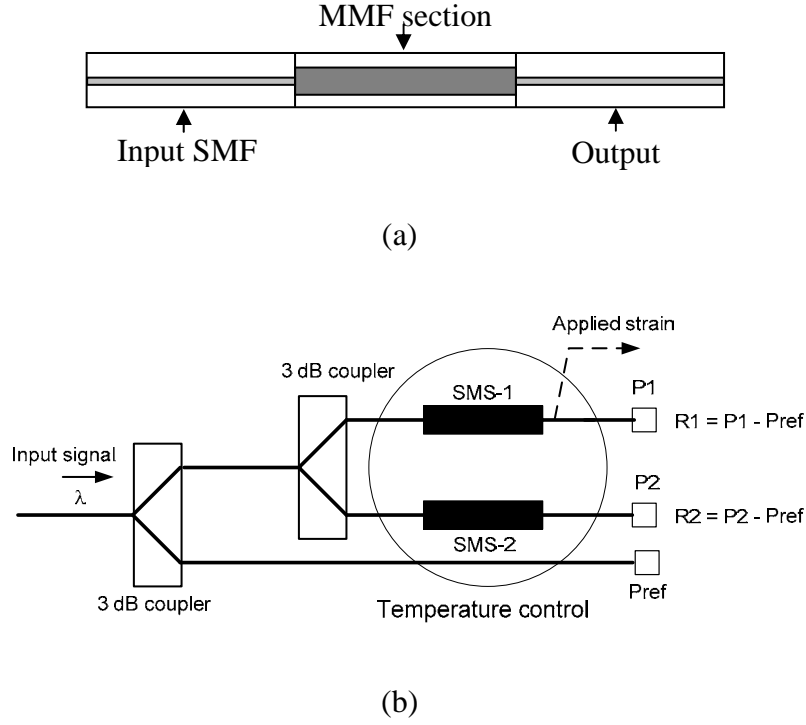


Figure 44 (a) Single SMS fibre structure (b) Schematic structure of strain measurement with a self-temperature monitoring in a ratiometric power measurement scheme using a pair of SMS fibre structures

For an applied strain (ε), the change in MMF length, core radius, and refractive index can be expressed as [112]:

$$\Delta L = L\varepsilon \quad (7.1a)$$

$$\Delta a_{(SMF,MMF)} = -\sigma a_{(SMF,MMF)}\varepsilon \quad (7.1b)$$

$$\Delta n_{(SMF,MMF)i} = -\frac{n_{(SMF,MMF)i}^3}{2} [p_{12} - \sigma(p_{11} + p_{12})]\varepsilon = -p_e\varepsilon \quad (7.1c)$$

where L is the length of the MMF section, a is the core radius, n_i represents the refractive index of the core and cladding of the MMF, p_{11} and p_{12} are the strain-optic coefficients for fused silica, p_e is the effective strain-optic coefficient, and

σ is the Poisson ratio. The change in length for the MMF, core radius, and refractive index due to the temperature can be expressed as [112]

$$\Delta L = \alpha L \Delta T \quad (7.2a)$$

$$\Delta a_{(SMF,MMF)} = \alpha a_{(SMF,MMF)} \Delta T \quad (7.2b)$$

$$\Delta n_{(SMF,MMF)_i} = \beta n_{(SMF,MMF)_i} \Delta T \quad (7.2c)$$

where α is a thermal expansion coefficient and β is a thermo-optic coefficient. The combined effect of strain and temperature on the length of the MMF, its core radius, and the refractive index are

$$\Delta L = L \varepsilon + \alpha L \Delta T \quad (7.3a)$$

$$\Delta a_{(SMF,MMF)} = -\sigma a_{(SMF,MMF)} \varepsilon + \alpha a_{(SMF,MMF)} \Delta T \quad (7.3b)$$

$$\Delta n_{(SMF,MMF)_i} = -p_e \varepsilon + \beta n_{(SMF,MMF)_i} \Delta T . \quad (7.3c)$$

In this paper, the core/cladding diameter of the SMF is 9/125 μm and of the MMF is 105/125 μm . It is known that MMF lengths from 44.53 to 42.45 mm provide a bandpass spectral response with a peak bandpass wavelength that depends on the length, ranging from 1490 to 1560 nm, respectively [116]. In this investigation a MMF length of 44.38 mm is chosen to provide an operating wavelength for the sensor in the region of 1490-1560 nm. The spectral response of the SMS fibre structure is calculated using modal propagation analysis and is shown in the inset figure in Fig. 45. To determine which wavelength is most sensitive to strain and temperature, the strain-dependent loss (SDL) and temperature-dependent loss (TDL) are calculated from 1490 to 1560 nm. The SDL is calculated at $\Delta \varepsilon = 1000 \mu\varepsilon$ and the TDL at $\Delta T = 30 \text{ }^\circ\text{C}$. The strain- and temperature-related coefficient values $p_e = 0.22$, $\sigma = 0.16$, $\alpha = 5 \times 10^{-7} / ^\circ\text{C}$, and

$\beta = 6.9 \times 10^{-6} / ^\circ\text{C}$ are used as in [112]. Fig. 45 shows the SDL and TDL of the SMS fibre structure, from which it is clear that some wavelengths are much more sensitive to strain and temperature, especially at the dip (1535-1545 nm) region of the bandpass response.

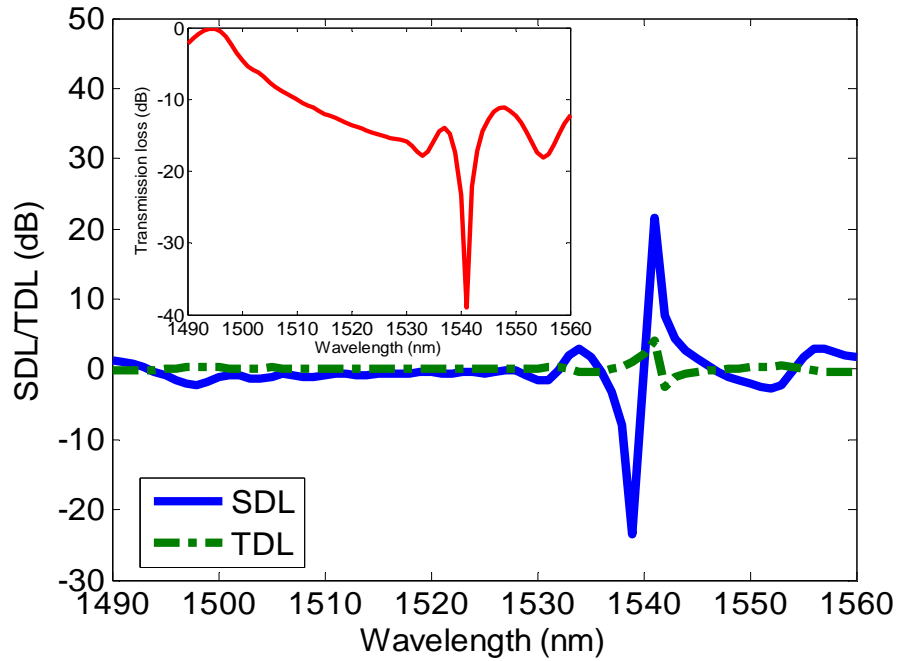
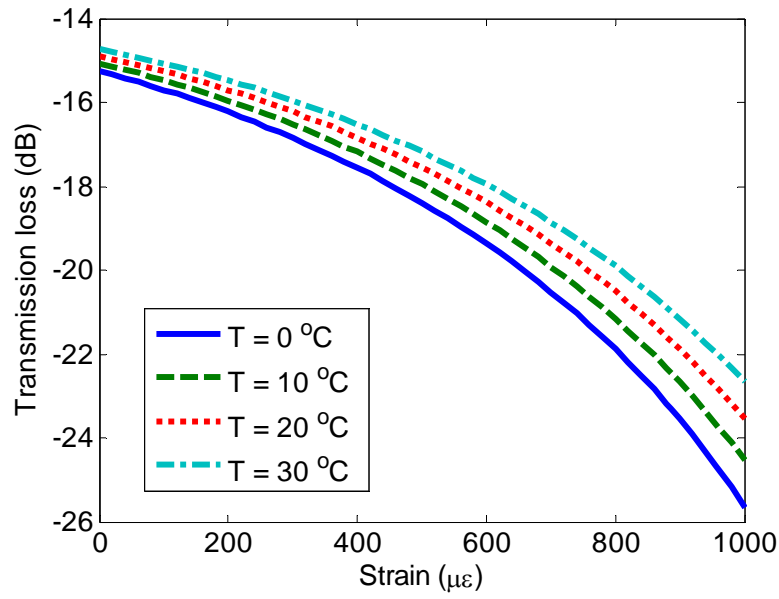


Figure 45 SDL and TDL of the SMS fibre structure (Inset, spectral response)

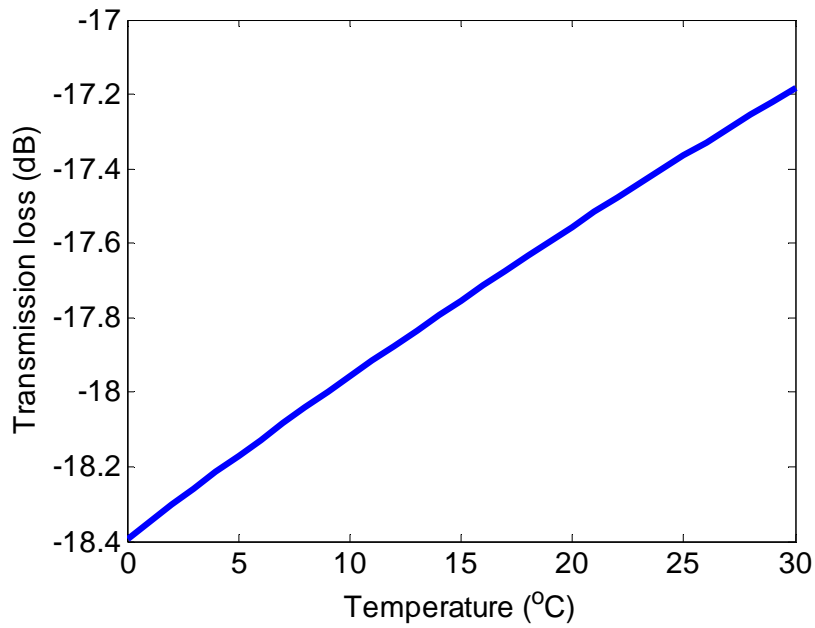
Given that a fixed wavelength ratiometric power measurement system is used for interrogation, the transmission losses responses due to strain and temperature are calculated at an operating wavelength of 1539 nm. This wavelength is chosen due to their high SDL value, which will improve strain sensitivity. In Fig. 46(a), the transmission loss responses due to an applied strain from 0 to 1000 $\mu\epsilon$ at $T = 0, 10, 20,$ and 30°C are shown. It is clear that the response to strain is monotonically decreasing but that the presence of a

temperature variation changes the transmission loss response to strain. At $T = 0$ °C, the discrimination range is -10.389 dB which is equivalent to strain sensitivity of 10.389×10^{-3} dB/ $\mu\epsilon$. To further illustrate the effect of temperature, the transmission loss response at 500 $\mu\epsilon$ due to a temperature variation from 0 °C to 30 °C is shown in Fig. 46(b). A temperature change of 30 °C alters the transmission loss response by 1.21 dB at 500 $\mu\epsilon$. Such a change in the transmission loss due to temperature is equivalent to a strain measurement error of 116.4 $\mu\epsilon$. It is clear from this result that the magnitude of transmission loss change, due to variations in temperature, is substantial and of the same order of magnitude as that due to the strain itself. Ambient temperature variations can thus significantly reduce the strain measurement accuracy if only one SMS fibre structure is used.

An SMS fibre structure when used as a strain sensor is clearly temperature sensitive. However, it is apparent from Fig. 46(a) that the transmission loss monotonically decreases for a decrease in temperature. This means that, by monitoring the system temperature, it is feasible to apply a calibration correction factor to minimize the temperature-induced strain measurement error. Furthermore, the monotonically decreasing transmission loss response with temperature means that by using two identical SMS fibre structures, one as the strain sensor and the other one as a temperature monitor, a strain sensor with a self-temperature monitoring can be implemented as presented in Fig. 44(b).



(a)



(b)

Figure 46 Transmission loss responses at the operating wavelength of 1539 nm (a) strain responses at different ambient temperatures, (b) temperature response for an applied strain of $500 \mu\epsilon$

7.3 Experimental results

The SMS fibre structure described above was fabricated using a precision Fujikura CT-07 cleaver and a Sumitomo type-36 three-axis fusion splicer. Two such SMS fibre structures were fabricated with a MMF length of 44.38 mm. The lengths of the two MMFs were carefully controlled and cleaved in order to minimise length differences. The transmission loss responses of the fabricated SMS fibre structures were measured using a tunable laser TUNIC PLUS and a power meter and the result of this is shown in Fig. 47. The measured results show a good agreement with the calculated result by comparison with the inset in Fig. 45. The measured results for the spectral responses of the two fabricated SMS structures are most identical. The small discrepancy between two measured spectral responses is most likely caused by residual MMF length errors^a and also fibre core splice offsets, occurring during the fabrication process [117].

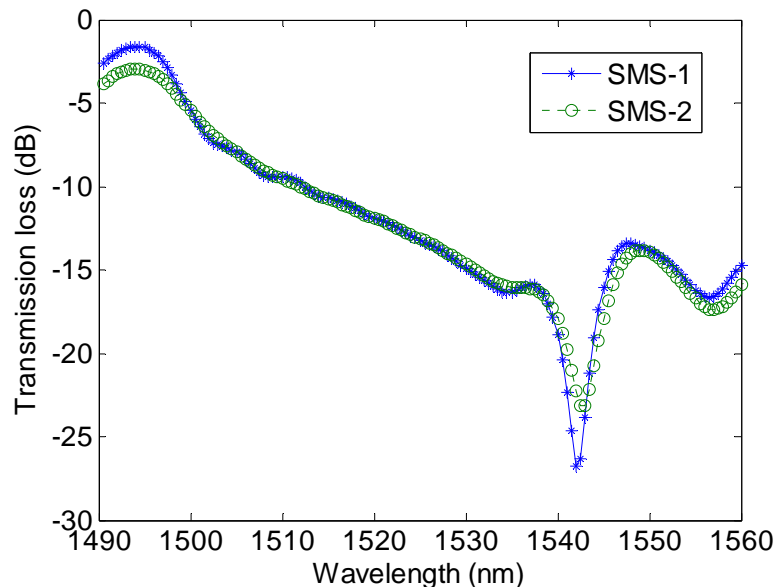


Figure 47 Measured spectral response of two SMS fibre structures

^a Estimated to be circa ± 0.05 mm which induces a peak wavelength bandpass response shift of ∓ 2 pm.

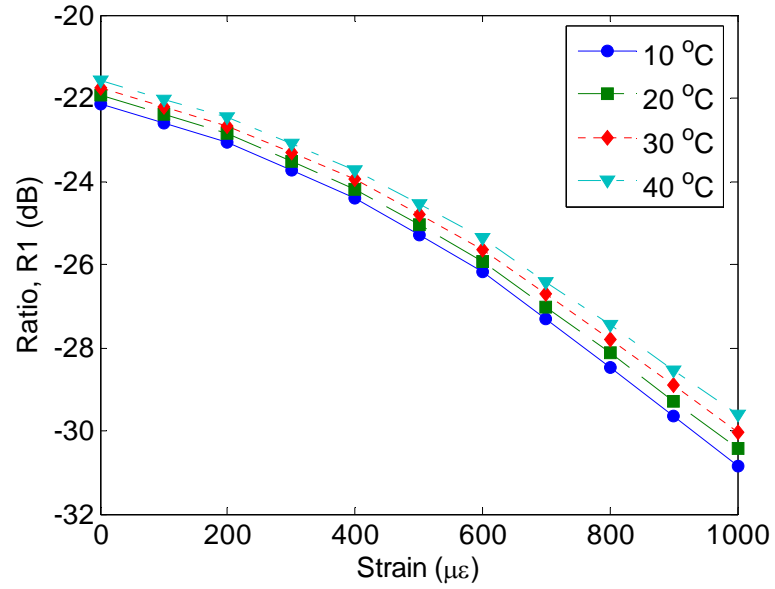
The two SMS fibre structures were utilised in a ratiometric measurement scheme as shown in Fig. 44(b). The input signal from the tunable laser was split into two equal intensity signals using a 3 dB fibre coupler^a. One of the signals was transmitted through the reference arm and the other via a second 3 dB fibre coupler to arms containing the pair of SMS fibre structures SMS-1 and SMS-2. Power meters were placed at the ends of all three arms. Axial strain was applied to SMS-1, and both of the SMS fibre structures were attached to the same thermoelectric Peltier cooler. At the selected wavelength of 1539 nm, the ratio response due to the applied strain was measured from 0 to 1000 $\mu\epsilon$ with an increment of 100 $\mu\epsilon$ at the temperature of 10 °C, 20 °C, 30 °C and 40 °C. The measured ratio R1, as defined in Fig. 44(b), is presented in Fig. 48 (a). Fig. 48(b) shows the calculated ratio responses from 0 to 1000 $\mu\epsilon$ at the temperature of 10 °C, 20 °C, 30 °C and 40 °C, with 3 dB coupler loss consideration. The strain measurement sensitivity at 10 °C is 8.732×10^{-3} dB/ $\mu\epsilon$ which is approximately equal to the calculated strain sensitivity of 9.463×10^{-3} dB/ $\mu\epsilon$ from Fig. 48(b). The measured and calculated ratio responses for strain with temperature variations also show a good agreement^b. Discrepancies can be attributed to splicing loss during fabrication and the accuracy of the strain and temperature coefficient values used in the calculations.

In the previous section it was found that temperature can significantly degrade the strain measurement accuracy of a single SMS fibre structure. It is shown in Fig. 48(a) that the ratio variation due to a temperature change from

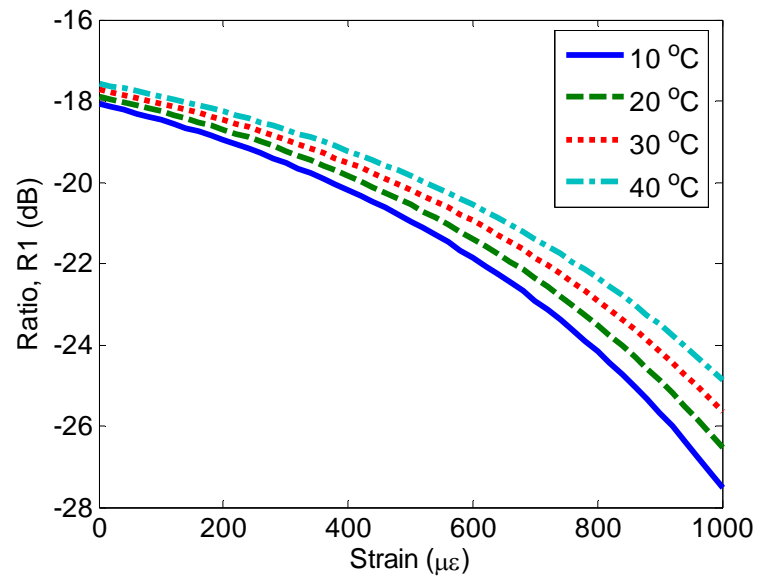
^a 10202A-50 - 2x2 SM Coupler

^b At an applied strain of 500 $\mu\epsilon$, the ratio variation due to a temperature variation for the measured and calculated values is 0.736 and 1.120 dB, respectively.

10 °C to 40 °C is 0.736 dB at 500 $\mu\epsilon$. This ratio variation induces a strain measurement error of 84.3 $\mu\epsilon$.



(a)



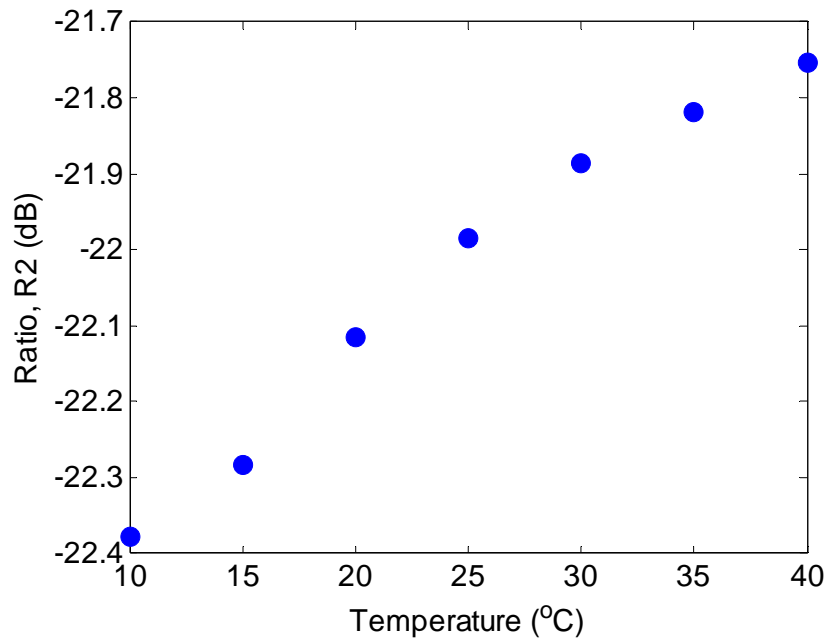
(b)

Figure 48 Ratio of SMS-1 as a function of strain with temperature variation at an operating wavelength of 1539 nm: (a) measured (b) calculated

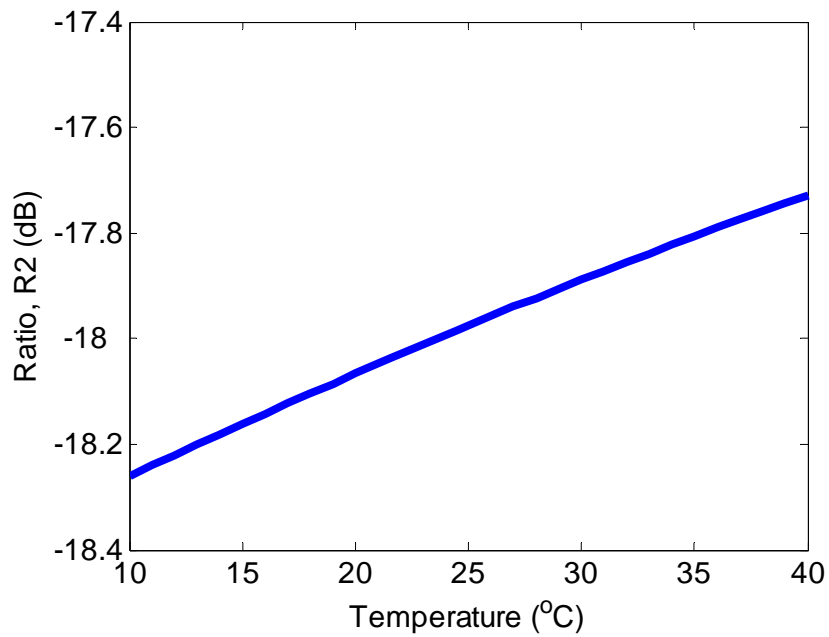
To minimise the temperature-induced strain measurement error, self-temperature monitoring can be carried out by employing SMS-2. The measured and calculated ratio responses due to a temperature variation from 10 °C to 40 °C are shown in Fig. 49(a) and Fig. 49(b), respectively. The ratio response is monotonically increasing, with an acceptable discrimination range of 0.623 dB (calculated value is 0.533 dB) which is suitable for the temperature monitoring. Discrepancies between the measured and the calculated values can be attributed to insertion loss, such as splice loss, the accuracy of the strain and temperature coefficient values used in the calculations, and, most important, residual MMF length errors.

To analyse the effect of residual MMF length errors on the temperature response, Fig. 50 shows the calculated ratio responses due to temperature variation from 10 to 40 °C with MMF length errors of $\Delta L_{mmf} = -20, 0, 20,$ and $40 \mu\text{m}$. It is clear that both the insertion loss and the discrimination range of the calculated ratio response are influenced by length errors in the MMF section. The discrimination ranges are 0.195, 0.533, 0.995, and 1.792 dB, respectively. The linearity of the calculated ratio response also depends on the length of the MMF. The calculated linear regression correlation coefficients for the various length errors in Fig. 50 are 0.993, 0.998, 0.999, and 0.996, respectively. By comparison the linear regression correlation coefficient of the measured ratio response is 0.975 as in Fig. 49(a).

From the measured results as in Fig. 48, it was estimated that a strain measurement resolution of $0.34 \mu\epsilon$ is possible, assuming the uncertainty in the measured power ratio is 0.003 dB [118].



(a)



(b)

Figure 49 Ratio response of SMS-2 due to temperature variation at an operating wavelength of 1539 nm: (a) measured (b) calculated

From Fig. 49, the temperature measurement resolution was estimated as 0.14 °C. From the extracted temperature information, an accurate strain value can be determined based on a suitable calibration of strain responses with temperature variations. The temperature-induced strain measurement error at 500 $\mu\epsilon$ can be reduced from 84.3 $\mu\epsilon$ to as low as 0.39 $\mu\epsilon$.

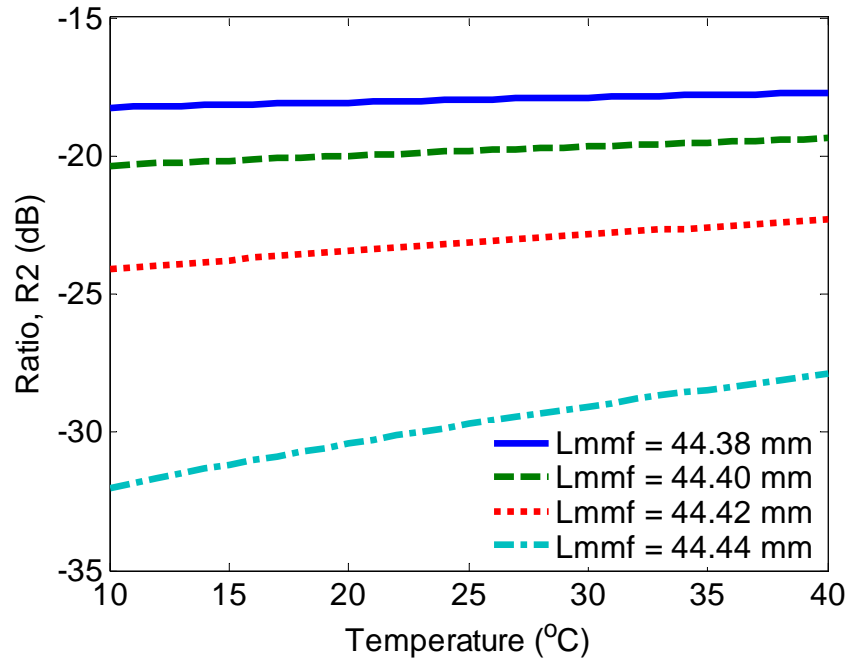


Figure 50 Calculated ratio response of SMS-2 with MMF length errors due to temperature variation at an operating wavelength of 1539 nm

For a given fixed signal source wavelength, the length of the MMF sections of SMS-1 and SMS-2 need to be optimized to achieve the highest strain and temperature dependence, respectively. It is shown in [116], that the peak wavelength of a bandpass filter can be tuned by selecting a suitable MMF length. It should be noted, that to achieve high sensitivity for strain measurement with low temperature-induced errors with a fixed wavelength source, the MMF lengths

of SMS-1 and SMS-2 need to be optimised in such a way that the edge of a dip of the SMS transmission spectrum coincides exactly with the operating wavelength.

In a radiometric power measurement, the influence of the signal-to-noise ratio of the laser source can degrade the measurement resolution [119], as well as the sensitivity of the sensor itself. According to [119], measurement resolution can be maintained if the signal-to-noise ratio of laser source is higher than 40 dB for a typical sensor response with a minimum ratio response of -35 dB. In this radiometric system, the signal-to-noise ratio of the laser source used is 55 dB and the minimum measured ratio response of R1 and R2 is higher than -35 dB as in Fig. 48(a) and Fig. 49(a), to maintain the measurement resolution.

7.4 Conclusions

The strain and temperature dependence of an SMS fibre structure has been investigated numerically and experimentally. It was found that a single SMS fibre structure for an intensity-based measurement strain sensor exhibits substantial strain error measurement due to temperature variations. It has also been demonstrated that strain measurement using a pair of SMS fibre structures within a radiometric power measurement scheme can minimize temperature induced strain measurement error. At an operating wavelength of 1539 nm, for strain measurement from 0 to 1000 $\mu\epsilon$ within a temperature range from 10 to 40 °C, the proposed configuration can provide strain and temperature measurement resolutions of 0.34 $\mu\epsilon$ and 0.14 °C, with temperature induced strain measurement error as low as 0.39 $\mu\epsilon$.

7.5 References

- [104] G. P. Brady, K. Kalli, D. J. Webb, D. A. Jackson, L. Reekie, and J. L. Archambault, “Simultaneous measurement of strain and temperature using the first- and second-order diffraction wavelengths of Bragg gratings”, *IEE Proc. Optoelec.*, vol. 144, pp. 156-161, 1997.
- [105] F. M. Hanran, J. K. Rew, and P. D. Foote, “A strain-isolated fibre Bragg grating sensor for temperature compensation of fibre Bragg grating strain sensors”, *Meas. Sci. Technol.*, vol. 9, pp. 1163-1166, 1998.
- [106] L. V. Nguyen, D. Hwang, D. S. Moon, and Y. Chung, “Simultaneous measurement of temperature and strain using a Lyot fibre filter incorporated with a fibre Bragg grating in a linear configuration”, *Meas. Sci. Technol.*, vol. 20, Article Number: 034006, 2009.
- [107] Q. Wang and G. Farrell, “All-fibre multimode-interference-based refractometer sensor: proposal and design,” *Opt. Lett.*, vol. 31, pp. 317–319, 2006.
- [108] W. S. Mohammed, P. W. E. Smith, and X. Gu, “All-fibre multimode interference bandpass filter,” *Opt. Lett.*, vol. 31, pp. 2547-2549, 2006.
- [109] A. M. Hatta, G. Farrell, Q. Wang, G. Rajan, P. Wang, and Y. Semenova, “Ratiometric wavelength monitor based on singlemode-multimode-singlemode fibre structure,” *Microw. Opt. Technol. Lett.*, vol. 50, pp. 3036-3039, 2008.
- [110] E. Li and G.-D. Peng, “Wavelength-encoded fibre-optic temperature sensor with ultra-high sensitivity,” *Opt. Commun.*, vol. 281, pp. 5768-5770, 2008.
- [111] A. M. Hatta, G. Rajan, Y. Semenova, and G. Farrell, “SMS fibre structure for temperature measurement using a simple intensity-based interrogation system,” *Electron. Lett.*, vol. 45, pp.1069-1071, 2009.
- [112] E. Li, “Temperature compensation of multimode-interference-based fibre devices,” *Opt. Lett.*, vol. 32, pp. 2064–2066, 2007.
- [113] S. M. Tripathi, A. Kumar, R. K. Varshney, Y. B. P. Kumar, E. Marin, and J. P. Meunier, “Strain and temperature sensing characteristics of single-

- mode–multimode–single-mode structures,” *J. Lightwav. Technol.*, vol. 27, pp. 2348-2356, 2009.
- [114] E. Li, “Sensitivity-enhanced fibre-optic strain sensor based on interference of higher order modes in circular fibres,” *IEEE Photon. Technol. Lett.*, vol. 19, pp. 1266-1268, 2007.
- [115] D. P. Zhou, L. Wei, W. K. Liu, Y. Liu, and J. W. Y. Lit, “Simultaneous measurement for strain and temperature using fibre Bragg gratings and multimode fibres,” *App. Opt.*, vol. 47, pp. 1668-1672, 2008.
- [116] Q. Wang, G. Farrell, and W. Yan, “Investigation on singlemode-multimode-singlemode fibre structure,” *J. Lightw. Technol.*, vol. 26, pp. 512-519, 2008.
- [117] A. M. Hatta, G. Farrell, P. Wang, G. Rajan, and Y. Semenova, “Misalignment limits for a singlemode-multimode-singlemode fibre-based edge filter,” *J. Lightw. Technol.*, vol. 27, pp. 2482-2488, 2009.
- [118] Q. Wang, G. Rajan, P. Wang, and G. Farrell, “Resolution investigation of a ratiometric wavelength measurement system,” *App. Opt.*, vol. 46, pp. 6362-6367, 2007.
- [119] Q. Wang, G. Farrell, and T. Freir, “Study of transmission response of edge filters employed in wavelength measurements,” *App. Opt.*, vol. 44, pp. 7789-7792, 2005.

Chapter 8

Conclusions and future research

This chapter presents achievements and conclusions from across the thesis. Future research as an extension of this PhD thesis is also discussed.

8.1 Conclusions from the research

The core aim of this research as stated in Chapter 1 was to investigate all-fibre multimode interference devices based on a step index singlemode-multimode-singlemode fibre structure for use as (A) a new type of edge filter for a ratiometric wavelength measurement system and as (B) novel stand alone sensors.

In this thesis, a new type of edge filter using a pair of SMS fibre structures with an X-type spectral response, has for the first time been proposed, designed, and demonstrated as an approach to improving the performance of a ratiometric wavelength measurement system. Several aspects of an SMS fibre structure edge filter have been investigated including the effect of misalignment of the SMS fibre cores during fabrication along with polarization and temperature dependence.

Novel SMS-based fibre sensors for temperature and strain measurements using an intensity-based measurement system have also been investigated. Three novel applications of SMS fibre structures have been proposed and demonstrated as a temperature sensor, a voltage sensor utilizing the strain effect, and a strain

sensor with self-temperature monitoring. For each of the research strands in this thesis, the key conclusions are summarized below, followed in each case by the research outcomes:

8.1.1. Multimode interference in an SMS fibre structure for an edge filter application

A numerical model for an edge filter was presented by using an MPA based on the LP_{0m} . Two SMS fibre structures were designed to provide an X-type edge filters spectral response as an alternative to the conventional single filter ratiometric wavelength measurement. The experimental results were presented and ratiometric wavelength measurement was demonstrated. For ratiometric wavelength measurement a discrimination range of 20.41 dB in the wavelength range 1530 to 1560 nm and a resolution better than 10 pm have been demonstrated. In addition, a comparison of performance between the use of a single edge filter and the X-type edge filters in a ratiometric wavelength measurement system was also investigated. It was shown that the use of X-type edge filters can increase measurement resolution and accuracy.

From these studies, it can be concluded that:

- An MPA based on LP_{0m} can be used successfully to investigate and design an SMS fibre structure-based edge filter.
- SMS fibre structures are suitable as X-type edge filters for a ratiometric wavelength measurement system.
- The use of X-type SMS-based edge filters can improve wavelength measurement resolution and accuracy compared to the use of a single

edge filter. At a wavelength of 1545 nm, the measurement resolution for the use of X-type and single edge filter is 4 and 8 pm, respectively; while the accuracy due to the PDL induced wavelength measurement error is 0.105 and 0.204 nm, respectively.

- The system proposed here provides a significantly better measurement sensitivity of 0.68 dB/nm compared to the sensitivity of 0.16 dB/nm reported for an the all-fibre ratiometric wavelength measurement system based on macro bending fibre-based edge filter as in [46].

8.1.2. The effect of misalignment in an SMS fibre structure on the spectral response of an edge filter

The effect of misalignment of SMS fibre cores due to the fabrication process on the spectral responses of X-type edge filters was investigated. When lateral core offsets exist, the use of an MPA based on LP_{0m} is not possible. As an alternative a numerical model based on an MPA with a set of calculated guided modes using the finite difference method (FDM) was developed to investigate the effect of misalignment of SMS fibre cores. It was proposed that a limit is needed on the tolerable misalignment of the SMS fibre cores in order to maintain the spectral performance of the edge filter. An experimental verification was also presented.

The conclusions from these studies are:

- The proposed MPA based on a set of all possible calculated modes using the FDM is a useful tool for investigating the effect of misalignment of SMS fibre cores.

- The misalignment of SMS fibre cores can affect the spectral performance of an edge filter based on an SMS fibre structure. A tolerable misalignment limit for the SMF core centre of 4 μm is proposed beyond which the spectral performance degrades unacceptably.
- While fabricating the SMS fibre structure, it is recommended that a fusion splicer with three axis adjustment is used to minimize misalignment.
- The numerical model used here, based on MPA using FDM, offers simplicity in its implementation compared to alternative models such as an MPA using a complete set of hybrid modes [60].

8.1.3. Polarization dependence of an SMS fibre structure-based edge filter

Polarization dependence in fibre optic devices can degrade measurement accuracy. The polarization dependence of an SMS fibre structure has not been investigated previously. In this thesis, the polarization dependent loss of an SMS fibre structure used as an edge filter was investigated using an MPA based on FDM. The PDL due to lateral and rotational core offsets was investigated numerically and experimentally. It was shown that the PDL of the SMS edge filter depends on its lateral and rotational core offsets. It was demonstrated that the core offset must be minimised to achieve low PDL for an SMS fibre structure-based edge filter. It was proposed that when lateral core offsets are unavoidable, the PDL of an SMS edge filter can still be minimized by introducing a rotational core offset of 90° . Supporting experimental results were also presented.

From the studies, it can be concluded that:

- The main source of PDL in an SMS fibre structure is SMS core offset.
- The PDL of an SMS edge filter depends on its lateral and rotational cores offsets.
- Lateral core offsets are undesirable as they will increase the PDL for the SMS edge filter. However, if lateral offsets do occur, then by introducing a deliberate rotational core offset of 90° , the PDL can be minimized considerably. The average PDL of SMS edge filter in the edge filter wavelength range can be reduced from 0.215 to 0.092 dB with a rotational core offset of 90° . This PDL is competitive with other filter implementations, for example for a macro-bending fibre edge filter, the average PDL within the wavelength range is about 0.2 dB [71].

8.1.4. Temperature dependence of an SMS fibre structure-based edge filter

The temperature dependence of an edge filter based on an SMS fibre structure was investigated numerically and experimentally. An MPA based on the LP_{0m} was used to investigate the temperature dependence of an SMS fibre structure-based edge filter. The influence of two parameters – the thermo optic coefficient (TOC) and the thermal expansion coefficient (TEC) on the temperature dependence of an SMS edge filter was investigated numerically. It was shown that the TOC makes a more significant contribution to the temperature dependence compared to the TEC. For ratiometric wavelength measurement using X-type edge filters based on SMS fibre structures, a small temperature variation can induce a ratio variation

and in turn a wavelength measurement error. It was proposed and demonstrated that self-monitoring of temperature can be carried out using an expanded ratiometric scheme. It was shown that self-monitoring of the temperature reduces temperature induced wavelength error to ± 10.7 pm at 1545.

The conclusions from these studies are:

- The TOC makes a more significant contribution to the temperature dependence of an SMS edge filter compared to the TEC.
- The linearity of the SMS edge filter's response to both wavelength and temperature potentially allows the use of the SMS structure to monitor its own temperature using an expanded ratiometric scheme.

8.1.5. Novel standalone sensors based on an SMS fibre structure

As an alternative to the FBG-based sensors, an SMS fibre structure is proposed as a novel stand alone sensor with the advantages of low cost and simple fabrication by comparison to FBGs. Furthermore, in this thesis, SMS fibre structure sensors are interrogated using an intensity-based measurement system, offering low cost, a simple configuration and the potential for high speed measurement compared to interrogation techniques that tracks a peak or a dip in a spectral response using an OSA. Three novel applications of the SMS fibre structure were investigated in this thesis as:

a) A temperature sensor.; An SMS fibre structure as a standalone sensor for temperature using interrogation based on intensity measurement was investigated numerically and experimentally. The SMS fibre structure was optimized to provide a strong temperature dependence that can be utilized as a temperature sensor. A temperature measurement range of 50 to 200 °C with a potential

resolution of 0.2 °C is demonstrated. It is simpler and can provide competitive resolution when compared to the FBG-based temperature sensor. In the FBG-based temperature sensor, to resolve a temperature change of ~ 0.1 °C requires a high wavelength resolution measurement of ~ 1 pm [12].

b) A voltage sensor; The application of an SMS fibre structure for voltage measurements based on utilizing the strain effect was investigated. Typical applications are voltage measurement in an area of high EM fields or at high voltages when dielectric breakdown must be avoided. For use as a voltage sensor, voltage was converted into a strain to be measured by an SMS structure, using a piezoelectric (PZT) transducer. The SMS fibre structure, attached to the PZT, was utilized in a ratiometric power measurement scheme. The sensor was investigated and demonstrated both numerically and experimentally. A DC voltage measurement range from 0 to 100 V with a resolution of about 0.5 V or 0.5% of full scale measurement was demonstrated. The proposed sensor offers a simple configuration, fast measurement capability, and the potential for kilovolt measurement with a suitable choice of PZT. For comparison for voltage measurement over the range from 0 to 5 kV using an FBG and a suitable PZT, a measurement resolution of 3% of full scale has been achieved, which is lower than the resolution achieved in this thesis [102].

c) A strain sensor; A strain sensor with a very low temperature induced strain measurement error was investigated. For this purpose two SMS fibre structures were proposed and demonstrated in a ratiometric power measurement scheme, one SMS structure acts as the strain sensor and the other SMS structure acts as a temperature monitor. The use of this configuration allows minimization of the

temperature induced strain measurement error. It was demonstrated that for strain measurement from 0 to 1000 $\mu\epsilon$ within the temperature range 10 to 40 $^{\circ}\text{C}$, the proposed configuration can provide a strain and temperature resolution of 0.34 $\mu\epsilon$ and 0.14 $^{\circ}\text{C}$, respectively, with a corresponding temperature induced strain measurement error as low as 0.39 $\mu\epsilon$.

From the studies, it can be concluded that:

- A linear relationship between intensity transmitted by the SMS structure at a fixed wavelength and temperature can be achieved by optimizing the length of the MMF and the operating wavelength. This effect can be utilized as a temperature sensor which can be used with a simple interrogation scheme and high speed measurement for a range of temperature sensor applications.
- It is also shown that a linear relationship between the transmitted intensity and strain applied to the SMS fibre structure can be achieved by optimizing the length of the MMF section and operating wavelength. Based on the strain effect, the SMS fibre structure attached to a PZT can be used for voltage measurement in a ratiometric power measurement scheme which offers a simple configuration, a fast measurement capability of 1 kHz measurement speed can be achieved, and the potential for kilovolt measurement with a suitable choice of PZT.
- The SMS fibre structure is sensitive to both strain and temperature. In a strain sensor application, the use of two SMS fibre structures in an expanded ratiometric power measurement system can effectively reduce

temperature induced strain measurement error from 84.3 $\mu\epsilon$ to 0.39 $\mu\epsilon$ at the strain of 500 $\mu\epsilon$.

8.2 Overall conclusions from the research

An SMS fibre structure is suitable as an edge filter and can be implemented as X-type edge filters in an all-fibre ratiometric wavelength measurement system for an interrogation of FBG-based sensors which are among the most common fibre sensors. Several aspects that can impair the performance of an SMS structure-based edge filter have been investigated, including the effect of misalignment of the SMS fibre cores (due to fabrication tolerances), polarization dependence, and temperature dependence. Several approaches have been proposed and demonstrated to achieve high performance for wavelength measurement. For the first time, a limit of 4 μm or lower on the maximum core offsets for an SMS structure has been shown to be required to ensure the desired spectral performance achieved. It is found, that the PDL of an SMS fibre edge filter depends on the lateral and rotational cores offsets. To achieve low PDL, the cores offset also must be reduced. If the lateral offsets do occur the PDL can be reduced considerably by introducing a rotational core offset of 90° during splicing. The temperature dependence of X-type edge filters based on SMS fibre structures can be minimized by using self-temperature monitoring in an expanded ratiometric wavelength measurement system.

An SMS fibre structure is also suitable for stand alone sensors using an intensity-based measurement system as an alternative to the FBG-based sensors. Based on studies of temperature and strain effects, an SMS fibre structure can be

utilized as a temperature sensor and a voltage sensor. The proposed sensors provide competitive resolution with the advantages of low cost, a simple fabrication process, and simple interrogation technique, compared to the FBG-based sensors. The cross sensitivity of the temperature and strain response, commonly found with an FBG sensor is also present for sensor based on an SMS fibre structure. The temperature induced strain measurement error for an SMS strain sensor can be minimized by using two SMS fibre structures in an expanded ratiometric power measurement system.

An SMS fibre structure has been shown to be an effective approach for both the interrogation of FBG sensor and for the development of new sensor types. By comparison to other edge filter for use in an interrogation system for an FBG, several advantages have been demonstrated such as the ability to implement X-type edge filters responses. Several successful sensors implementations have also been demonstrated and the potential exists for other sensing applications, for example for vibration sensing, bend sensing, and refractive index sensing or bio-sensing. Finally, the use of MMI for sensing has been proved which potentially expands the range of applications for other photonic devices that are based on MMI. Overall, the work has expanded and improved understanding and knowledge of optical sensing, for a diverse range of potential applications, including structural health monitoring, industrial processes and power system measurement.

8.3 Future research

This thesis has described numerical and experimental investigation of SMS fibre structure as a new type of edge filter and as novel stand alone sensors. There remain a number of unanswered research questions and challenges, such as:

8.3.1. Implementation of ANN for self temperature monitoring

Temperature dependence does affect the performance of an SMS fibre structure-based edge filter. An expanded ratiometric utilizing two SMS fibre structures-based the X-type edge filters has been proposed. An inverse matrix approach can be used to extract the wavelength and temperature information. However, the measurement accuracy is limited due to the matrix coefficient variations on the wavelength and temperature responses. To increase the measurement accuracy, an artificial neural network (ANN) approach will be used. The ANN can model the nonlinear or linear relationship between the input and output data. The ANN architectures and their parameters will be investigated to achieve a high measurement accuracy.

8.3.2. Bending and vibration in an SMS fibre structure

In this thesis, a straight SMS fibre structure has been investigated numerically and experimentally. An MPA based on LP_{0m} or based on FDM has been successfully used to investigate the light propagation in SMS fibre structures. For future research, bending and vibration effects in the SMS fibre structure will be investigated. A theoretical model based on MPA will be extended or a suitable modelling platform such as a beam propagation method (BPM) will be considered

to simulate the light behaviour in a bending or vibrating SMS fibre structure. Potential applications such as an airflow sensor and a vibration sensor based on this effect will be investigated.

8.3.3. Novel fibre hetero structure of SMMS fibre structure

A new type of a fibre hetero-structure, a singlemode-multimode-multimode-singlemode (SMMS) fibre structure, with two different types of MMF fibres, will be investigated in future research. A theoretical model will be developed to simulate the light behaviour in the SMMS fibre structure. Since the two MMF sections of SMMS fibre structure will have a different refractive index profile, core radius and length, the effect of strain and temperature will be different compared to the SMS fibre structure. There is a cross sensitivity of strain and temperature response in an SMS fibre structure. The cross sensitivity of strain and temperature in a SMMS fibre structure will be investigated theoretically and experimentally. Preliminary experimental results suggest that this new structure may allow for temperature independent strain detection.

8.3.4. Development of integrated ratiometric wavelength monitor

In this thesis, the all-fibre ratiometric wavelength measurement system utilizing an X-type SMS fibre structure edge filter based on MMI have been demonstrated. An integrated optic version of a ratiometric wavelength monitor will be developed as a part of future research. Introductory theoretical modelling and design for an integrated version of the X-type edge filter based on MMI have been carried out earlier. Two designs are presented in Appendix C and Appendix D. In Appendix C, a Y-branch and two MMIs based on planar lightwave circuit (PLC) of silica on

silicon buried channel waveguides were designed and optimized to provide the X-type spectral response. In Appendix D, a simple configuration for an integrated ratiometric wavelength monitor with the X-type spectral response based on a single MMI structure has been proposed and presented. The fabrication and characterization of an integrated ratiometric wavelength monitor will be carried out with the support of Science Foundation Ireland (SFI) under the National Access Programme (NAP) at Tyndall National Institute, Cork, Ireland.

Appendix A

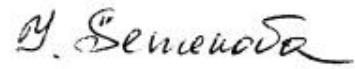
Statement of Contribution

For the publications presented within this thesis, the co-authors listed below certify that:

1. Agus Muhamad Hatta is the first author for all the publications.
2. As first author, Agus Muhamad Hatta undertook all aspects of the research described in each publication, including preparation and submission of the publication and the preparation of any revisions requested by referees, with the support and advice of the co-authors.
3. The co-authors agree to the use of the publications in this thesis.



Prof. Gerald Farrell



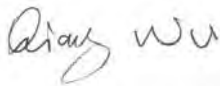
Dr. Yuliya Semenova



Dr. Ginu Rajan



Dr. Pengfei Wang



Dr. Qiang Wu



Dr. Qian Wang



Prof. Jie Zheng

Appendix B

Ratiometric wavelength monitor based on “X-type spectral response” using two edge filters^a

Keywords: fibre optics, multimode interference, edge filter, wavelength monitor

Abstract: The performance of an all-fibre ratiometric wavelength measurement system is compared for the case of two edge filters and the case of one edge filter. The two fibre edge filters are used with overlapping and opposite slope spectral responses, a so called “X-type spectral response”, each based on singlemode-multimode-singlemode (SMS) fibre structures. Noise and polarization dependent loss (PDL) are the two parameters that determine the resolution and an accuracy of the system. It is demonstrated that the use of two SMS edge filters for a ratiometric wavelength measurement system can increase the resolution and the accuracy when compared with a system using only one edge filter.

^a A. M. Hatta, G. Rajan, G. Farrell and Y. Semenova, “Ratiometric wavelength monitor based on X-type spectral response using two edge filters,” *Optical Sensors 2009, Proceeding of SPIE*, 7356, 73561N, 2009.

B.1 Introduction

A wavelength monitor is a key component for a fibre-Bragg-grating (FBG) sensing system. An FBG-based optical sensing system requires a wavelength demodulation system to detect the wavelength shift of reflected light from the FBG elements induced by strain or temperature changes. There are several different schemes for wavelength measurement/monitoring. Among the available schemes, an all-fibre ratiometric power measurement technique offers a simple configuration, an easy connection all-fibre configuration, the potential for high-speed measurement, and the absence of mechanical movement compared to wavelength-scanning-based active measurement schemes. A ratiometric scheme converts a wavelength measurement into a signal intensity measurement. A ratiometric wavelength monitor usually consists of a splitter with two outputs to which are attached an edge filter arm with a well defined spectral response and a reference arm. Alternatively, two edge filters arms with overlapping opposite slope spectral responses [120], a so-called “X-type spectral response”, can be used to increase the resolution of the measurement system. The main element of the all-fibre ratiometric scheme, the edge filter, can be implemented by biconical fibre couplers [121], bending fibre [122], and singlemode-multimode-singlemode (SMS) fibre structure [123].

A resolution and an accuracy of wavelength measurement of ratiometric system need to be considered. In a previous study, it is shown that the resolution of wavelength measurement of ratiometric system is determined by the signal-to-noise ratio of the input signal and the noise of the photodetectors associated with optical-to-electronic conversion [124]. It is also shown in [125], that the

polarization dependent loss (PDL) of a ratiometric system determines the accuracy of wavelength measurement. In [124] and [125], the ratiometric system utilized one edge filter based on a macrobend fibre. In this paper, further investigation on the resolution due to the noise and the accuracy induced by PDL of ratiometric wavelength measurement based on “X-type spectral response” using two edge filters is carried out. The two edge filters are based on SMS fibre structure [123]. The performance of ratiometric measurement system is compared for the case of two edge filters and the one edge filter case.

B.2 Ratiometric wavelength measurement

Fig. 51(a) and 51(b) show the schematic configuration of an all-fibre configuration of a ratiometric wavelength measurement system either employing two edge filters with X-type spectral response or one edge filter, respectively. The input signal is divided into two signals, one passes through the edge filter 1 (E1) arm and the other passes through the edge filter 2 (E2) arm or reference (ref) arm. Two photodetectors are placed at the ends of both arms. The target spectral responses in a wavelength range from λ_L to λ_U of the edge filters and the reference are shown in the Fig. 51(c). The corresponding ratios of the two outputs over the wavelength range are presented in Fig. 51(d) for the use of two edge filters and one edge filter. In both cases the wavelength of an unknown input signal can be determined by measuring the ratio of the electrical outputs of the two photodetectors, assuming a suitable calibration has been carried out. In this investigation the edge filters are based on singlemode-multimode-singlemode (SMS) fibre structures as shown in Fig. 51(e). The SMS fibre edge filter is

fabricated by splicing a specified length of a multimode fibre (MMF) with two singlemode fibres (SMF) at the ends of MMF.

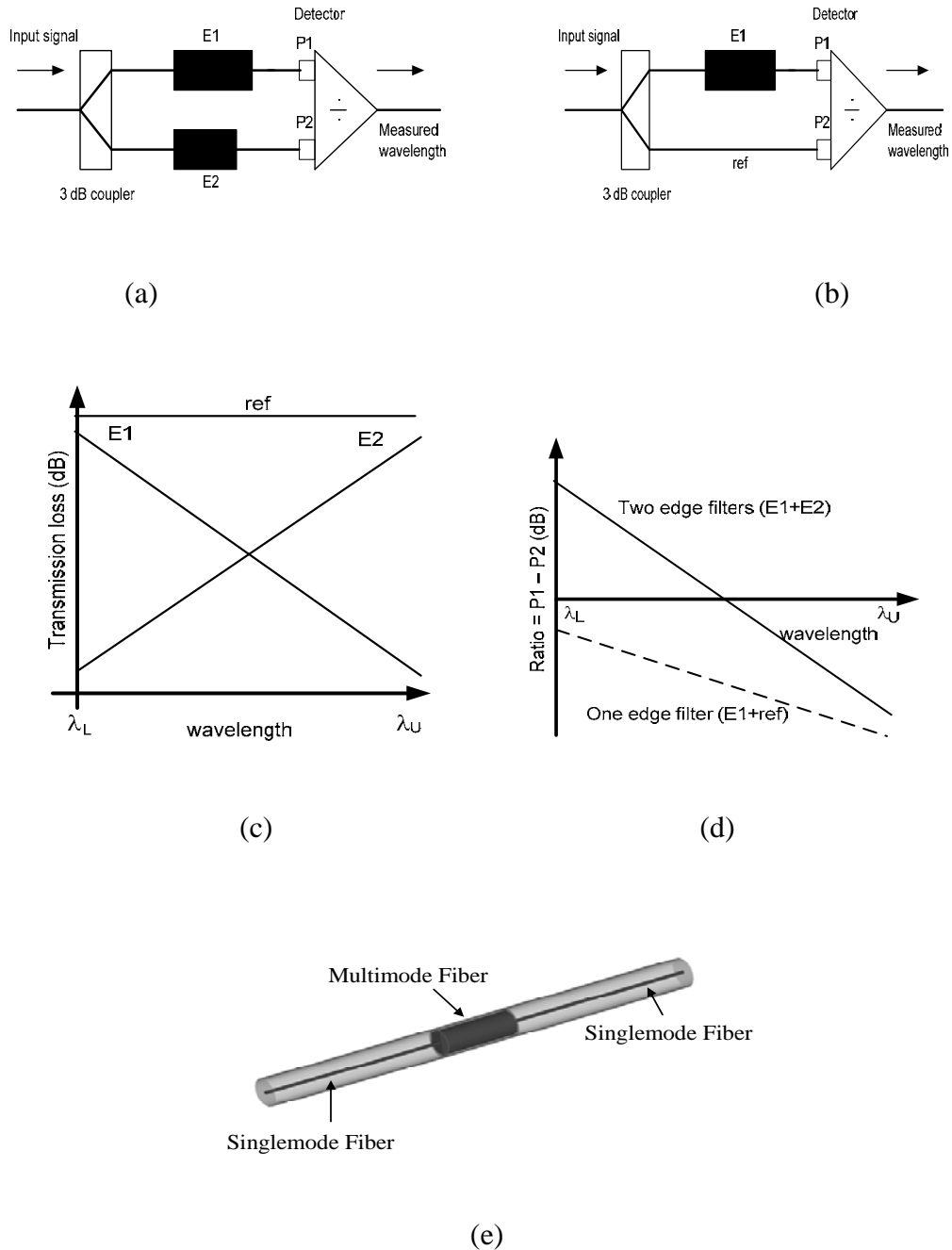


Figure 51 Schematic configuration of the proposed MMI ratiometric wavelength monitor (a) using two edge filters (b) using one edge filter, (c) Desired spectral response of two edge filter arms and (d) The output ratio between two arms (e) SMS fibre edge filter

It is useful to initially consider the design of the SMS edge filter(s). In order to design an SMS fibre edge filter, a modal propagation analysis (MPA) for linearly polarized (LP) modes is used [126], [127]. A brief review of the design, fabrication and measurement of the SMS edge filter(s) can be found in [123]. A target wavelength range for wavelength measurement from 1530 to 1560 nm is chosen. This range is chosen as it corresponds to the typical centre wavelengths for many FBG sensors. The calculated and measured results of SMS edge filters, as described in [123], E1 and E2, are shown in Fig. 52. The measured results show a good agreement with the numerical results. The discrepancy between the calculated and measured results is most likely a consequence of splice insertion losses.

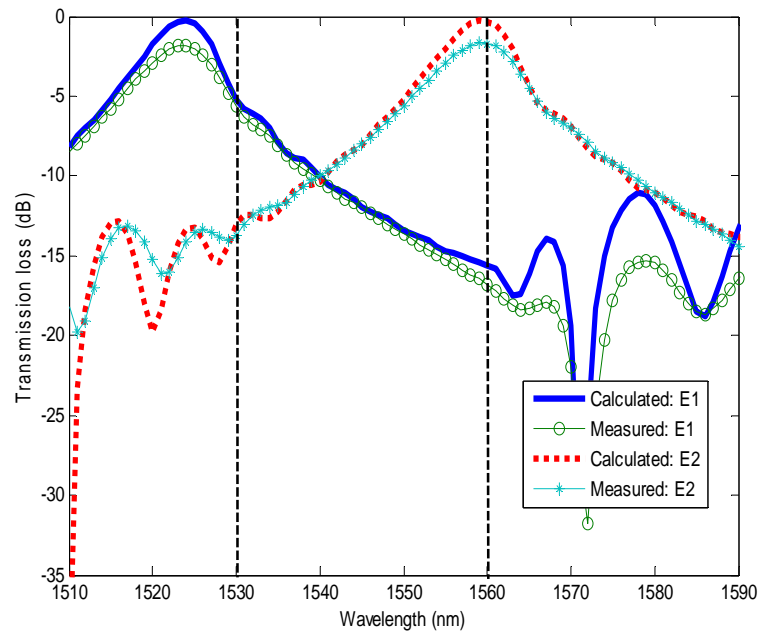


Figure 52 Calculated and measured two SMS fibre edge filters X-type spectral response

To demonstrate the use of the two SMS fibre edge filters in a functioning wavelength measurement system a ratiometric measurement system is built as shown in Fig. 51(a). The input signal is split into two equal intensity signals using a 3 dB fibre splitter. One signal passes through E1 and the other passes through E2. A high speed dual channel power meter is placed at the ends of both arms. Fig. 53 shows the measured ratio of the optical power. The ratio measured between 1530 to 1560 nm has a linear slope with a discrimination range of 25.37 dB from 10.13 to -15.25 dB which is suitable for wavelength measurement. As a comparison, the ratio response for the case of one SMS fibre edge filter as in Fig. 51(b) is also presented in Fig. 53. The use of two edge filters compared to the one edge filter increases the slope of ratio response, from 0.40 dB/nm to 0.84 dB/nm.

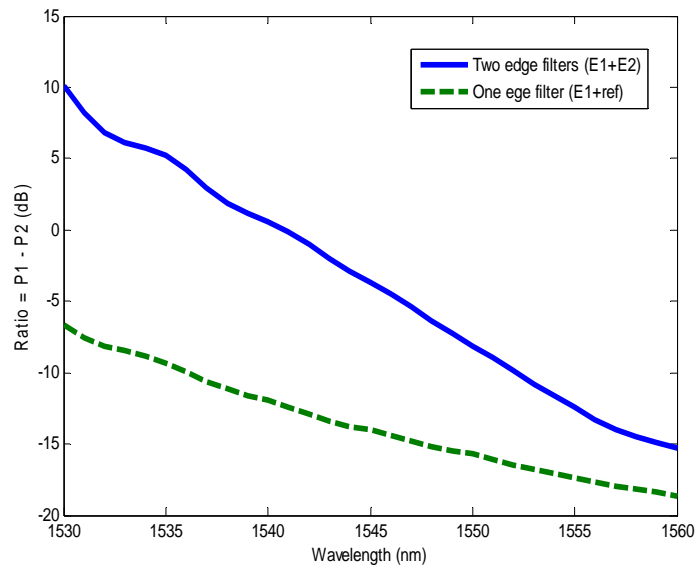


Figure 53 Measured ratio response for the use of two edge filters and one edge filter

B.3 Resolution and accuracy investigation

B.3.1 Resolution

The minimum wavelength shift or resolution of wavelength measurement due to the noise in ratiometric system is investigated. The output ratio at wavelength λ_0 for a ratiometric system [124], utilizing two edge filters as in Fig. 51(a) is

$$R(\lambda_0) = -10 \cdot \log_{10} \left[\frac{\int C_1(\lambda) I_{\lambda_0}(\lambda) E_1(\lambda) d\lambda}{\int C_2(\lambda) I_{\lambda_0}(\lambda) E_2(\lambda) d\lambda} \right] = P_1 - P_2 \quad (\text{B.1a})$$

and for the ratiometric system using one edge filter as in Fig. 51(b) is

$$R(\lambda_0) = -10 \cdot \log_{10} \left[\frac{\int C_1(\lambda) I_{\lambda_0}(\lambda) E_1(\lambda) d\lambda}{\int C_2(\lambda) I_{\lambda_0}(\lambda) d\lambda} \right] = P_1 - P_2 \quad (\text{B.1b})$$

where $C_1(\lambda)$ and $C_2(\lambda)$ are the outputs of the 3db fibre coupler which for an ideal case it is assumed wavelength independent and thus $C_1(\lambda) = C_2(\lambda) = 0.5$ in measurable wavelength range. $E_{1,2}(\lambda)$ is the transmission loss response of the edge filter, and $I_{\lambda_0}(\lambda)$ is the spectrum of the input signal. $P_{1,2}$ is the output from each arm. The spectrum of the input signal, $I_{\lambda_0}(\lambda)$, also takes account of the limited signal-to-noise-ratio (SNR) of the source as described in [128]. As in [124], taking into account of the noise generated by the photodetectors and the electronic circuitry, the output ratio is modelled with a random number value within the resolution range as:

$$\text{Ratio}(\lambda_0) = R(\lambda_0) + rR_M \quad (\text{B.2})$$

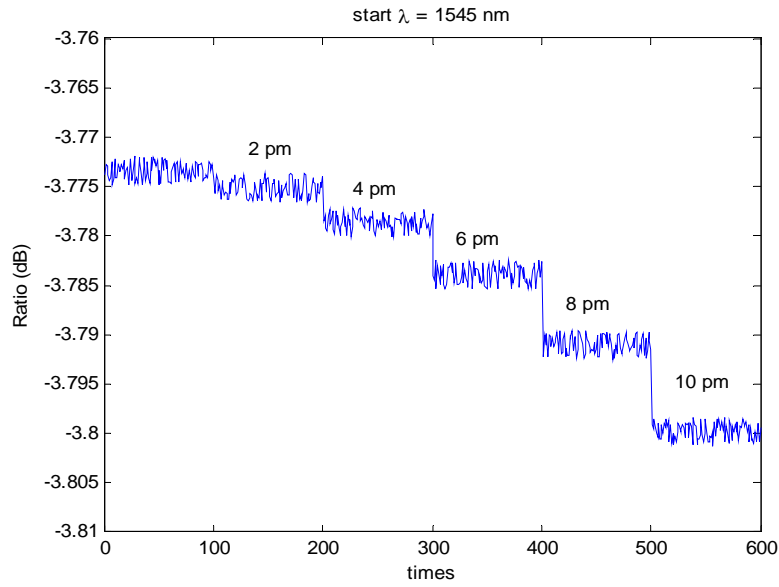
where R_M is the range of variation of the output ratio, and r is a Gaussian random number produced for each measurement. Gaussian statistics are used as they

closely approximate the statistical nature of the noise arising from optoelectronic conversion.

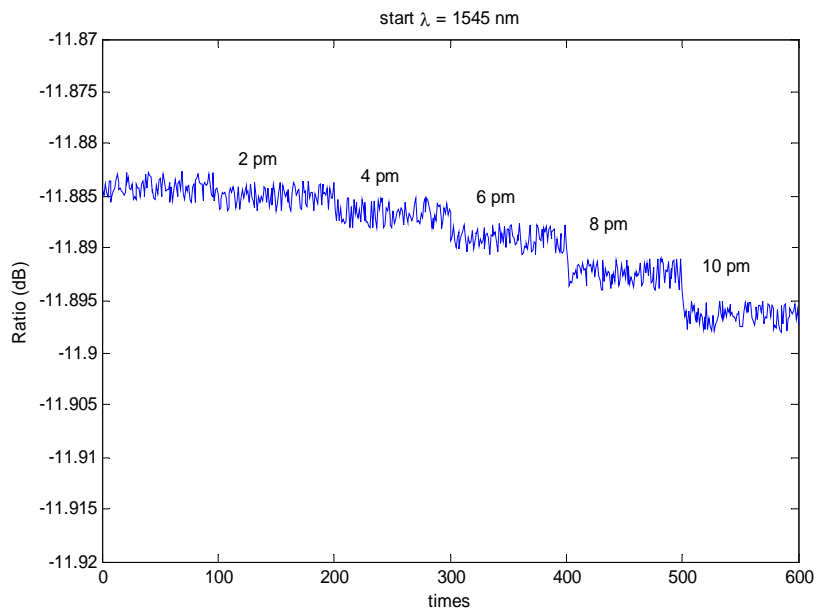
A numerical example is presented to illustrate the resolution of ratiometric system. The input signal from the tunable laser is assumed to have an SNR of 50 dB at $\lambda_0 = 1545$ nm within the wavelength range and the corresponding variation R_M due to the photodetectors' noise is 0.003 dB [124]. The calculated ratio for the ratiometric system using two edge filters is shown in Fig. 54(a) as the wavelength is tuned from $\lambda_0 = 1545$ nm by successively increasing increments of 2, 4, 6, 8 and 10 pm. It is shown that the minimum wavelength shift or resolution of this ratiometric is about 4 pm. To compare the resolution of a ratiometric system utilizing one edge filter, the calculated ratio is shown in Fig. 54(b) with a minimum resolution is about 8 pm.

To experimentally confirm the resolution performance of the ratiometric system, the tunable laser was used to provide an input signal and the corresponding output ratio was recorded. The minimum tuning step for the available laser used is 10 pm. The source wavelength is set to 1545 nm and is tuned by successively increasing increments of 10, 20 and 30 pm. The dual channel power meter is used to sample the SMS outputs for 4-6 s and the ratio in dB of the power levels is determined for each sample with a sampling rate of 50 measurements/second. Fig. 55 shows the complete time series of the measured ratio values as a function of sample time and the wavelength increments. Fig. 55(a) and 55(b) show the measured ratio for the ratiometric system with two edge filters and one edge filter, respectively. From Fig. 55, one can see that the use of

two edge filters can resolve wavelength increments with greater significantly greater success than the use of one edge filter.

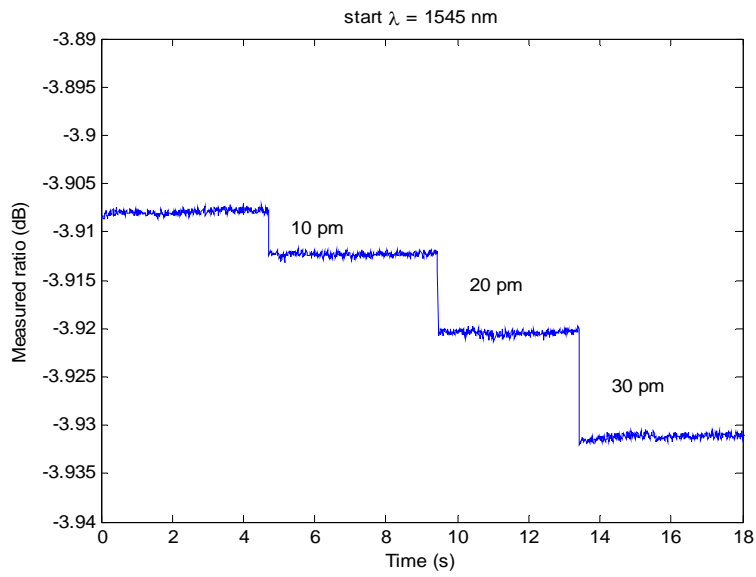


(a)

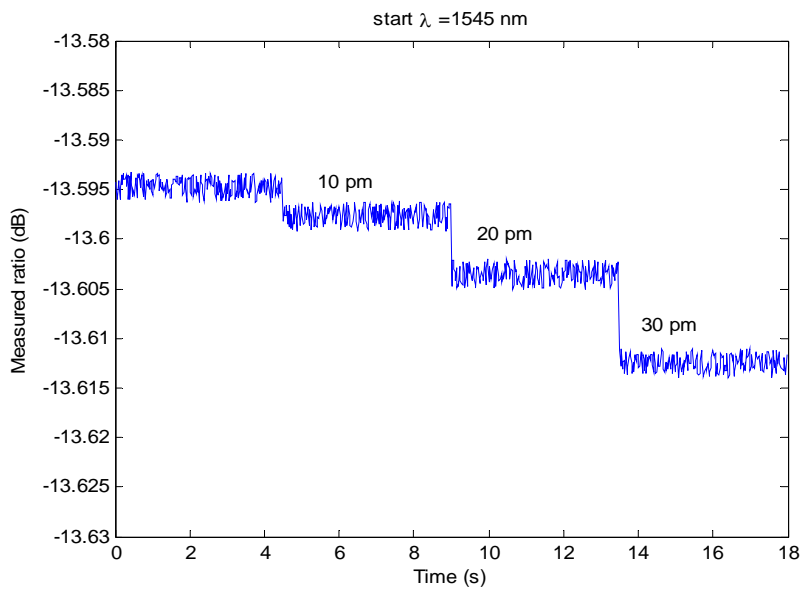


(b)

Figure 54 Calculated ratio with tuning increment from 2 to 10 pm (a) two edge filters, (b) one edge filter



(a)



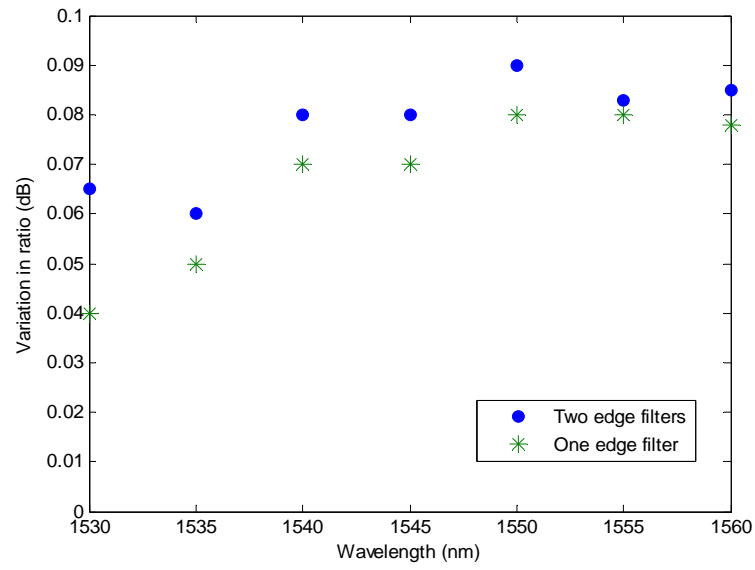
(b)

Figure 55 Measured ratio with tuning increment from 10 to 30 pm (a) two edge filters, (b) one edge filter

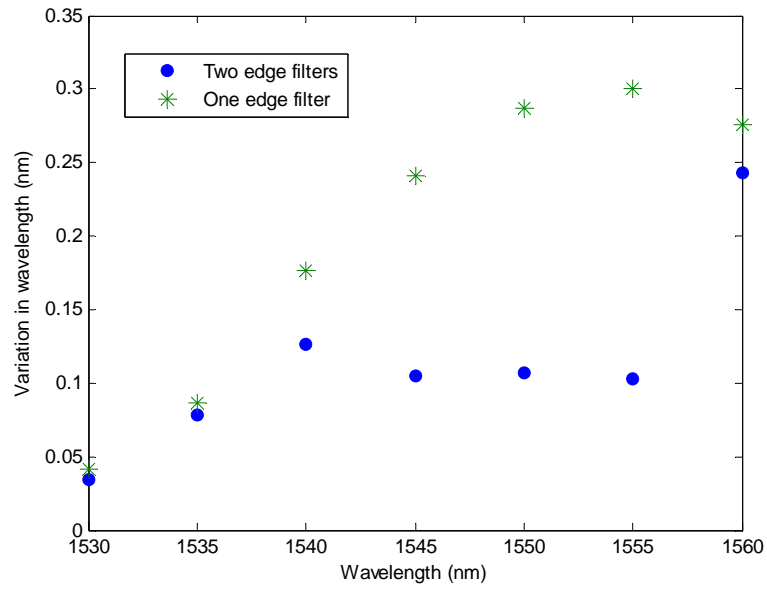
B.3.2 Accuracy and the effect of Polarization Dependent Loss

The polarization dependent loss (PDL) of an edge filter(s) is known to have a serious impact on the accuracy of a radiometric wavelength measurement system [125]. To experimentally compare the influence of PDL on the wavelength accuracy of a system based on the use of one or two edge filters, a polarization controller was used to change the input polarization state of the input light. The systems were calibrated at a fixed polarization state. The polarization state is changed over the measurable wavelength range so as to induce the maximum variation in the measured value by comparison to the calibrated value for both the measured ratio and wavelength shift [125]. Fig. 56 presents the measured variation in ratio and variation in wavelength. The measured variation in wavelength is obtained from the calibrated ratio response. It is shown in Fig. 56(a), the use of two edge filters increases slightly the variation in ratio induced by PDL.

However, the use of two edge filters can reduce the PDL induced wavelength variation, as shown in Fig. 56(b). This occurs because of the higher slope of the ratio response as in Fig. 53. The wavelength variation or a wavelength error at 1545 nm is 0.105 and 0.240 nm for the use of two edge filters and one edge filter, respectively. Thus the use of two SMS fibre edge filters can increase the accuracy even when the input polarization state changes.



(a)



(b)

Figure 56 Measured variation in ratio (a) and wavelength (b) due to the PDL of the system for the use of two edge filters and one edge filter

B.4 Conclusion

The performance of an all-fibre ratiometric wavelength measurement based on SMS edge filter(s) has been investigated. The resolution due to the noise in a ratiometric system and the accuracy induced by PDL is demonstrated. It is shown the ratiometric wavelength measurement system using two SMS fibre edge filters with the X-type spectral response can increase the resolution and the accuracy compared to the use of one SMS edge filter.

B.5 References

- [120] S. M. Melle, K. Liu, and R. M. Measures, "Practical fibre optic Bragg grating strain gauge system", *App. Opt.*, vol. 32, pp. 3601–3609, 1993.
- [121] A. B. L. Ribeiro, L. A. Ferreira, M. Tsvekov, and J. L. Santos, "All-fibre interrogation technique for fibre Bragg sensors using a biconical fibre filter," *Electron. Lett.*, vol. 32, pp. 382–383, 1996.
- [122] Q. Wang, G. Farrell, T. Freir, G. Rajan, and P. Wang, "Low-cost wavelength measurement based on a macrobending single-mode fibre," *Opt. Lett.*, vol. 31, pp. 1785-1787, 2006.
- [123] A. M. Hatta, G. Farrell, Q. Wang, G. Rajan, P. Wang, and Y. Semenova, "Ratiometric wavelength monitor based on singlemode-multimode-singlemode fibre structure", *Microw. Opt. Technol. Lett.*, vol. 50, pp. 3036-3039, 2008.
- [124] Q. Wang, G. Rajan, P. Wang, and G. Farrell, "Resolution investigation of a ratiometric wavelength measurement system," *App. Opt.*, vol. 46, pp. 6362-6367, 2007.
- [125] G. Rajan, Q. Wang, Y. Semenova, G. Farrell, and P. Wang, "Effect of polarization dependent loss on the performance accuracy of a ratiometric wavelength measurement system," *IET Optoelectronics*, vol. 2, pp. 63-68, 2008.

- [126] W. S. Mohammed, P. W. E. Smith, and X. Gu, "All-fibre multimode interference bandpass filter," *Opt. Lett.*, vol. 31, pp. 2547-2549, 2006.
- [127] Q. Wang, G. Farrell, and W. Yan, "Investigation on singlemode-multimode-singlemode fibre structure," *J. Lightw. Technol.*, vol. 26, pp. 512-519, 2008.
- [128] Q. Wang, G. Farrell, and T. Freir, "Study of transmission response of edge filters employed in wavelength measurements," *App. Opt.*, vol. 44, pp. 7789-7792, 2005.

Appendix C

Design of the optical core of an integrated ratiometric wavelength monitor^a

Abstract: The optical core of an integrated ratiometric wavelength monitor which consists of a Y-branch and two edge filters, with opposite spectral responses, based on a pair of symmetrical multimode interference (MMI) structures is proposed. The designed ratiometric structure demonstrates a suitable spectral response, with potentially a 20 pm resolution over a 100 nm wavelength range.

C.1 Introduction

Wavelength monitoring and measurement is required in many optical systems such as multi-channel dense wavelength-division multiplexing optical communication systems and fibre-Bragg-grating-based optical sensing systems. In one wavelength monitoring scheme, the so-called a ratiometric detection scheme, the wavelength of an input signal is determined by the measurement of the ratio of two signal powers. It has a simple configuration and offers the potential for high-

^a A. M. Hatta, G. Farrell, Q. Wang and J. Zheng, "Design of the optical core of an integrated ratiometric wavelength monitor," *Proceeding of 14th European Conference on Integrated Optics (ECIO), ECIO'08*, pp. 273-276, 2008.

speed measurement as compared with wavelength-scanning-based active measurement schemes. A ratiometric wavelength measurement scheme can be implemented with bulk devices, an all-fibre-based configuration or integrated optical circuits. Integrated wavelength monitors have a compact size, a fast response, are more robust and have a low fabrication cost compared to bulk optical devices. Examples of the designed and developed integrated wavelength monitors include multimode interference (MMI) couplers, a Y-branch with an S-bend structure, and a Y-branch with an MMI structure [129]-[131].

In [129], the wavelength monitor consists of a central MMI waveguide, two output waveguides, and one input waveguide. For wavelength measurement it offers a 100 nm range and 200 pm resolution. Previously, in [131], we have shown that an MMI structure can be used as an edge filter for a ratiometric wavelength monitor. In [131], the length and width of the multimode section, and the positions of the input and output waveguides are optimised according to a desired spectral response by using the global optimisation algorithm-adaptive simulated annealing. We propose here a further improvement, with a ratiometric scheme which employs two opposite slope edge filters offering a higher resolution compared with the ratiometric scheme with one edge filter and one reference arm [132]. In this paper, two edge filters with opposite slope spectral responses based on a symmetrical MMI are designed and can be used for high resolution wavelength monitoring.

C.2 Proposed configuration and design method

Fig. 57(a) shows a schematic configuration of an integrated ratiometric structure. It contains a Y-branch splitter and two edge filter arms, containing symmetrical MMI structures. The desired spectral responses of the two arms are shown in Fig. 57(b), while the corresponding ratio of the two outputs over a wavelength range is presented in Fig. 57(c). The wavelength of an input signal can be determined through measuring the power ratio of the output ports at the outputs of the two arms, assuming a suitable calibration has taken place.

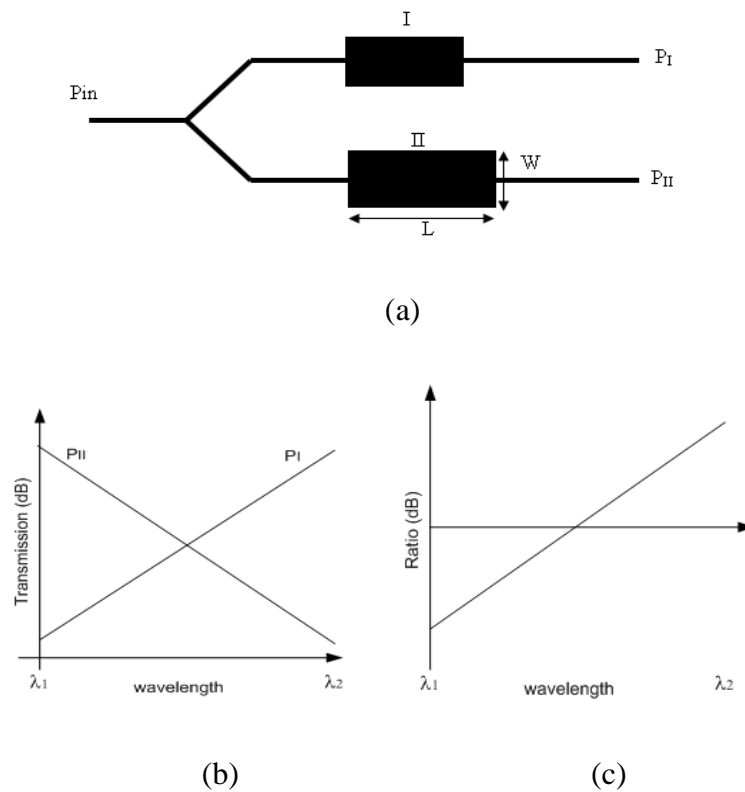


Figure 57 (a) Schematic configuration of ratiometric structure with two edge filter arms with MMI structures (b) Desired spectral response of two edge filter arms and (c) The output ratio between two arms

The design steps for each MMI structure are identical. To optimise an individual MMI structure for an edge filter application, the width (W) and length (L) of the MMI are adjusted. The transmission response of the MMI is calculated for each W and L of MMI. A modal propagation analysis (MPA) can be used to calculate the transmission response in the multimode waveguide [133]. It is known that the desired edge filter corresponds to either an increasing or decreasing transmission as the wavelength increases over the wavelength range. Therefore, it is necessary to calculate the transmission response between the lower and upper limits [λ_1 and λ_2] of the desired wavelength range over a range the W and L values for the MMI. For each W of the each MMI, we scan the length L in increments of $0.01 L_\pi$ (where L_π is the beat length) and determine the transmission value at λ_1, λ_2 as $P(\lambda_1), P(\lambda_2)$ and then calculate the corresponding discrimination range $D = |P(\lambda_1) - P(\lambda_2)|$ (thus $P(\lambda_1)$ and $P(\lambda_2)$ should be in dB). A symmetrical MMI produces a self image at a distance $L = \frac{3}{4} L_\pi$, so we can set the scanning range of L as $0 \leq L \leq 2 \frac{3}{4} L_\pi(\lambda_1)$.

After calculating $P(\lambda_1)$ and $P(\lambda_2)$ for each W and L for an MMI we select some structures as possible candidates. We select the structures based on the constraints that the discrimination, D , should be better than 10 dB and that the baseline loss (either $P(\lambda_1)$ and $P(\lambda_2)$ depending on whether the slope is negative or positive) should also be less than 8 dB. Then we calculate the spectral response for each selected structures. An ideal response for the edge filter should give a linear dependence for wavelength versus transmission. We can use a linear curve fitting and get a slope (m) of linear function ($T(\lambda) = m\lambda + c$) and a norm residual

(nxr) from a QR decomposition of the Vandermonde matrix [134], as the parameters to choose the best spectral response. The ideal spectral response has high m and low nxr . The optimal edge filter with positive or negative slope is chosen based on a figure of merit:

$$F = \exp \left[- \left(\frac{c_n nxr}{c_m |m|} \right) \right] \quad (C.1)$$

where c_n and c_m are weighting coefficients. The best edge filter occurs when $F = 1$ and the worst when $F = 0$.

C.3 Numerical example and discrimination demonstration

As a numerical example, a buried silica-on-silicon waveguide is chosen where the refractive index of the core and cladding is 1.4553 and 1.4444, respectively. The waveguide cross section is $5.5 \mu\text{m} \times 5.5 \mu\text{m}$ and the multimode section thickness is $5.5 \mu\text{m}$. The effective index method is used to simplify the calculation. The wavelength range for this example is taken to be 1500 – 1600 nm. The width of the MMI is chosen to be in the range $30 - 50 \mu\text{m}$ and the length $0 - 2\frac{3}{4}L_\pi(\lambda_1)$.

Based on the above procedure, the optimal edge filters are found to have the dimensions $W = 45 \mu\text{m}$, $L = 3478 \mu\text{m}$ and $W = 46 \mu\text{m}$, $L = 3250 \mu\text{m}$ for the positive slope MMI (P_I) and the negative slope MMI (P_{II}), respectively. The spectral responses are plotted in Fig. 58(a) from which it is clear that the discrimination range (from 1500 to 1600 nm) is 10.97 dB, while the baseline loss is 6.57 dB for the positive slope edge filter. For the negative slope edge filter the

discrimination range is 11.39 dB with a baseline loss of 5.96 dB. To calculate the ratio of the whole integrated ratiometric structure, a Pade (1,1) beam propagation method with a GD scheme is used [135] below [135] below. The ratio of the spectral response is from -10.91 to 11.49 dB and is shown in Fig. 59.

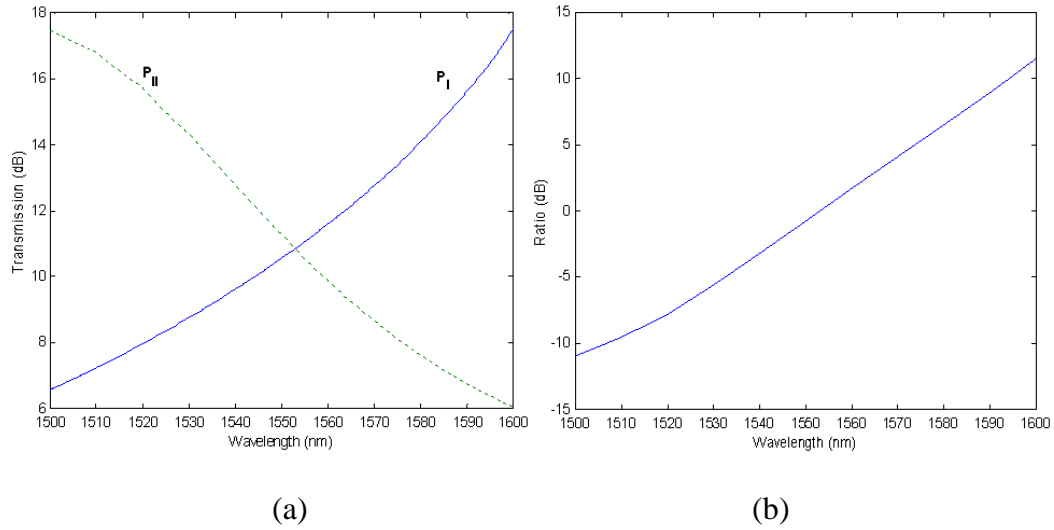


Figure 58 (a) Spectral response of optimised edge filters with opposite slopes (b) Spectral response of the ratiometric

To confirm the wavelength discrimination capability of the designed structure, the ratiometric wavelength measurement process is modelled numerically [136] below by taking account of the optical noise of the source signal and the electrical noise of the photodetectors. Assuming the SNR of the input signal is about 55 dB, the best resolution achievable for power measurement is 0.001 dB and the noise generated by photodetectors and electronic circuitry is equivalent to an uncertainty in the ratio measurement of 0.002 dB. The source wavelength is set to 1550 nm. This wavelength is changed by successively

increasing increments of 5, 10, 15 and 20 pm. The photodetector outputs are sampled 100 times and the ratio of the photodetectors outputs is calculated for each wavelength. The wavelength is incremented again and the process of sampling is repeated. Fig. 59 shows the complete time series of the calculated ratio values as a function of sample time and the wavelength increments. From Fig. 59, it is clear that the detectable ratio due to the wavelength tuning has a potential resolution at least better than 20 pm.

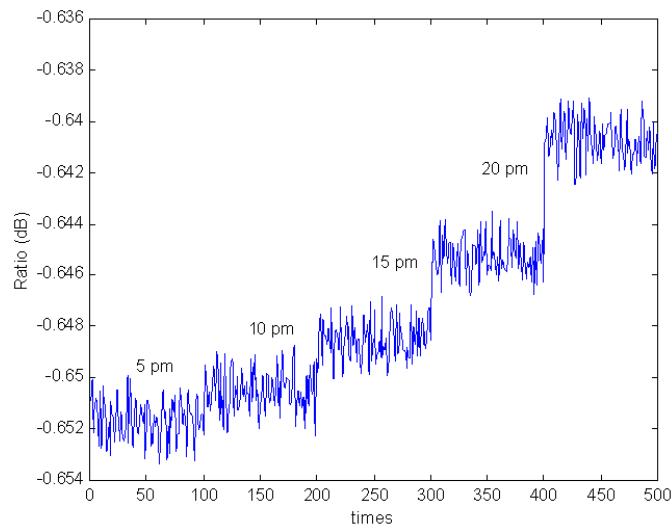


Figure 59 Output ratio as the wavelength is tuned

C.4 Conclusion

An integrated ratiometric wavelength monitor based on a pair of MMI structures with symmetrical responses has been presented. The width and length of the two MMI edge filters with opposite slope spectral responses are optimised based on a defined figure of merit. The wavelength discrimination of the designed ratiometric

structure has been demonstrated numerically and shows a competitive resolution (20 pm) for wavelength measurement.

C.5 References

- [129] C. Sookdhis, T. Mei, and H. S. Djie, "Wavelength monitoring with low contrast multimode interference waveguide", *IEEE Photon. Technol. Lett.*, vol.17, pp.822-824, 2005.
- [130] Q. Wang, G. Farrell, and A. M. Hatta, "Global optimization of multimode interference structure for ratiometric wavelength measurement," *Proc. SPIE*, vol. 6619, Third European Workshop on Optical Fibre Sensors 2007.
- [131] Q. Wang, G. Farrell, P. Wang, G. Rajan, and T. Freir, "Design of integrated wavelength monitor based on a Y-branch with an S-bend waveguide," *Sensors and Actuators A*, vol. 134, pp. 405-409, 2007.
- [132] S. M. Melle, K. Liu, and R. M. Measures, "Practical fibre-optic Bragg grating strain gauge system," *App. Opt.*, vol. 32, pp. 3601-3609, 1993.
- [133] L.B. Soldano and E.C.M. Pennings, "Optical multi-mode interference devices based on self-imaging: principles and applications," *J. Lighth. Technol.*, vol.13, pp. 615-627, 1995.
- [134] www.mathworks.com
- [135] J. Yamauchi, *Propagating Beam Analysis of Optical Waveguides*, Research Studies Press, pp. 89-97, 2003.
- [136] Q. Wang, G. Rajan, P. Wang, and G. Farrell, "Resolution investigation of a ratiometric wavelength measurement system," *App. Opt.*, vol. 46, pp. 6362-6367, 2007.

Appendix D

A simple integrated ratiometric wavelength monitor based on multimode interference structure^a

Keywords: Integrated optics, multimode interference, wavelength monitor

Abstract: Wavelength measurement or monitoring can be implemented using a ratiometric power measurement technique. A ratiometric wavelength monitor normally consists of a Y-branch splitter with two arms: an edge filter arm with a well defined spectral response and a reference arm or alternatively, two edge filters arms with opposite slope spectral responses. In this paper, a simple configuration for an integrated ratiometric wavelength monitor based on a single multimode interference structure is proposed. By optimizing the length of the MMI and the two output port positions, opposite spectral responses for the two output ports can be achieved. The designed structure demonstrates a spectral

^a A. M. Hatta, G. Farrell and Q. Wang, "A simple integrated ratiometric wavelength monitor based on multimode interference structure," *Optical Design and Engineering III, Proceeding of SPIE 7100*, 710023, 2008.

response suitable for wavelength measurement with potentially a 10 pm resolution over a 100 nm wavelength range.

D.1 Introduction

A measurement of unknown wavelength is essential for many systems such as multi-channel dense wavelength-division multiplexing (DWDM) optical communication systems and Fibre Bragg Grating (FBG)-based optical sensing systems. As an example, an FBG-based optical sensing system requires a wavelength demodulation system to detect the wavelength shift of reflected light from the FBG elements induced by strain or temperature changes. There are different schemes of wavelength measurement/monitoring. A ratiometric wavelength monitoring has a simple configuration, the potential for high-speed measurement and the absence of mechanical movement compared to wavelength-scanning-based active measurement schemes. A ratiometric wavelength monitor converts the wavelength measurement into a signal intensity measurement. The ratiometric wavelength monitor usually consists of a splitter with two arms: an edge filter arm with a well defined spectral response and a reference arm or alternatively, two edge-filters arms with opposite slope spectral responses. It has been shown that the use of two opposite slope edge filters can increase the resolution of a ratiometric system [137]. The main element of the ratiometric scheme, the edge filter, can be implemented by a bulk thin filter [137], biconical fibre couplers [138], bending fibre [139], [140], integrated optics based on multimode interference [141], [142], an S-bend waveguide [143], and directional coupler [144]. Compared to bulk optical devices and fibre-based edge filters,

integrated wavelength monitors have a compact size, high scalability, and also benefit from a fast response and physical robustness.

MMI structures have been utilized as edge filters [141], [142] and a wavelength monitor [145]. Depending on the position of the input port on the MMI section, there are three interference mechanisms: paired, symmetrical, and general interference mechanisms, as described in the modal propagation analysis in [146]. In [145], a MMI wavelength monitor based on a paired interference mechanism has been proposed which offers a 100 nm range and 200 pm resolution. Previously, in [141], we have shown that an MMI structure can be used as an edge filter for a ratiometric wavelength monitor. In [141], the length and width of the MMI section, and the positions of the input and output waveguides, are optimized according to a desired spectral response by using the global optimisation algorithm-adaptive simulated annealing. A further improvement [142] has been proposed, in which the ratiometric scheme employs two opposite slope MMI edge filters based on symmetrical interference mechanism and which offers a 100 nm range and 15 pm resolution. In this paper, a single MMI structure with one input and two output ports based on a general interference mechanism is proposed as the ratiometric wavelength monitor. The two output ports have opposite spectral response slopes. This structure is simpler and more compact than the conventional ratiometric scheme which utilizes a Y-branch splitter and separate edge filter(s).

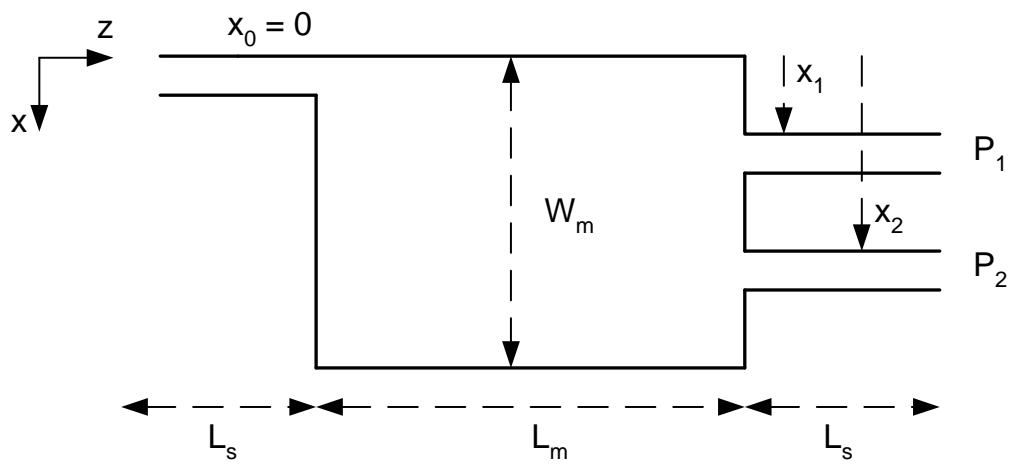
D.2 Proposed structure and design method

Fig. 60(a) shows the schematic configuration of an integrated ratiometric structure utilizing the general interference mechanism of a MMI structure. It contains an input port, an MMI section, and two output ports. The input port and the two output ports positions are denoted as x_0 , x_1 , and x_2 . The width and the length of MMI section are W_m and L_m respectively and the thickness of the waveguide is h . The desired spectral responses of the two arms are shown in Fig. 60(b), while the corresponding ratio of the two outputs over a wavelength range is presented in Fig. 60(c). The wavelength of an input signal can be determined by measuring the power ratio of the output ports at the outputs of the two arms, assuming a suitable calibration has taken place.

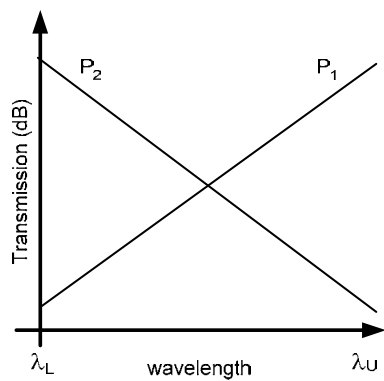
To design such an MMI-based device, a modal propagation analysis (MPA) is used [146]. The procedure for an MPA is as follows: the input light is assumed to have the field distribution $\psi(x,0)$ of the fundamental mode of the input port. The input field can be decomposed into the eigenmodes of the MMI section, $\varphi_\nu(x)$, when the light enters the MMI section. The input field to the MMI can be written as:

$$\psi(x,0) = \sum_{\nu=0}^{m-1} c_\nu \varphi_\nu(x, y) \quad (\text{D.1})$$

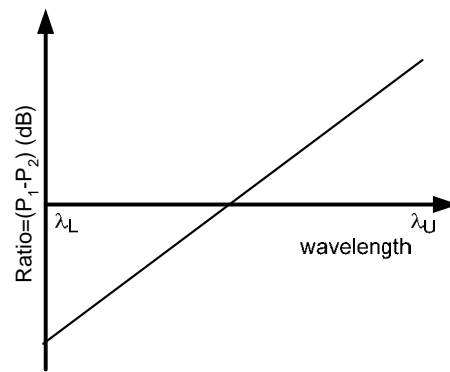
where m is the number of eigenmodes and c_ν is the excitation coefficient of each mode.



(a)



(b)



(c)

Figure 60 Schematic configuration of the proposed MMI ratiometric wavelength monitor (b) Desired spectral response of two edge filter arms and (c) The output ratio between two arms

The coefficient c_v can be calculated by an overlap integral between $\psi(x,0)$ and $\varphi_v(x)$

$$c_v = \frac{\int \psi(x,0) \cdot \varphi_v(x) dx}{\sqrt{\int \varphi_v^2(x) dx}}. \quad (\text{D.2})$$

As the light propagates in the MMI section, the field at a propagation distance z can be calculated by

$$\psi(x, z) = \sum_{v=0}^{m-1} c_v \varphi_v(x) \exp[j(\beta_0 - \beta_v)z] \quad (\text{D.3})$$

where β_v is the propagation constant of each eigenmode of the MMI. The transmission loss in dB can be determined by using the overlap integral method between $\psi(x, z)$ and the eigenmode of the output port of x_1 or x_2 , $\psi_{1,2}(x)$:

$$P_{1,2}(z) = -10 \cdot \log_{10} \left(\frac{\left| \int \psi(x, z) \psi_{1,2}(x) dx \right|^2}{\int |\psi(x, z)|^2 dx \int |\psi_{1,2}(x)|^2 dx} \right). \quad (\text{D.4})$$

To optimise the MMI structure as a ratiometric wavelength monitor, for a certain W_m , the L_m of the MMI and the output port positions, x_1 and x_2 , are adjusted. The transmission response of the each port position is calculated for each L_m of MMI. The desired spectral response of the overall structure is such that the two output ports have opposite slope transmission responses (eg., one increasing and one decreasing) as the wavelength increases over the wavelength range as shown in Fig. 60(b). Therefore, it is necessary to calculate the transmission response between the lower and upper limits $[\lambda_L$ and $\lambda_U]$ of the desired wavelength range over a range the L_m values for the MMI. For each L_m , we scan the output positions across the width of MMI, x_1 and x_2 and determine

the transmission value at λ_L , λ_U as $P_{1,2}(\lambda_L)$, $P_{1,2}(\lambda_U)$, respectively, then calculate the corresponding discrimination range $D_{1,2} = |P_{1,2}(\lambda_L) - P_{1,2}(\lambda_U)|$.

After calculating $P_{1,2}(\lambda_L)$ and $P_{1,2}(\lambda_U)$ for each L_m , x_1 and x_2 , we select some structures as possible candidates. We select the structures based on the constraints that the discrimination, D , should be better than 10 dB and that the baseline loss (either $P_{1,2}(\lambda_L)$ and $P_{1,2}(\lambda_U)$) depending on whether the slope is negative or positive) should be less than 8 dB [139], [140]. Then, we calculate the spectral response for each selected structures. An ideal response for the output port should give a quasi linear dependence for wavelength versus transmission. We can use a linear curve fitting and get a slope (a) of linear function ($P(\lambda) = a\lambda + b$) and a norm residual (nxr) from a QR decomposition of the Vandermonde matrix, as the parameters used to choose the best spectral response. The ideal spectral response has a high slope a and low nxr . The optimal structure with opposite spectral response slopes of the two output ports is chosen based on a figure of merit

$$F = 0.5 \left\{ \exp \left[- \left(\frac{nxr_+}{a_+} \right) \right] + \exp \left[- \left(\frac{nxr_-}{|a_-|} \right) \right] \right\} \quad (D.5)$$

where the subscript + and – indicates the positive and negative slope of the output port spectral response, respectively. The best structure occurs when $F = 1$ and the worst when $F = 0$.

The design procedure can be summarized as follow:

1. Calculate $P_{1,2}(\lambda_L)$, $P_{1,2}(\lambda_U)$, and $D_{1,2}$ for the range of L_m .

2. Choose the appropriate structures with a parameter set of L_m , x_1 and x_2 , subject to the constraints: i) $D_{1,2} > 10$ dB, ii) the baseline loss (either $P_{1,2}(\lambda_L)$ and $P_{1,2}(\lambda_U)$) < 8 dB.
3. Choose the optimal structure: L_m , x_1 , and x_2 based on maximising the value of F .

D.3 Numerical Example

To demonstrate the design method and performance achieved, we present here a numerical example. The refractive indices of the core and the cladding for a buried silica-on-silicon waveguide are $n_{co} = 1.4553$ and $n_{cl} = 1.4444$, respectively. The height of the waveguide is $5.5 \mu\text{m}$ and the width of the input/output port is $5.5 \mu\text{m}$. We set $W_m = 55 \mu\text{m}$ (this value allows for an output port spacing that avoids unwanted coupling between the ports) and the input port is positioned at the lateral end side of the MMI, i.e. $x_0 = 0 \mu\text{m}$. The wavelength range is $\lambda_L = 1500 \text{ nm}$ to $\lambda_U = 1600 \text{ nm}$. The MPA and an effective index method are used to simplify the calculation of 3D into 2D which can reduce significantly the computational time. Undertaking the first step in the design procedure, we choose the range of L_m to be calculated as $0.5L_\pi \leq L_m \leq 1.5L_\pi$ ($L_\pi = \frac{\pi}{\beta_0 - \beta_1}$) at $\lambda_L = 1500 \text{ nm}$ is the coupling length of the two lower modes of the MMI), with an increment $0.01L_\pi$. Following the above procedure, after the second step, some appropriate structures with the parameter set of $[L_m, x_1, x_2]$ can be selected. Based on the third step, the figure of merit of the appropriate structures with the parameter set is depicted in Fig. 61. It is shown that the highest figure of merit, $F = 0.71$, is

the optimal structure with $L_m = 1.04$ $L_\pi = 4538$ μm , $x_1 = 10$ μm , $x_2 = 35$ μm . The corresponding spectral response is shown in Fig. 62. The positive (P_1) and negative (P_2) slope spectral response of the output ports in the wavelength range 1500 to 1600 nm are 7.16 to 17.28 dB and 20.96 to 6.59 dB, respectively.

To calculate the ratio of the whole integrated ratiometric structure as in Fig. 60(a), with $L_s = 2000$ μm ; the effective index method and a Pade (1,1) beam propagation method (BPM) with a GD scheme [147] are used. The output port spectral responses P_1 and P_2 are 7.36 to 17.72 dB and 20.55 to 6.47 dB, respectively, and the corresponding ratio is from -13.19 to 11.25 dB and is shown in Fig. 63. There are slight differences in the spectral responses resulting from the MPA and BPM calculations. It should be noted that the BPM calculation is intrinsically more accurate in that it considers all the radiation modes, compared to the MPA which only considers the guided modes. Furthermore, the BPM calculations apply to the whole structure while the MPA calculations apply only to the MMI section. However, the MPA is computationally faster than the BPM and suitable for scanning and optimization of parameters, while the BPM can be used as a verification tool to check the accuracy of results.

To validate the wavelength discrimination ability of the designed structure, the ratiometric wavelength measurement process is modeled numerically using the method in ref. [148] by taking account of the optical noise of the source signal and the electrical noise of the photodetectors. Assuming the SNR of the input signal is about 55 dB, the best resolution achievable for power measurement is 0.001 dB and the noise generated by the photodetectors and electronic circuitry is equivalent to an uncertainty in the ratio measurement of 0.002 dB. The source

wavelength is set to 1550 nm. This wavelength is changed by successively increasing increments of 2.5, 5, 7.5, 10, 12.5, 15, and 17.5 pm. The photodetector outputs are sampled 100 times and the ratio of the photodetectors outputs is calculated for each wavelength. The wavelength is incremented again and the process of sampling is repeated. Fig. 64 shows the complete time series of the calculated ratio values as a function of sample time and the wavelength increments. From Fig. 64, it is clear that the detectable ratio due to the wavelength tuning has a potential resolution of 10 pm.

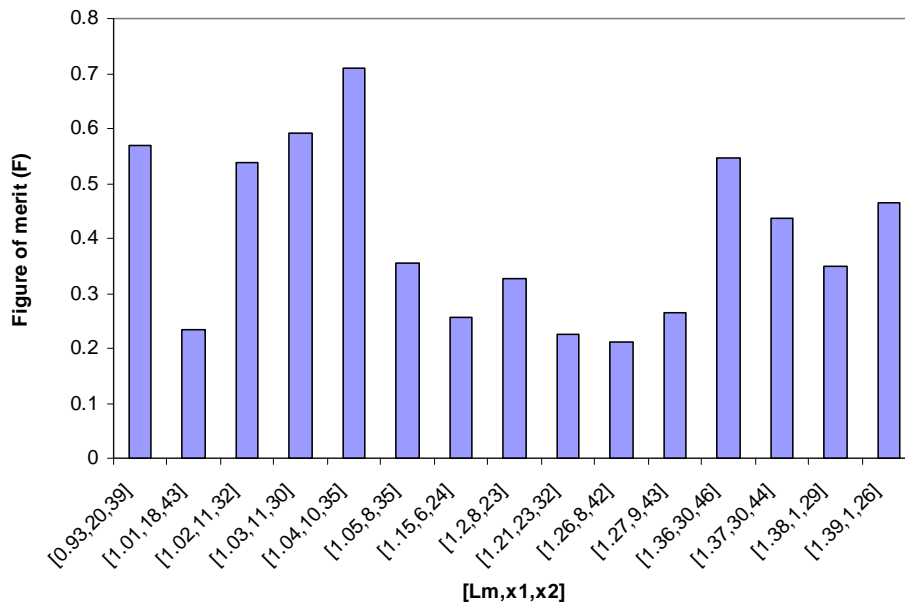


Figure 61 Figure of merit of the appropriate structures with a set of parameter $[L_m, x_1, x_2]$

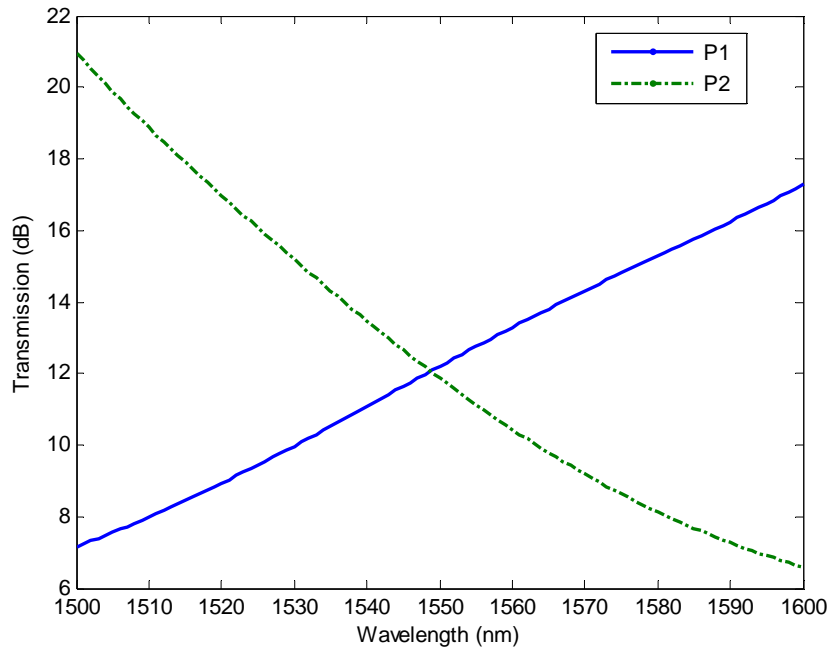


Figure 62 Spectral responses of the output ports of the optimal structure

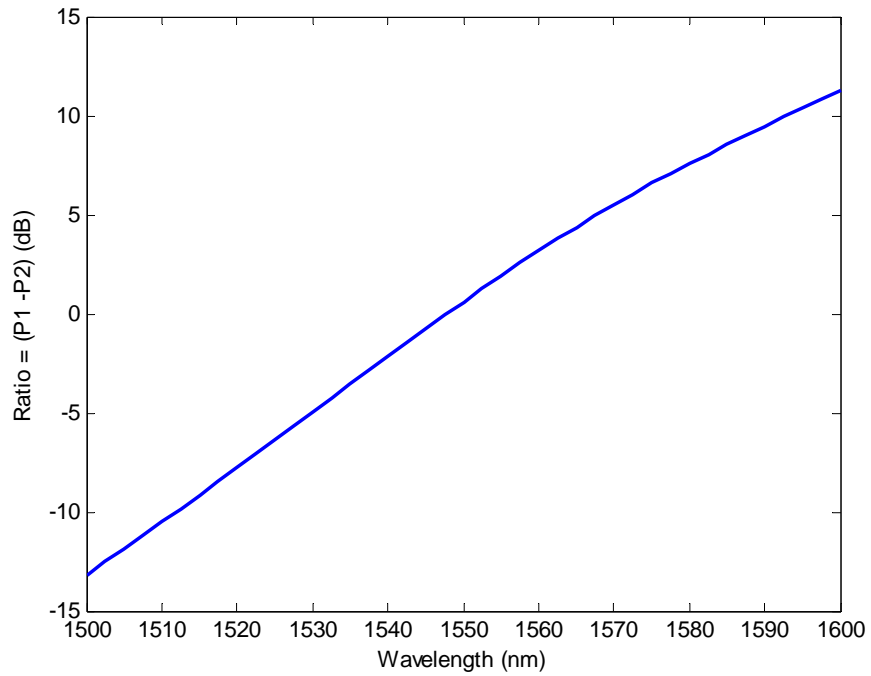


Figure 63 The output ratio calculated using BPM

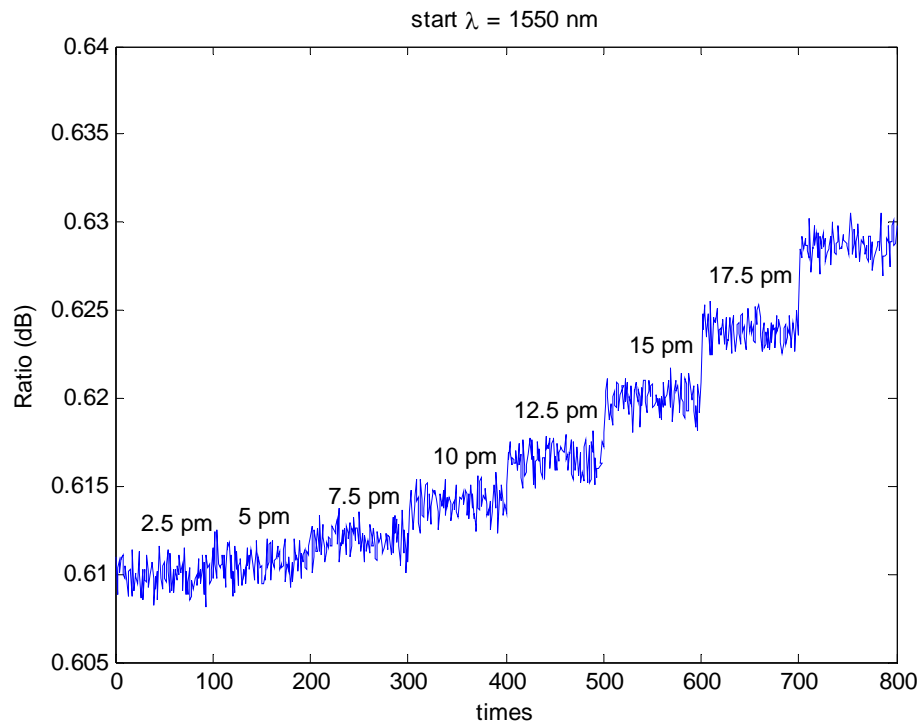


Figure 64 Output ratio as the wavelength is tuned

D.4 Conclusion

An integrated wavelength monitor based on an MMI structure has been presented. This integrated ratiometric monitor offers a simpler structural configuration compared to the conventional one that includes a Y-branch structure and two opposite slope edge filters. The length of the MMI and the position of the output ports are optimized based on the defined figure of merit. The wavelength discrimination of the simple ratiometric structure has been demonstrated numerically and shows a viable resolution (10 pm) for wavelength measurement.

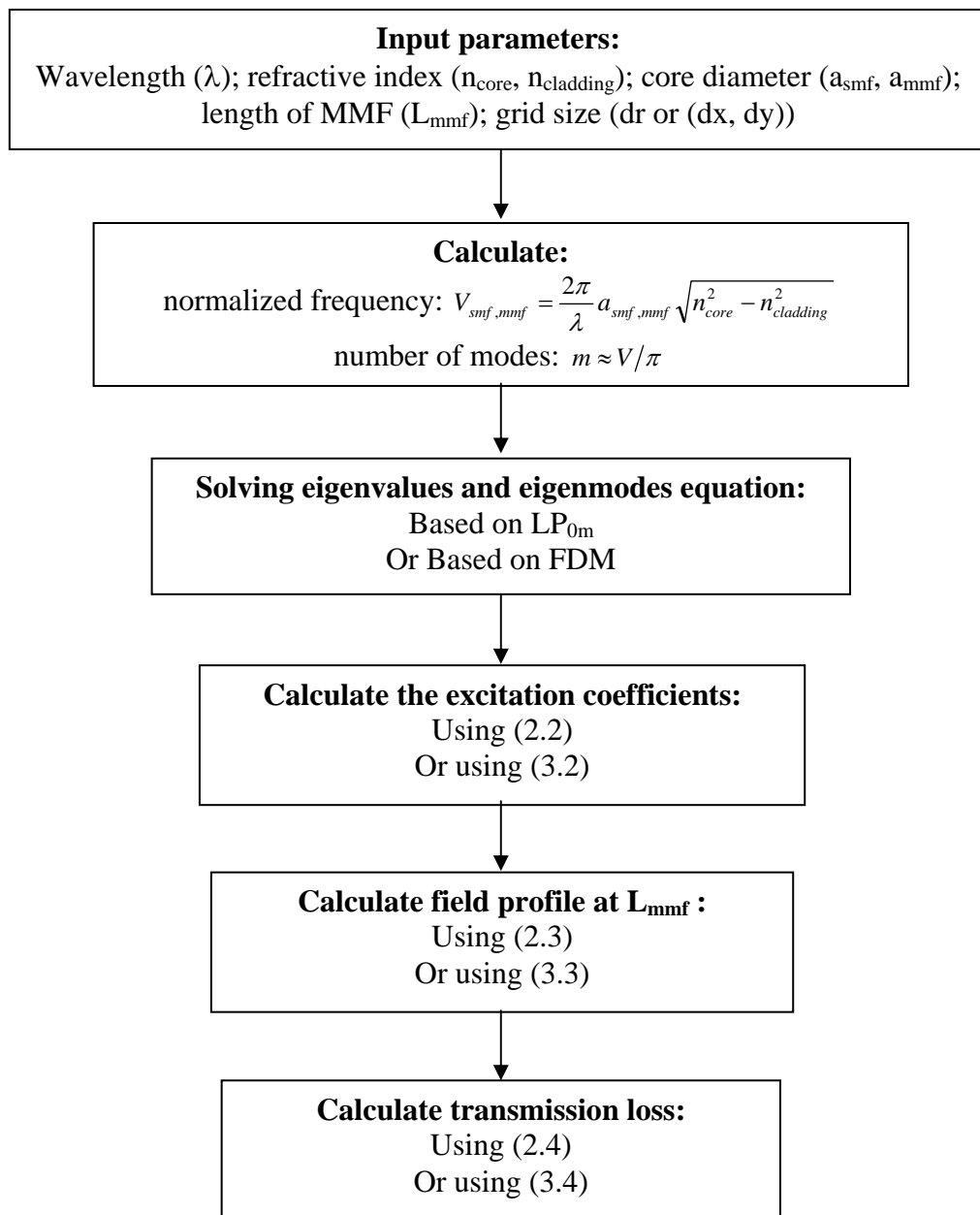
D.5 References

- [137] S. M. Melle, K. Liu, and R. M. Measures, "Practical fibre-optic Bragg grating strain gauge system," *App. Opt.*, vol. 32, pp. 3601-3609, 1993.

- [138] A. B. L. Ribeiro, L. A. Ferreira, M. Tsvekov, and J. L. Santos, "All-fibre interrogation technique for fibre Bragg sensors using a biconical fibre filter," *Electron. Lett.*, vol. 32, pp. 382–383, 1996.
- [139] Q. Wang, G. Farrell, T. Freir, G. Rajan, and P. Wang, "Low-cost wavelength measurement based on a macrobending single-mode fibre," *Opt. Lett.*, vol. 31, pp. 1785-1787, 2006.
- [140] P. Wang, G. Farrell, Q. Wang, and G. Rajan, "An optimized macrobending-fibre-based edge filter," *IEEE Photon. Technol. Lett.*, vol. 19, pp. 1136-1138, 2007.
- [141] Q. Wang, G. Farrell, and A. M. Hatta, "Global optimization of multimode interference structure for ratiometric wavelength measurement," *Proc. SPIE*, vol. 6619, 66192M, 2007.
- [142] A. M. Hatta, G. Farrell, Q. Wang, and J. Zheng, "Design on the optical core of an integrated ratiometric wavelength monitor," *Proc. ECIO 2008*, pp. 273-276, 2008.
- [143] Q. Wang, G. Farrell, P. Wang, G. Rajan, and T. Freir, "Design of integrated wavelength monitor based on a Y-branch with an S-bend waveguide," *Sensors and Actuators A*, vol. 134, pp. 405-409, 2007.
- [144] A. M. Hatta, Q. Wang, G. Farrell, and J. Zheng, "A design method for a ratiometric wavelength monitor using a pair of directional couplers acting as edge filters," *Proc. SPIE*, vol. 6996, 69961T, 2008.
- [145] C. Sookdhis, T. Mei, and H. S. Djie, "Wavelength monitoring with low contrast multimode interference waveguide", *IEEE Photon. Technol. Lett.*, vol.17, pp.822-824, 2005.
- [146] L.B. Soldano and E.C.M. Pennings, "Optical multi-mode interference devices-based on self-imaging: principles and applications," *J. Lighth. Technol.*, vol.13, pp. 615-627, 1995.
- [147] J. Yamauchi, *Propagating Beam Analysis of Optical Waveguides*, Research Studies Press, pp. 89-97, 2003.
- [148] Q. Wang, G. Rajan, P. Wang, and G. Farrell, "Resolution investigation of a ratiometric wavelength measurement system," *App. Opt.*, vol. 46, pp. 6362-6367, 2007.

Appendix E

Flowchart of the Modal Propagation Analysis



```

% =====
% Main program
% Modal Propagation Analysis Based on LP0m
% The DIT-PRC
% =====

%Parameters
% =====
%Input wavelength (in mikrometer)
lambda =1.55;
% Referactive index (ncore, ncladding)
% SMF
ncosmf=1.4504;nclsmf=1.4447;
%MMF
ncommf=1.4446;nclmmf=1.4271;
% core radius, a (in mikrometer)
% SMF
as=4.15;
% MMF
am=52.5;
% Length of MMF (in mikrometer)
Lmmf = 44818;
% grid size
dr=0.05;
% =====

% Calculate (normalized frequency, number of modes)
% =====
k=2*pi/lambda;
Vsmf=k*asmf*sqrt(ncosmf^2-nclsmf^2);
Vmmf=k*ammf*sqrt(ncommf^2-nclmmf^2);
modes=fix(v/pi);
% =====

% Solving eigenvalue and eigenmode equation
% =====
% MMF
[betam,phim]=modesolvermmf(ncommf,nclmmf,ammf,dr,k,Vmmf,modes);
% SMF
[betas,phis]=modesolversmf(ncosmf,nclsmf,asmf,dr,k,Vsmf);
% =====

%Calculated the excitation coefficient
% =====
[Cm]=excitationcoeff(phis,phim,dr);
% =====

%Calculate field profile at Lmmf
% =====
[phiz]=fieldprofile(Cm,betam,Lmmf);
% =====

% Calculate transmission loss
% =====
[Pout]=transmissionloss(phis,phiz,dr);
% =====

```

```

% =====
% Main program
% Modal Propagation Analysis Based on FDM
% The DIT-PRC
% =====

%Parameters
% =====
%Input wavelength (in mikrometer)
lambda =1.55;
% Referactive index (ncore, ncladding)
% SMF
ncosmf=1.4504;nclsmf=1.4447;
%MMF
ncommf=1.4446;nclmmf=1.4271;
% core radius, a (in mikrometer)
% SMF
as=4.5;
% MMF
am=52.5;
% Length of MMF (in mikrometer)
Lmmf = 44818;
% grid size
dx=0.25;dy=0.25;
% =====

% Calculate (normalized frequency)
% =====
k=2*pi/lambda;
Vsmf=k*asmf*sqrt(ncosmf^2-nclsmf^2);
Vmmf=k*ammf*sqrt(ncommf^2-nclmmf^2);
% =====

% Solving eigenvalue and eigenmode equation
% =====
% MMF
[betam,phim]=modesolvermmfFDM(ncommf,nclmmf,ammf,dx,dy,k,Vmmf,nmodes);
% SMF
[betas,phis]=modesolversmfFDM(ncosmf,nclsmf,asmf,dr,k,Vsmf);
% =====

%Calculated the excitation coefficient
% =====
[Cm]=excitationcoeff(phis,phim,dx,dy)
% =====

%Calculate field profile at Lmmf
% =====
[phiz]=fieldprofile(Cm,betam,Lmmf)
% =====

% Calculate transmission loss
% =====
[Pout]=transmissionloss(phis,phiz,dx,dy)
% =====

```

Appendix F

Equipment and accessories

The details of main equipment and accessories used in the experimental work presented in this thesis are described in this appendix. Important specification and operational characteristics of fibre fusion splicer, the tunable laser source, optical spectrum analyzer, power meters, polarization controller, temperature controller,.. are described in this section.

Sumitomo Type 36 Fusion Splicer

A Sumitomo Type 36 Fusion Splicer was used to splicing fibres together. The splicer can handle fibre types such as, singlemode, multimode, dispersion shifted, dispersion compensated, cut off shifted and Er doped fibres. A fibre cladding diameter of 125 microns is preferable for the splicer. A precision CCD camera examines the fibre from the X and Y view and precisely aligns the fibres, before doing the arc splicing. After splicing, high resolution direct core monitoring image processing software incorporated into the 180 splicer calculates the estimated splice loss. There are two main splicing modes: automatic mode and attenuation mode. By using automatic mode, typical splice loss for singlemode fibres is less than 0.05 dB. By using attenuation mode, a pre-setting of 1 dB attenuation correspond core offset of 3.3 μm .

Nettest OSICS ECL Tunable Laser

The Nettest OSICS tunable laser system is designed for fibre optic component testing, particularly for DWDM. It is a fully integrated system with onboard hardware and software. The OSICS system may be remotely operated via standard RS232 and IEEE-488 interfaces. The main specifications of the OSICS ECL tunable laser are listed below:

Wavelength range : 1500 nm - 1620 nm

Output Power range: -5 dBm - +7dBm

Wavelength resolution: 0.01 nm

Wavelength accuracy: 0.01nm

Tuning speed: 10nm/s

Power stability: 0.01dB

Side mode suppression ratio: 45 dB

Relative intensity noise: 145 dB/Hz

Agilent Optical Spectrum Analyzer

The key specifications of the Agilent 86140B Optical Spectrum analyzer are given below:

Wavelength range: 600 nm to 1700 nm

Wavelength accuracy: 0.01 nm

FWHM: 0.06 nm

Sensitivity: -90 dB in the wavelength range 1250 nm -1610 nm

Maximum safe power: 30 dBm

Polarization dependence: 0.3 dB in the range 1250 nm -1650 nm

Optical Fiber Power Meters

Two dual channel power meters are used to measure power in the experiments:

PXIT 306 dual channel fiber optic power meter, and a custom made power meter with a dual channel amplifier board and two photodiodes. The PXIT 306 is a high performance dual channel power meter compatible with the PXI format. Its two channels were independent and high speed data acquisition is possible when used in the sequence mode. The power meter was able to measure power level up to -70 dBm.

Temperature Controller

A Thermoelectric cooler (Marlow Industries DT12-8 driven by a temperature controller was used for the temperature studies. The Thorlabs ITC 510 Laser Diode Current and TEC Controller provide current and temperature control in one unit. The instruments provide a maximum laser drive current range of pm1 A, and a TEC drive current of up to pm4A (32W). The ITC 510 Current Controller exhibits exceptionally low current noise and low temperature drift, making this instrument one of the best performing combination controller. The key specifications of the TEC controller of ITC 510 are listed below:

Control range: -4A to -4A

Maximum output power: 32 W

Thermistor: 2k/20 K

Other Equipment

Other main equipments used in this thesis were Thorlabs FPC560 manual polarization controller, PZT stack AE0505D18, a single channel piezo controller MDT694A (Thorlabs), etc. The polarization controller utilizes stress induced birefringence to alter the polarization in a single-mode fiber. The loop diameter of the paddle was 2.2". The PZT stack translates the DC voltage of 0 to 100 V into displacement of 0 to 19 μm . A single channel piezo controller MDT694A (Thorlabs) was used to supply DC voltages from 0 to 100 V.